

UNIVERSIDADE FEDERAL DO AMAZONAS  
PRÓ-REITORIA DE PESQUISA  
PROGRAMA DE PÓS-GRADUAÇÃO EM FÍSICA

MARCUS VINICIUS ALVES RIBEIRO

**THEORETICAL MODELS OF SCALE-FREE POLYMER  
NETWORKS**

Manaus - AM  
2023

Support:



MARCUS VINICIUS ALVES RIBEIRO

**THEORETICAL MODELS OF SCALE-FREE POLYMER  
NETWORKS**

Thesis presented to the Postgraduate Program in  
Physics at the Federal University of Amazonas as  
partial fulfillment to obtain the title of Doctor in  
Physics.

Advisor: Prof. Dr. Mircea Daniel Galiceanu

Manaus - AM  
2023

©All rights reserved.

## Ficha Catalográfica

Ficha catalográfica elaborada automaticamente de acordo com os dados fornecidos pelo(a) autor(a).

R484t Ribeiro, Marcus Vinicius Alves  
Theoretical Models of Scale-Free Polymer Networks / Marcus  
Vinicius Alves Ribeiro . 2023  
59 f.: il. color; 31 cm.

Orientador: Mircea Daniel Galiceanu  
Tese (Doutorado em Física) - Universidade Federal do  
Amazonas.

1. Complex Polymer Networks. 2. Scale-free Networks. 3. Rouse  
Model. 4. Semiflexible Model. 5. Copolymer Model. I. Galiceanu,  
Mircea Daniel. II. Universidade Federal do Amazonas III. Título

*To my wife and my daughters, with love.*

---

---

# ACKNOWLEDGMENTS

---

To Prof. Dr. Mircea Daniel Galiceanu for his valuable guidance in this work, as well as for his exemplary attention and dedication. Also, I express my thanks to all the professors of the Department of Physics as well as the Physics Postgraduate Program (PPGFIS) for their understanding and patience.

To my parents, I thank you every day for the great example you gave me and continue to give me. Unfortunately, my mother is no longer present, but I know she would be happy both for my undergraduate education and now for my doctorate.

To my wife and daughters for their patience, understanding, and support throughout this academic period. Lorraine, you know that this would not be possible without your companionship.

To my colleagues at work and postgraduate studies, I am grateful for the support and motivation in continuing this journey.

Lastly, I want to thank all the workers who always fight for public universities to remain public, accessible with quality.

---

---

# ABSTRACT

---

Scale-free Networks (SFNs) are structures built with nodes that show a degree distribution that follows a power law. SFNs are used with great success in several real networks. In this work, the networks are modeled from an algorithm that constructs scale-free networks without loops by changing the minimum,  $K_{min}$  and the maximum,  $K_{max}$ , allowed degrees,  $\gamma$ , which measures the density of links and  $N$ , total number of monomers. In this work, we will study the theoretical polymers dynamics models focused on Generalized Scale-Free Networks (GSFNs) on arbitrary tree-like polymers. For the Rouse Model, we monitor the influence of each of the parameters  $K_{min}$ ,  $K_{max}$ ,  $\gamma$ , and  $N$ . In the Semiflexible Model, which fixes the angles between the bonds between the nearest neighbors, we add one more parameter: the stiffness parameter  $q$ . In the Copolymer Model, we consider of the parameters:  $\eta = \frac{N_A}{N_B}$ , the ratio between the number of monomers of type  $A$  and  $B$ , and  $\sigma = \zeta_A/\zeta_B$ , where  $\zeta_A$  and  $\zeta_B$  are friction constants of monomers of the  $A$  and  $B$ , respectively. In all the cases, we will analyze the eigenvalue ( $\lambda$ ) spectra of the connectivity matrix  $\mathbf{A}$  and the dynamical behavior of these networks, focusing on the Complex Dynamic Modulus, with its two parts: the Storage Modulus ( $G'$ ) and the Loss Modulus ( $G''$ ) and on the average displacement  $\langle\langle Y(t) \rangle\rangle$ . For eigenvalues, we can notice the influence of the parameters of the Rouse and Flexibility model in terms of the degeneracy of  $\lambda = 1$ . Differently, in the Copolymer Model, we have two eigenvalues with high degeneracy:  $\lambda = 1$  and  $\lambda = \sigma$ . In all models are encountered two situations: connectivity-independent behaviors at very small and very large  $\omega$ , namely for very small  $\omega$  one has  $G'(\omega) \sim \omega^2$  and  $G''(\omega) \sim \omega^1$ , for very large  $\omega$  has  $G'(\omega) \sim \omega^0$  and  $G''(\omega) \sim \omega^{-1}$ .

Keywords: **Complex Polymer Networks. Scale-free Networks. Rouse Model. Semiflexible Model. Copolymer Model.**

---

# RESUMO

---

Redes de Livre de Escala, ou em inglês Scale-free Networks (SFNs), são estruturas contruídas com nós, que demonstra uma distribuição de grau de tipo lei de potência. SFNs são usadas com grande sucesso em vários modelos de redes reais. Neste trabalho, as redes são modeladas usando um algoritmo que constrói redes livre de escala sem "loops" alterando os graus mínimos  $K_{min}$  e máximos  $K_{max}$  permitidos,  $\gamma$ , que mede a densidade de graus e  $N$ , que representa o número total de monômeros. Neste trabalho estudamos os modelos teóricos focados em redes livres de escala generalizadas (GSFNs) em polímeros tipo árvores arbitrários. Para o Modelo Rouse, monitoraremos a influência de cada um dos parâmetros  $K_{min}$ ,  $K_{max}$ ,  $\gamma$  e  $N$ . No Modelo Semiflexível, que fixa os ângulos entre as ligações entre os vizinhos mais próximos, adicionamos mais um parâmetro: a rigidez. No modelo copolímero, acrescentamos os parâmetros:  $\eta = \frac{N_A}{N_B}$ , que é a razão quantidade de monômeros do tipo  $A$  e  $B$ , e  $\sigma = \zeta_A/\zeta_B$ , onde  $\zeta_A$  e  $\zeta_B$  são as constantes de fricção dos monômeros  $A$  e  $B$ , respectivamente. Em todos os casos, analisaremos os espectros de autovalores da matriz de conectividade  $\mathbf{A}$  e o comportamento dinâmico dessas redes, com foco no Módulo Dinâmico Complexo, com suas duas partes: o Módulo de Armazenamento ( $G'$ ) e o Módulo de Perda ( $G''$ ) e deslocamento médio  $\langle\langle Y(t) \rangle\rangle$ . Para autovalores, podemos ver a influência dos parâmetros no Modelos Rouse e Semiflexibilidade em termos da degenerescência para  $= 1$ . Diferentemente, no Modelo de Copolímero, temos dois autovalores com alta degenerescência:  $= 1$  e  $= \sigma$ . Em todos os modelos são observadas duas situações: independentes para comportamentos em  $\omega$  muito pequeno e muito grande; para  $\omega$  muito pequeno tem-se  $G'(\omega) \sim \omega^2$  e  $G''(\omega) \sim \omega^1$ , para muito grande  $\omega$  tem  $G'(\omega) \sim \omega^0$  e  $G''(\omega) \sim \omega^{-1}$ .

Palavras-chave: **Redes Poliméricas Complexas. Redes Livre de Escala. Modelo de Rouse. Modelo Semiflexível. Modelo Copolímero.**

---



---

# LIST OF FIGURES

---

1.1	Visualization of the structure of the Internet network. The nodes represent an IP's address. The colors were based on Class A allocation of IP space to different registrars in the world. Source: [6]. . . . .	2
1.2	Human disease network. Nodes are diseases and two diseases are connected if they share a genetic component. Source: Adapted of the Goh <i>et al</i> [2]. . . . .	2
1.3	(Left) ER model for $N = 12$ nodes and $L = 20$ links. (Right) Small-World Model for $N = 8$ , $L = 4$ and $p = 0.2$ . . . . .	3
1.4	Type of Polymers, in which bead represents a monomer: (a) Homopolymer (b) Copolymer	4
1.5	(A) Schematic of the polypeptoid sequences. Each sequence contains 2 types of monomers: hydrophilic and uncharged N-methoxyethyl (Nme) glycine (black circle), and negatively charged Nce glycine (red circle). (B) Attachment scheme to form long polypeptoids through end-to- end click reactions between 24mer polypeptoids. Source: [30]. . . . .	4
2.1	Map of Königsberg in Euler's time showing the actual layout of the seven bridges. Source: [46]. . . . .	6
2.2	Here the various parts of the lands (A, B, C, D) of Fig. 2.1 are stylized as vertices. The various bridges are represented by the edges of the graph. . . . .	7
2.3	A small subset of (a) the Internet, where routers (specialized computers) are connected to each other; (b) a protein-protein interaction network, where two proteins are connected if there is experimental evidence that they can bind to each other in the cell. Source: [4]. . . . .	8
2.4	(a) A Random Network with $N = 50$ , (b) Degree Rank Plot, (c) Degree Histogram. Source: Made in Program Python . . . . .	9
2.5	Complex Network with four vertex. . . . .	9
2.6	Degree distribution for Scale-Free Polymer Networks with $N = 100000$ and $S = 100$ realizations of the algorithm. . . . .	16
2.7	Construction procedure in detail. . . . .	17
2.8	Realizations of GSFNs with $N = 1000$ , $\gamma = 2.5$ and the parameters' set $(K_{min}, K_{max})$ : (Top left) (2, 999), (Top right) (2, 50), (Down left) (5, 999), and (Down right) (5, 50). Source: [39] . . . . .	18
2.9	(a) Schematic representation of a scale-free network of size $N = 50$ , $\gamma = 2.5$ , $K_{min} = 2$ , and $K_{max} = 49$ and ten random walkers, shown by red color. (b) The visualization of the one step evolution of the infectious randomwalkers on the network. The black color represents susceptible individuals, red the infectious, and blue the individuals removed from the network. Source: [17] . . . . .	19
3.1	Rouse Model. . . . .	21

3.2	Schematic drawing of the nearest and next-nearest neighbors of a bead $i$ in a treelike network. Source: [86] . . . . .	28
3.3	Construction procedure of a GSFN: (a) and (b) Construction procedure in detail for realization of the GSFN construction procedure with $N = 20$ and the parameters' set $(\gamma, K_{min}, K_{max})$ equal to: (c) (1.0, 2, 19) and (d) (4.0, 2, 19). (d) Copolymer GSFN obtained from network (c) by choosing at random the $A$ -type (green) and $B$ -type (gray) monomers. . . . .	30
4.1	(a-d) Eigenvalues in progressive order for GSFPNs with $N = 1000$ and $K_{min} = 4$ . . . . .	34
4.2	Eigenvalue spectra for SGSFNs with $N = 4000$ nodes and $S = 250$ realizations. Other parameters are: $(\gamma, K_{min}, K_{max}, q)$ : (a)(2, 2, 3999, variable), (b) (2.5, 2, 3999, variable). . . . .	35
4.3	Eigenvalue spectra for SGSFNs with $N = 4000$ nodes and $S = 250$ realizations for the parameters $(\gamma, K_{min}, K_{max}, q)$ being (2.5, variable, 3999, 0.3). . . . .	35
4.4	Eigenvalue spectra for SGSFNs with $N = 4000$ nodes and $S = 250$ realizations for the parameters $(\gamma, K_{min}, K_{max}, q)$ are variable, 2, 3999, 0.1. . . . .	36
4.5	Eigenvalue spectra for GSFCNs with $N = 4000$ . The parameters $(\gamma, K_{min}, K_{max}, \sigma, \eta)$ are: (2.5, 2, 3999, variable, 1.0). . . . .	37
4.6	Eigenvalue spectra for GSFCNs with $N = 4000$ . The parameters $(\gamma, K_{min}, K_{max}, \sigma, \eta)$ are: (variable, 2, 3999, 0.01, 1.0). . . . .	38
4.7	Eigenvalue spectra for GSFCNs with $N = 4000$ . The parameters $(\gamma, K_{min}, K_{max}, \sigma, \eta)$ are: (2.5, variable, variable, 0.01, 1.0). . . . .	39
4.8	Eigenvalue spectra for GSFCNs with $N = 4000$ . The parameters $(\gamma, K_{min}, K_{max}, \sigma, \eta)$ are: (2.5, 2, 3999, 0.01, variable). . . . .	40
4.9	The storage modulus $G'(\omega)$ for GSFPNs with $N = 1000$ and $\gamma = variable$ . The parameters' set $(K_{min}, K_{max})$ is equal to: (Left) (3, 20) and (Right) (3, 100). . . . .	41
4.10	The loss modulus $G''(\omega)$ for GSFPNs with $N = 1000$ and $\gamma = variable$ . The parameters' set $(K_{min}, K_{max})$ is equal to: (Right) (5, 50), and (Left) (5, 1000). . . . .	42
4.11	The average monomer displacement for GSFPNs with $N = 1000$ its derivative for GSFPNs corresponds to $K_{min} = 2, K_{max} = 50, \gamma = variable$ . . . . .	43
4.12	The average monomer displacement and its derivative for GSFPNs with $N = 1000$ . Left-hand side panel corresponds to $K_{min} = variable, K_{max} = 1000, \gamma = 25$ . . . . .	44
4.13	Storage modulus and its derivative for SGSFNs with $N = 4000$ and $S = 100$ realizations for the parameters $(\gamma, K_{min}, K_{max}, q)$ are (variable, 2, 3999, 0.1). . . . .	44
4.14	Storage modulus and its derivative for SGSFNs with $N = 4000$ and $S = 100$ realizations for the parameters $(\gamma, K_{min}, K_{max}, q)$ are (2.5, variable, 3999, 0.3). . . . .	45
4.15	Storage modulus and its derivative for SGSFNs with $N = 4000$ and $S = 100$ realizations. The parameters $(\gamma, K_{min}, K_{max}, q)$ are (2, 2, 3999, variable). . . . .	46
4.16	Loss modulus and its derivative for SGSFNs with $N = 4000$ and $S = 100$ realizations. Other parameters are: $(\gamma, K_{min}, K_{max}, q)$ : (Left) (variable, 2, 3999, 0.3) and (Right) (variable, 2, 3999, 0.7). . . . .	47
4.17	Loss modulus and its derivative for SGSFNs with $N = 4000$ and $S = 100$ realizations for the parameters $(\gamma, K_{min}, K_{max}, q)$ are (2.5, 2, variable, 0.1). . . . .	48
4.18	Loss modulus and its derivative for SGSFNs with $N = 4000$ and $S = 100$ realizations for the parameters $(\gamma, K_{min}, K_{max}, q)$ are (2.5, 2, 3999, variable). . . . .	49

4.19	Average monomer displacement and its derivative for SGSFNs. The parameters' set is: $(N, \gamma, K_{min}, K_{max}, q)$ : (Left) (4000, 2, 2, $N1$ , variable), (Right) (4000, 2.5, 2, 3999, variable) . . . . .	50
4.20	Average monomer displacement and its derivative for SGSFNs. The parameters' set is: $(N, \gamma, K_{min}, K_{max}, q)$ : (a) (4000, variable, 2, 3999, 0.3), (b) (4000, 2.5, variable, 3999, 0.3). . . . .	50
4.21	Storage modulus $G'(\omega)$ and your derivative for GSFCNs with $N = 4000$ with the parameters $(\gamma, K_{min}, K_{max}, \sigma, \eta) = (2.5, 2, 3999, variable, 1.0)$ . . . . .	52
4.22	Loss modulus $G''(\omega)$ and your derivative $\alpha''$ for GSFCNs with $N = 4000$ with the parameters $(\gamma, K_{min}, K_{max}, \sigma, \eta) = (2.5, 2, 3999, variable, 1.0)$ . . . . .	52
4.23	Storage modulus $G'(\omega)$ and your derivative for GSFCNs with $N = 4000$ with the parameters $(\gamma, K_{min}, K_{max}, \sigma, \eta) = (variable, 2, 3999, 0.01, 1.0)$ . . . . .	53
4.24	Loss modulus $G''(\omega)$ and your derivative $\alpha''$ for GSFCNs with $N = 4000$ with the parameters $(\gamma, K_{min}, K_{max}, \sigma, \eta) = (variable, 2, 3999, 0.01, 1.0)$ . . . . .	53
4.25	Storage modulus $G'(\omega)$ and your derivative for GSFCNs with $N = 4000$ with the parameters $(\gamma, K_{min}, K_{max}, \sigma, \eta) = (2.5, variable, variable, 0.01, 1.0)$ . . . . .	54
4.26	Loss modulus $G''(\omega)$ and your derivative $\alpha''$ for GSFCNs with $N = 4000$ with the parameters $(\gamma, K_{min}, K_{max}, \sigma, \eta) = (2.5, variable, variable, 0.01, 1.0)$ . . . . .	55
4.27	Storage modulus $G'(\omega)$ and your derivative for GSFCNs with $N = 4000$ with the parameters $(\gamma, K_{min}, K_{max}, \sigma, \eta) = (2.5, 2, 3999, 0.01, variable)$ . . . . .	56
4.28	Loss modulus $G''(\omega)$ and your derivative $\alpha''$ for GSFCNs with $N = 4000$ with the parameters $(\gamma, K_{min}, K_{max}, \sigma, \eta) = (2.5, 2, 3999, 0.01, variable)$ . . . . .	56

---

---

# LIST OF ABBREVIATIONS AND ACRONYMS:

---

**HDN** - Human Disease Network

**ER** - Erdos and Rényi

**WS** - Watts-Strogatz

**SFNs** - Scale-Free Networks

**GGs** - Generalized Gaussian Structures

**WWW** - World Wide Web

**BA** - Barabási and Albert

**GSFNs** - Generalized Scale-Free Networks

**STPs** - Semiflexible Treelike Polymers

**SGSFNs** - Semiflexible Generalized Scale-Free polymer Networks

**GSFCNs** - Generalized Scale-Free Copolymer Networks



---

# CONTENTS

---

<b>1</b>	<b>Introduction</b>	<b>1</b>
<b>2</b>	<b>Complex Network</b>	<b>6</b>
2.1	Complex Network Properties . . . . .	8
2.2	Scale-Free Networks (SFNs) . . . . .	12
<b>3</b>	<b>Theoretical Models</b>	<b>20</b>
3.1	Rouse Model . . . . .	20
3.1.1	Viscoelastic Relaxation Moduli . . . . .	24
3.2	Semiflexible Model . . . . .	26
3.3	Copolymer Model . . . . .	29
<b>4</b>	<b>Results</b>	<b>33</b>
4.1	Eigenvalue spectra . . . . .	33
4.1.1	Rouse Model . . . . .	33
4.1.2	Semiflexible Model . . . . .	34
4.1.3	Copolymers Model . . . . .	36
4.2	Mechanical Relaxation . . . . .	40
4.2.1	Rouse Model . . . . .	41
4.2.2	Semiflexible Model . . . . .	43
4.2.3	Copolymers Model . . . . .	50
<b>5</b>	<b>Conclusion</b>	<b>57</b>
	<b>REFERENCES</b>	<b>59</b>
	<b>Bibliography</b>	<b>59</b>

---

# Introduction

---

Networks are present in all aspects of our lives: networks of friends, communication, transportation networks, or the Web are all examples that we experience outwardly, while the neurons in our brain and the proteins within our body form networks that determine our intelligence and survival. The study of network science predicated its basic foundations on the development of graph theory, which was early examined by Leonhard Euler in 1736, when he published the famous Seven Bridges of Königsberg paper [1]. In the context of the network theory, a complex network system could be defined as a system composed of *nodes* (e.g., structural or functional relation) and the direct interactions between them, called *links*. Nodes can represent some entities like people, cities, computers, websites, concepts, cells, genes, species, etc. Links represent relationships or interactions between these entities: friendships among people, flights between airports, packets exchanged among computers through Internet, links between Web pages, synapses between neurons, and so on.

One of the best-known and most widely studied examples of a network is the Internet, the computer data network in which the nodes are computers and the links are physical data connections between them, such as optical fiber cables or telephone lines. In Fig. 1.1, we visualize the network of the Internet where nodes represent servers, and links represent fiber-optic links. Another example is the map of the human disease network (HDN) show in Fig 1.2 where nodes represent disorders, and two disorders are connected if they share at least one gene and in which mutations are associated with both disorders [2].

Various network models have been built. The random graph developed by Erdős and Rényi can be considered the most basic model of complex networks. Erdos and Rényi (ER) introduced a model to generate random graphs consisting of  $N$  vertices (nodes) and  $L$  edges (links). Starting with  $N$  disconnected nodes, the network is constructed by adding  $L$  links randomly, avoiding multiple and self connections [3, 4]. This model builds a network with  $N$  nodes and a probability  $p$  of connecting each pair of nodes. Fig. 1.3 (left) represents the ER model for  $N = 12$  and  $L = 20$ . The most popular model of random networks with small-world characteristics and an abundance of short loops was developed by Watts and Strogatz and is called the Watts-Strogatz (WS) *small-world model*. To construct a small-word network, we begin with a regular lattice of  $N$  nodes in which each node is connected to nearest neighbors in each direction, totalizing 2 connections, where  $N \geq \log(N) \geq 1$ . Next, each link is randomly rewired with probability  $p$ . When  $p = 0$  we have an ordered lattice with many loops but large distances, and when  $p \rightarrow 1$ , the network becomes a random graph with short distances but few loops [5]. In Fig. 1.3 (right)

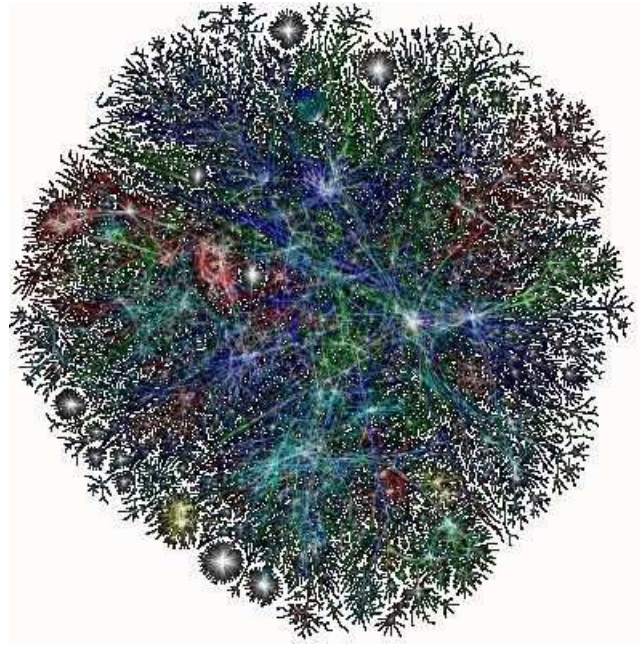


**Figure 1.1** - Visualization of the structure of the Internet network. The nodes represent an IP's address. The colors were based on Class A allocation of IP space to different registrars in the world. Source: [6].

### *Human Disease Network (HDN)*

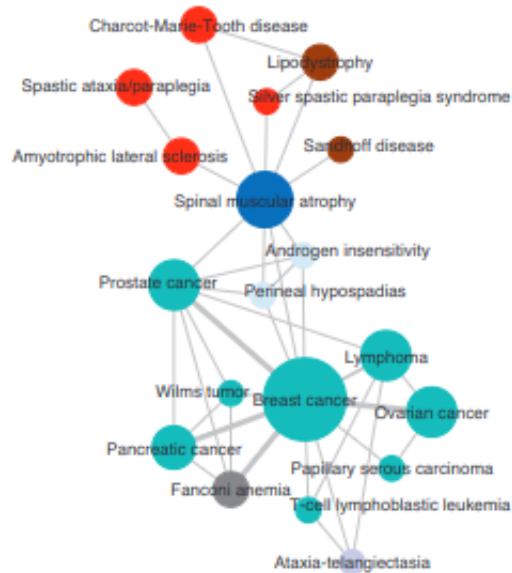


**Figure 1.2** - Human disease network. Nodes are diseases and two diseases are connected if they share a genetic component. Source: Adapted of the Goh *et al* [2].

represents the Small World model for  $N = 8$ ,  $L = 16$  and  $p = 0.2$ .

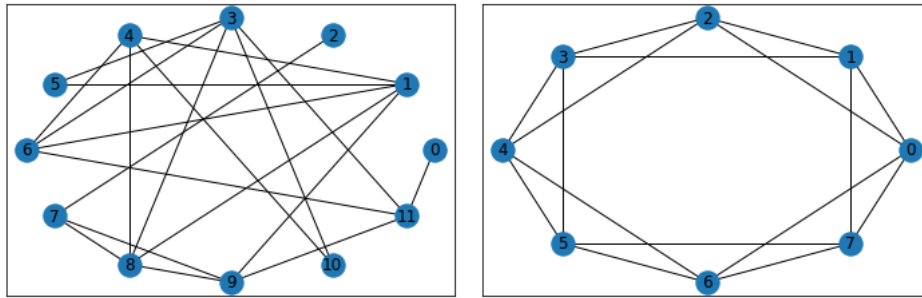


**Figure 1.3** - (Left) ER model for  $N = 12$  nodes and  $L = 20$  links. (Right) Small-World Model for  $N = 8$ ,  $L = 4$  and  $p = 0.2$

After Watts and Strogatz's model, Barabási and Albert showed that the degree distribution of many real systems is characterized by a degree distribution that has been found to follow a power law for large  $k$ ,  $P(k) \sim k^{-\gamma}$  where  $k$  is the number on the links and  $\gamma$  represents the density those links. These networks are called *Scale-Free Networks* (SFNs) [4, 7]. This thesis was focused on SFNs, because they were used with great success to model various real networks, such as protein-protein interaction network [9, 10], metabolic networks [11, 12], river networks [13], food webs [14], internet [15], epidemic processes [16, 17], the author collaboration networks of scientific papers [18, 19], financial networks [20, 21], transport networks [22, 23], to name only a few examples. In this work, the nodes are the polymer's monomers and follow a scale-free degree distribution.

Over the past 50 years, the uses for and production of synthetic polymers have increased exponentially. This is largely due to the undeniable fact that these materials provide many social benefits, including those strongly and positively connected to sustainability (e.g., lightweight transportation to reduce fuel consumption, membranes for efficient water purification, and food packaging to prevent spoilage). Unfortunately, most synthetic polymers are not biodegradable. Ultimately, the long-term sustainability of the polymer industry will hinge on the successful introduction of new polymers derived from annually renewable resources. [25].

Polymer is used to mean a particular class of macromolecules composed of molecules that have long sequences of one or more species of atoms or groups of atoms linked to each other by primary, usually covalent, bonds. If there is only one type of chemical unit (monomer), the corresponding polymer is a *homopolymer* (Fig. 1.4 (a)); if there is more than one type, it is a *copolymer* (Fig. 1.4 (b)) [26]. Copolymers have played an essential part in developing polymeric materials for different applications. Ethylene–vinyl acetate (EVA), acetonitrile–butadiene–styrene (ABS), and styrene–butadiene–styrene (SBS) are just a few examples of copolymers with commercial importance. Depending on the copolymer type, *i.e.*, random/alternating, graft, or block, copolymers with different properties can be obtained [27].

Nowadays, polymer networks are not only widely used in many everyday commodity applications such as automotive tires or various structural vibration and noise-cutting solutions but are also increasingly employed as advanced functional materials for drug delivery systems,



**Figure 1.4** - Type of Polymers, in which bead represents a monomer: (a) Homopolymer (b) Copolymer

selective membranes and gas storage, water purification, shape memory polymers, soft robotics, materials for medical applications, stretchable electronics, light-controlled contractible gels, and additive manufacturing [28]. The knowledge of dynamics in associative macromolecular networks is extremely important for understanding biophysical processes and designing soft materials for applications spanning drug delivery, tissue engineering, and organic electronics [29]. Truong *et al* [30] have shown that a study of the charge sequence on polyelectrolyte conformation is important to understand many biophysical processes and advancing the design of sequence-defined polymeric material. Modulating a polyelectrolyte's charge sequence has been shown to significantly alter its conformational behavior and activity in many biophysical processes [30]. In Fig. 1.5 are shown three polypeptoid sequences, each with equally spaced charged monomers and a net charge per monomer.

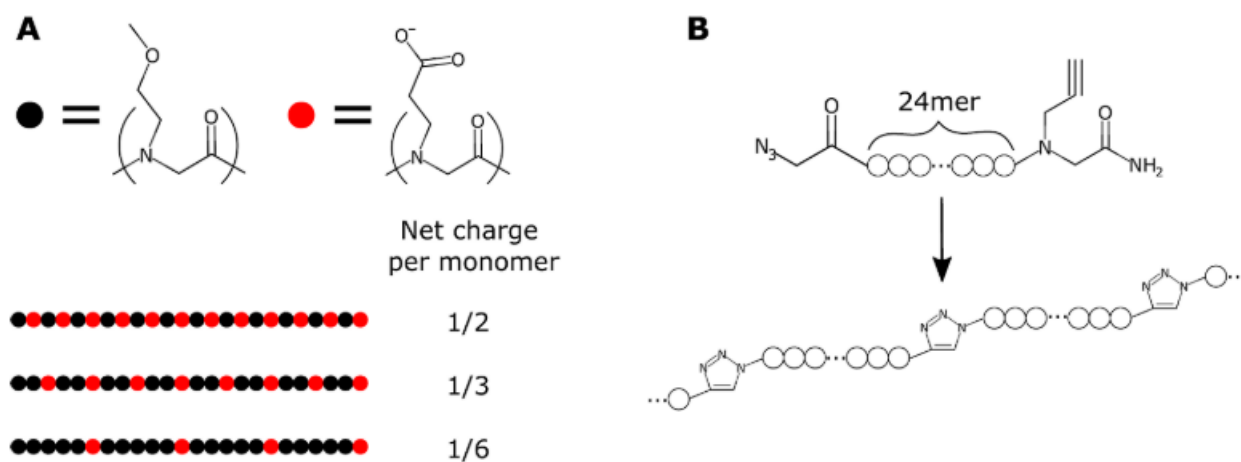


**Figure 1.5** - (A) Schematic of the polypeptoid sequences. Each sequence contains 2 types of monomers: hydrophilic and uncharged N-methoxyethyl (Nme) glycine (black circle), and negatively charged Nce glycine (red circle). (B) Attachment scheme to form long polypeptoids through end-to-end click reactions between 24mer polypeptoids. Source: [30].

In polymer physics, one of the most challenging problems is understanding the connection between polymeric materials' topology and their dynamics. The pioneering ideas of Rouse, starting with the bead-and-spring model for linear flexible chains, resulted in a basic approach that could be used to treat the dynamics of polymers [31]. In this model, the polymer is considered as being a sequence of beads connected via harmonic springs (Gaussian chain). Generalized Gaussian

---

Structures (GGS) which represent the extension of the classical Rouse model to arbitrary topology [32, 33]. Nowadays, its range of applicability is extended to the dynamics of polymers with much more complex architectures. Many theoretical studies have been devoted to treelike structures, such as dendrimers (which are regular subsets of the Cayley tree) and their derivatives, star polymers, hyperbranched polymers, fractal polymer networks, and small-world networks [33, 34]. However, the GGS formalism neglects some important polymer features, such as the excluded volume and the hydrodynamic interactions; moreover, in the original GGS approach, the semiflexibility of polymer strands taken into account. In our theoretical approach, the semiflexibility was introduced by restricting the orientations of the bonds, which can be monitored through the related stiffness parameter in the GGS model [35–39]. The stiffness effect is often fundamental, e.g., in biological macromolecular structures like DNA [40], actins [41, 42], and intermediate filament networks [43]. The GGS model is also applied to copolymers, for which there are two kinds of monomers with different mobilities, i.e., different friction coefficients [44, 45].

In summary, this work focuses on the theoretical investigations of the relaxation dynamics (Storage and Loss Moduli) and statics (topology) of Scale-Free Polymer Networks following the framework established by Generalized Gaussian Structures applying the Rouse, the Semiflexibility, and the Copolymer Model. The algorithm that creates the networks from a scale-free degree distribution with additional modularity parameters will be described. The dynamics will be studied by analyzing the behavior of the relaxation patterns of the average monomer displacement and the two mechanical relaxation moduli.

This thesis consists of four chapters. Chapter 1 describes the definitions of Network Science, the difference between graph and network science, the scale-free network, and the model used for constructing the polymers with a scale-free degree distribution. Chapter 2 recalls the general formalism of GGSs in the Rouse model and briefly show the equations that govern the mechanical relaxation and the folding and unfolding dynamics of polymers under applied external forces. After this, the semiflexible and the copolymers models theory is developed. All the models are describe by displacement  $\langle\langle Y \rangle\rangle$  and the complex dynamical shear modulus ( $G^*(\omega)$ ) or, equivalently, its real  $G'(\omega)$  and imaginary  $G''(\omega)$  components. Chapter 3 presents the results of the relaxation patterns of polymer networks modeled in Chapter 1. Finally, Chapter 4 concludes the work and outlines future perspectives.

# Complex Network

The mathematical idea of a *graph* can be traced back at least as far as the 1730s when Leonhard Euler posed and answered the question of whether it is possible to walk through the city of Königsberg (now Kaliningrad, Russia) crossing each of its seven bridges only once, see Fig. 2.1.

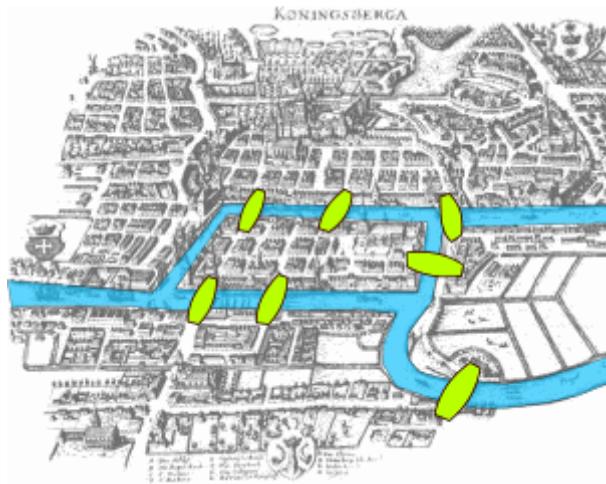


**Figure 2.1** - Map of Königsberg in Euler's time showing the actual layout of the seven bridges. Source: [46].

Despite Euler's solving this problem without using a picture representing the network of bridges in Königsberg, he reformulated it in a way that was the equivalent of what is now referred to as a 'graph'. A representation derived from Euler's formulation of Königsberg's bridges problem is illustrated in Fig. 2.2 by continuous lines, which are superposed on the scheme of the island and bridges of Fig. 2.1. Euler represented the four land areas separated by the river with letters *A*, *B*, *C*, and *D*. They are linked by a bridge and we draw a line (called an edge) between them. Then Euler made a simple observation: if a path crosses all bridges but never the same bridge twice, nodes with an odd number of links must be either the starting or the end point of this path. Indeed, if you arrive at a node with an odd number of links, you may have no unused link to leave it [4, 57].

As we will see, Graph theory has become a mainstream activity in pure mathematics, and the notion of a graph has a long history of applications in areas such as chemistry, physics, the social sciences, and computer science. Now, there is a small difference between a Graph and a Complex Network, therefore Barabási, in his book "Network Science" [4], is using them interchangeably (see Table 2.1).

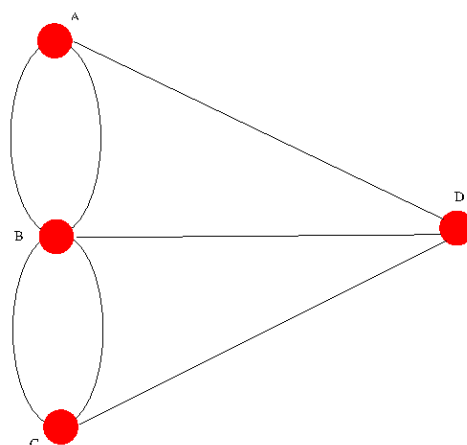


**Figure 2.2** - Here the various parts of the lands (A, B, C, D) of Fig. 2.1 are stylized as vertices. The various bridges are represented by the edges of the graph.

Complex Network	Graph Theory
Network	Graph
Node	Vertex
Link	Edge

Table 2.1 - Comparison between Complex Network and Graph Theory formulations.

For Complex Networks, the terms *network*, *node* and *link* represent real systems: The WWW (World Wide Web) is a network of web documents linked by URLs; society is a network of individuals linked by family, friendship or professional ties; the metabolic network is the sum of all chemical reactions that take place in a cell [4].

Complex networks occur everywhere: in artificial and human social systems, organic and non-organic matter from nano to macro scales, and natural and anthropogenic structures [23, 47]. Over the past two decades, many studies have applied network science methodologies across diverse scientific fields to study complex systems. Complex systems involve multiple components that interact with each other to give rise to complex behavior. Network science, which started within the Physics community, is now a mature multidisciplinary field with many applications ranging from Ecology to biology, medicine, social sciences, engineering, and computer science. Famous examples include the findings about sexual partners [48], the Internet and WWW [4, 49], epidemic spreading [17], immunization strategies [50], citation networks [51], the structure of financial markets [21], social percolation and opinion dynamics [52–54], the structure of mobile communication networks [55], and many others. Among the phenomena that have been shown to fall in this conceptual framework are cascading failures, blackouts, crashes, bubbles, crises, viral attacks and defense against them, introduction of new technologies, infrastructure, understanding measuring and predicting the emergence and evolution of networks and their stylized features, spreading phe-

nomena and immunization strategies, as well as the stability and fragility of airline networks [47]. Very recently, we have seen the application of network science; Bellingeri *et al.* present a complex networks-based epidemic model in the framework of the COVID-19 spread. The authors elaborate on the connection between removing social links and the diffusion of pandemics in the light of non-pharmaceutical interventions [56]. Also, Galiceanu *et al.* try to understand the evolution of a pandemic situation focused on a situation in which the spread occurs on a predefined network. In this case, we understand a network to be a collection of individuals connected through links based on familiarity, friendship, or professional reasons. A justifiable number of these networks, also called social networks, are scale-free [17]. It provides an essential tool in a systems approach to understanding many complex systems.

## 2.1 Complex Network Properties

To understand a complex system, we first need to know some basic quantities.

- **Number of nodes (N)** represents the number of components of the system. To distinguish the nodes, we label them with  $i = 1, 2, \dots, N$ . Each node can be considered an actor-movie network, a gene biological network, computers, people (Social Networks) and others things.
- **Number of links (E)**, or number of edges, represents the total number of interactions between the nodes.

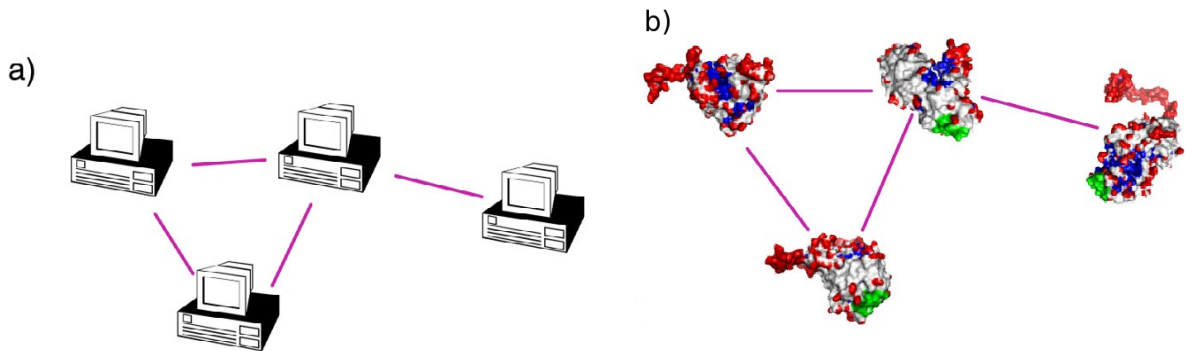


**Figure 2.3** - A small subset of (a) the Internet, where routers (specialized computers) are connected to each other; (b) a protein-protein interaction network, where two proteins are connected if there is experimental evidence that they can bind to each other in the cell. Source: [4].

- **Degree of a node ( $k$ )** is the number of edges attached to it. In an undirected network the total number of links can be expressed as the sum of the node degrees:

$$E_{total} = \frac{1}{2} \sum_{i=1}^N k_i, \quad (2.1)$$

here the  $1/2$  factor stands for the fact that in the sum (2.1) each link is counted twice.

- **The degree distribution,  $p_k$** , provides the probability that a randomly selected node in the network has degree  $k$ . Since  $p_k$  is a probability, it must be normalized:

$$\sum_{k=1}^{\infty} p_k = 1. \quad (2.2)$$

For a network with  $N$  nodes the degree distribution is a normalized histogram (Fig. 2.4) is given by

$$p_k = \frac{N_k}{N}, \quad (2.3)$$

where  $N_k$  is the number of nodes with degree  $k$ .

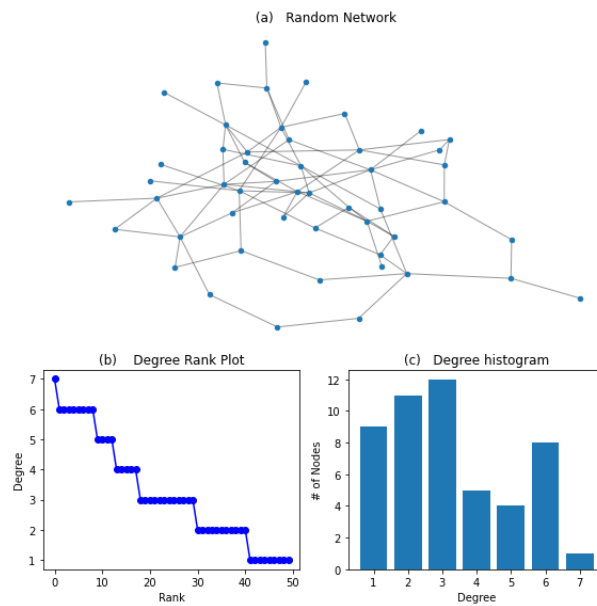


**Figure 2.4** - (a) A Random Network with  $N = 50$ , (b) Degree Rank Plot, (c) Degree Histogram. Source: Made in Program Python

- **Adjacency Matrix** of a network is an matrix  $N \times N$  with elements  $A_i$  given by

$$B_{ij} = \begin{cases} 1, & \text{if there is a link between node } j \text{ and node } i; \\ 0, & \text{otherwise.} \end{cases} \quad (2.4)$$

Let's consider the example displayed in Fig. 2.5.

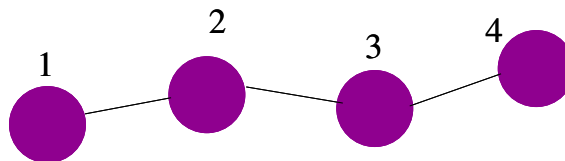


**Figure 2.5** - Complex Network with four vertex.

The Adjacency Matrix of the Fig. (2.5) can be expressed as

$$\mathbf{B} = \begin{pmatrix} B_{11} & B_{12} & B_{13} & B_{14} \\ B_{21} & B_{22} & B_{23} & B_{24} \\ B_{31} & B_{32} & B_{33} & B_{34} \\ B_{41} & B_{42} & B_{43} & B_{44} \end{pmatrix}.$$

Using Eq. (2.4), we have:

$$\mathbf{B} = \begin{pmatrix} 0 & 1 & 0 & 0 \\ 1 & 0 & 1 & 0 \\ 0 & 1 & 0 & 1 \\ 0 & 0 & 1 & 0 \end{pmatrix}.$$

There is another matrix, closely related to the adjacency matrix but differing in some important aspects, that can also tell us much about network structure. This is the *Laplacian*( $\mathbf{L}$ ), because its relation with the Laplacian Operator  $\nabla^2$  [57]. For an introduction to the Laplacian Matrix, we choose the problem of diffusion.

Diffusion is, among other things, the process by which gas moves from regions of high density to regions of low density, driven by the relative pressure (or partial pressure) of the different regions [57]. We can consider diffusion processes on networks, and such processes are sometimes used as a simple model of spread across a network, such as the spread of information or a disease. Suppose we have some commodities on the vertices of a network, and there is an amount  $\psi_i$  at node  $i$ . Moreover, now let us suppose that the commodity moves along the edges, flowing from one node  $j$  to an adjacent one  $i$  at a rate  $C(\psi_i - \psi_j)$  where  $C$  is a constant called the *diffusion constant*, is a measure of the rate of material transport as a result of the random movement of particles (diffusion) [58]. That is, in a small interval of time, the amount of fluid flowing from  $j$  to  $i$  is  $C(\psi_i - \psi_j)dt$ . Then the rate at which  $\psi_i$  is written in function of the Adjacency Matrix as

$$\frac{d\psi_i}{dt} = C \sum_j B_{ij}(\psi_j - \psi_i). \quad (2.5)$$

In this expression, the adjacency matrix elements  $B_{ij}$ , Eq. (2.4), insure that the only terms appearing in the sum are those that correspond to node pairs that are actually connected by an edge. Separating the two terms in Eq. (2.5), we can rewrite

$$\begin{aligned} \frac{d\psi_i}{dt} &= C \sum_j B_{ij}\psi_j - C\psi_i \sum_j B_{ij} \\ &= C \sum_j B_{ij}\psi_j - C\psi_i k_i \\ &= C \sum_j (B_{ij} - \delta_{ij}k_i)\psi_j, \end{aligned} \quad (2.6)$$

where  $k_i$  is the degree of node  $i$  and we have made use of the result  $k_i = \sum_j B_{ij}$  [57], while  $\delta_{ij}$  is the Kronecker delta.

Eq. (2.6) can be written in matrix form as

$$\frac{d\psi}{dt} = C(\mathbf{B} - \mathbf{D})\psi, \quad (2.7)$$

where  $\psi$  is the vector whose components are numbers  $\psi_i$ ,  $\mathbf{B}$  is the adjacency matrix, and  $\mathbf{D}$  is the diagonal matrix with the node degrees along its diagonal:

$$\mathbf{D} = \begin{pmatrix} k_1 & 0 & 0 & \cdots \\ 0 & k_2 & 0 & \cdots \\ 0 & 0 & k_3 & \cdots \\ \vdots & \vdots & \vdots & \ddots \end{pmatrix}. \quad (2.8)$$

It is common to define the new matrix

$$\mathbf{L} \equiv \mathbf{D} - \mathbf{B}. \quad (2.9)$$

The Eq. (2.6) can also be rewritten as

$$\frac{d\psi}{dt} + C\mathbf{L}\psi = 0, \quad (2.10)$$

which has the same form as the ordinary diffusion equation for a gas, except that the Laplacian operator  $\nabla^2$  that appears in that equation has been replaced by the matrix  $\mathbf{L}$  that can be called *Laplacian matrix*. In chapter 3 we will call it as *Connectivity Matrix*.

The elements of the Laplacian matrix are

$$L_{ij} = \begin{cases} k_i, & \text{if } i = j, \\ -1, & \text{if } i \neq j \text{ and there is an edge } (i, j), \\ 0, & \text{otherwise,} \end{cases} \quad (2.11)$$

We rewrite this expression as

$$\mathbf{L}_{ij} \equiv \delta_{ij}k_i - \mathbf{B}_{ij}. \quad (2.12)$$

For example, we write the matrix  $L_{ij}$  of the network displayed in Fig. 2.5,

$$L_{ij} = \begin{pmatrix} L_{11} & L_{12} & L_{13} & L_{14} \\ L_{21} & L_{22} & L_{23} & L_{24} \\ L_{31} & L_{32} & L_{33} & L_{34} \\ L_{41} & L_{42} & L_{43} & L_{44} \end{pmatrix} = \begin{pmatrix} 1 & -1 & 0 & 0 \\ -1 & 2 & -1 & 0 \\ 0 & -1 & 2 & -1 \\ 0 & 0 & -1 & 1 \end{pmatrix}. \quad (2.13)$$

We can solve the diffusion Eq. (2.10) by writing the vector  $\psi$  as a linear combination of the eigenvectors  $\mathbf{v}_i$  of the Laplacian thus:

$$\psi(t) = \sum_i a_i(t)\mathbf{v}_i, \quad (2.14)$$

with the coefficients  $a_i(t)$  varying over time. Substituting this form into Eq. (2.10) and making use of  $\mathbf{L}\mathbf{v}_i = \lambda_i\mathbf{v}_i$ , where  $\lambda_i$  is the eigenvalue corresponding to the eigenvector  $\mathbf{v}_i$ , we get

$$\sum_i \left( \frac{da_i(t)}{dt} + C\lambda_i a_i(t) \right) \mathbf{v}_i = 0. \quad (2.15)$$

But the eigenvectors of a symmetric matrix such as the Laplacian are orthogonal, and so, taking the dot product of this equation with any eigenvector  $\mathbf{v}_j$ , we get

$$\frac{da_i(t)}{dt} + C\lambda_i a_i(t) = 0, \quad (2.16)$$

for all  $i$ , which has the solution

$$a_i(t) = a_i(0)e^{-C\lambda_i t}. \quad (2.17)$$

Given an initial condition for the system, as specified by the quantities  $a_i(0)$ , we can find the state at any later time, if we know the eigenvalues and eigenvectors of the Laplacian matrix. In chapter 3, we will use these definitions.

## 2.2 Scale-Free Networks (SFNs)

Motivated by such many applications, many theoretical models were proposed aiming to reproduce or describe real-world networks. In many of these models, the degree distribution is power law, and the corresponding network is said to be scale-free [4, 59]. Scale-free and power-law are sacral words in network science. This mature field studies complex systems in nature and society by representing these systems as networks of interacting elements [60]. The concept of SFNs was used with great success in real networks such WWW [7, 61], the author collaboration network of scientific papers [18], networks in biological organisms [10], and reaction-diffusion processes [9, 62], to name only a few examples.

The study of scale-free networks has been extensively investigated over the last two decades. A key indicator for a network to be scale-free is the power-law degree distribution,  $p(k) \propto k^{-\gamma}$ , where  $k$  is the degree of a node, the parameter is typically in the range, and  $\gamma$  measures the density of network's connections. Many networks have been reported scale-free, ranging from metabolic to protein networks and from information networks to social networks [63]. That is, the probability distribution for the degree is a power law. In other words we can write

$$p_k \propto k^{-\gamma}. \quad (2.18)$$

If we plot the data in a double logarithmic scale, we should obtain a straight line. For this, we take a logarithm of Eq. (2.18) and we obtain

$$\log p_k \sim -\gamma \log k. \quad (2.19)$$

In more precise terms, we discuss the discrete and the continuum formalism with the objective to define power-law distribution.

The **discrete formalism** provides the probability  $p_k$  that a node has exactly  $k$  links

$$p_k = Ck^{-\gamma}, \quad (2.20)$$

where constant  $C$  and determined by the normalization condition

$$\sum_{k=1}^{\infty} p_k = 1. \quad (2.21)$$

Using Eq. (2.20) we obtain,

$$C \sum_{k=1}^{\infty} k^{-\gamma} = 1, \quad (2.22)$$

hence

$$C = \frac{1}{\sum_{k=1}^{\infty} k^{-\gamma}} = \frac{1}{\zeta(\gamma)}, \quad (2.23)$$

where  $\zeta(\gamma)$  is the Riemann-zeta function. As node degrees are positive integers,  $k = 0, 1, 2, \dots$ , the discrete power-law distribution has the form

$$p_k = \frac{k^{-\gamma}}{\zeta(\gamma)}. \quad (2.24)$$

See that Eq. (2.24) diverges at  $k = 0$ .

For **continuum formalism**, in analytical calculations it is often convenient to assume that the degrees can have any positive real value [4]. In this case we write the power-law degree distribution as

$$p(k) = Ck^{-\gamma}. \quad (2.25)$$

With the normalization condition

$$\int_{k_{min}}^{\infty} p(k)dk = 1. \quad (2.26)$$

Using Eq.(2.25) in Eq.(2.26), we obtain

$$C = \frac{1}{\int_{k_{min}}^{\infty} Ck^{-\gamma}dk} = (\gamma - 1)k_{min}^{(\gamma-1)}. \quad (2.27)$$

Then, applying Eq.(2.27) in Eq.(2.25), the continuum formalism the degree distribution has the form

$$p(k) = (\gamma - 1)k_{min}^{(\gamma-1)}k^{-\gamma}. \quad (2.28)$$

Therefore, in the case Discrete formalism has a precise meaning: it is the probability that a randomly selected node has degree  $k$ . However, only the integral of  $p(k)$  encountered in the continuum formalism has a physical interpretation:

$$\int_{k_1}^{k_2} p(k)dk, \quad (2.29)$$

is the probability that a randomly chosen node has degree between  $k_1$  and  $k_2$ .

There is a difference between a random and a scale-free network, and this comes in the *tail* of the degree distribution, representing the high- $k$  region of  $p_k$ . For small  $k$  the power law represents that a scale-free network has many small degree nodes, most of which are absent in a random network. For large  $k$  the power law indicates that the probability of observing a high-degree node, or hub, is higher in a scale-free than in a random network.

The first scale-free (SF) network model, introduced by Barabási and Albert (BA), postulated that there are two fundamental ingredients of many real networks [4,7,61]: their growing character and the preferential attachment rule.

- *Growth*: Starting with a small number ( $m_0$ ) of nodes, at every timestep, a new vertex is added with  $m(\leq m_0)$  links (that will be connected to the vertices already present in the system).
- *Preferential attachment*: When choosing the nodes to which the new node connects, the probability  $\Pi(k)$  that a link of the new node connects to node  $i$  depends on its degree  $k_i$  as

$$\Pi(k) = \frac{k_i}{\sum_j k_j}. \quad (2.30)$$

After  $t$  timesteps the Barabási-Albert model generates a network with  $N = t + m_0$  nodes and  $m_0 + mt$  links. Thus, older (with smaller  $t_i$ ) nodes increase their connectivity at the expense of the younger (with larger  $t_i$ ) ones, leading over time to some nodes that are highly connected, a “rich-get-richer” phenomenon [4]. The *growth* and *preferential attachment* are responsible for the emergence of scale-free networks.

In the Barabási-Albert model, the node’s growth rate is determined solely by its degree. However, in real systems, a node’s connectivity and growth rate depend not on its degree alone. For example, in social systems, some individuals are better at turning a random meeting into a lasting social link than others. The webpage can bring us back daily despite the many other pages competing for our attention. Finally, some research papers in a short timeframe acquire many citations. A common feature of these successful nodes is some intrinsic property, such as an individual’s social skills, the content of a web page, or the content of a scientific article, that propels them ahead of the pack. The examples discussed above indicate that nodes have different abilities (fitness) to compete for links. This different abilities is called *fitness property* [4, 64]. To incorporate the role of fitness, we assume that preferential attachment is driven by the product of a node’s fitness,  $\eta$ , and its degree  $k$ . The resulting model, called the Bianconi-Barabási, consists of the following two steps:

- *Growth*: In each timestep a new node  $j$  with  $m$  links and fitness  $\eta_j$  is added to the network, where  $\eta_j$  is a random number chosen from a fitness distribution  $\tau(\eta)$ . Once assigned, a node’s fitness does not change.
- *Preferential Attachment*: The probability that a link of a new node connects to node  $i$  is proportional to the product of node  $i$ ’s degree  $k_i$  and its fitness  $\eta_i$ ,

$$\Pi(k) = \frac{\eta_i k_i}{\sum_j \eta_j k_j}. \quad (2.31)$$

This generalized preferential attachment Eq.(2.31) incorporates in the simplest possible way that fitness and connectivity jointly determine the rate at which new links are added to a given node, i.e., even a relatively young node with a few links can acquire links at a high rate if it has a large fitness parameter than the rest of the nodes [4, 64].

Differently from the Barabási-Albert and Bianconi-Barabási model, in the building of the network, we choose to employ a growth algorithm [34, 39, 67, 68] that provides treelike structures with nodes obeying the power-law degree distribution. This model contains two additional parameters:  $K_{min}$ , which represents the minimum allowed degree, and  $K_{max}$ , which gives the maximum allowed degree. In order to keep the total probability equal to 1 we assume that the probability of a node having degree  $k$  should be written as

$$p_k = \begin{cases} \frac{k^{-\gamma}}{\sum_{j=K_{min}}^{K_{max}} j^{-\gamma}}, & K_{min} \leq k \leq K_{max} \\ 0, & otherwise. \end{cases} \quad (2.32)$$

The two modularity parameters,  $K_{min}$  and  $K_{max}$ , and the exponent  $\gamma$ , give us the possibility to study a larger variety of network's topologies by smothering the transition between different topologies.

In Fig. 2.6, we show the degree distribution  $p_k$  constructed networks through the Eq. (2.32), facilitating a direct comparison. Displayed are the results obtained for networks consisting of  $N = 100000$  nodes and the number of realizations of the construction algorithm,  $S = 100$ . Here, we set the parameters  $K_{min} = 2$  and  $K_{max} = N - 1$ . The exponent  $\gamma$  allows us to study a more extensive variety of network topologies.

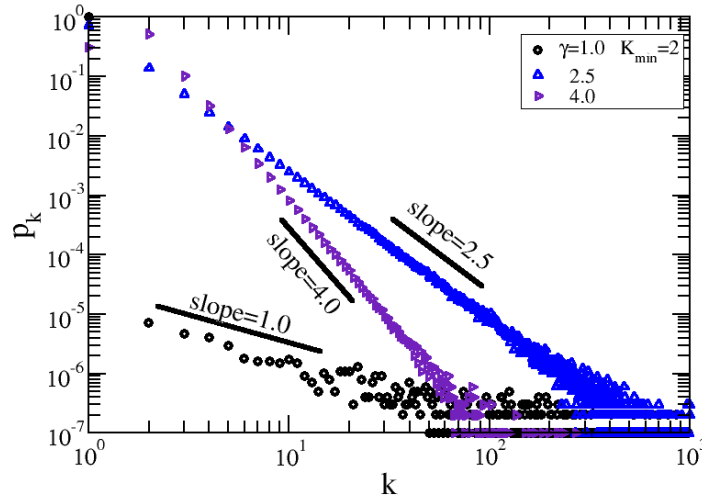


**Figure 2.6** - Degree distribution for Scale-Free Polymer Networks with  $N = 100000$  and  $S = 100$  realizations of the algorithm.

We start the construction procedure by fixing these three parameters' values and determining all the probabilities  $p_k$ , according to Eq. (2.32). Fig. 2.6, demonstrates how we built the network used in thesis. We create the first node, 1, blue node, and we choose at random its number of links,  $k_1$ , by making use of the degree distribution (2.32). Thus, we add  $k_1$  new nodes, which are all directly connected to the first node, in this case with 3 nodes. Now, we have three black nodes, namely, 2, 3 and 4. In the second construction step, we choose randomly one of the black nodes and we give its degree accordingly to the degree distribution (2.32), in our case the chosen node is 2 and its degree is 4. In the next step, we add  $k_2 - 1$  links, because the node 2 already has a direct connection with node 1, and  $k_2 - 1$  new nodes (5, 6 and 7). The numbering is according to the chronological order in which the nodes were created. This process is repeated until reaching the target number of nodes, denoted as  $N$ . Once the desired network size is achieved, growth is

halted, and any remaining black nodes are assigned a degree of one. This algorithm ensures that network construction does not stop on its own due to lack of available nodes. Additionally, every internal node in the network has a minimum of  $K_{min}$  and a maximum of  $K_{max}$  neighbors, while all peripheral nodes remain, with a degree of one. In chapter 3, we apply this algorithm that construct treelike Generalized Scale-Free Networks (GSFNs) in the context of polymer network relaxation dynamics [34, 38, 65].

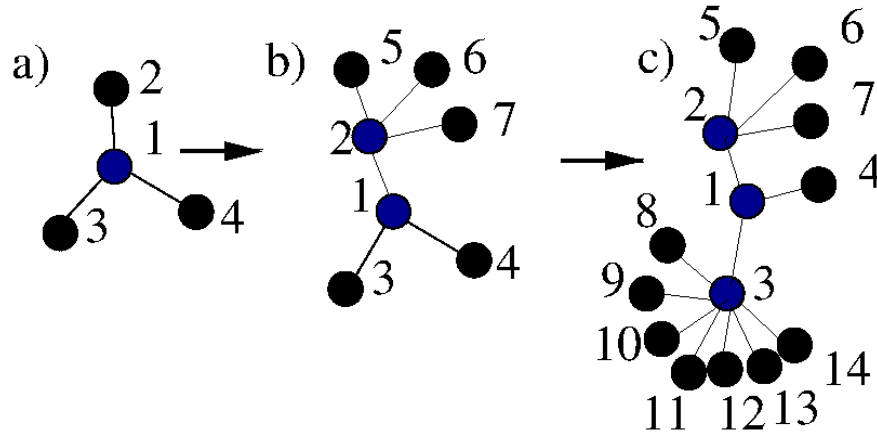


**Figure 2.7** - Construction procedure in detail.

In Fig. 2.8, by making use of the graphical software Gephi [66], we display several realizations of the algorithm for Generalized Scale-Free Networks (GSFNs) with  $N = 1000$  nodes and fixed  $\gamma = 2.5$  are formed by nodes with high degree Networks with smaller  $\gamma$ , *i.e.* GSFNs are mainly composed of coupled stars, while GSFNs with higher  $\gamma$  contain longer linear segments and fewer nodes with a high degree; for more details, see [39, 68]. Here, we can show how the two modularity parameters,  $K_{min}$  and  $K_{max}$ , influence the topology of the networks. In Fig. 2.8, we consider a network with the parameter  $K_{min}$  equal to 2 in the first row and 5 in the second row, while  $K_{max}$  is equal to 999 in the first column and 50 in the second column. We notice that the number of nodes with a high degree, which is higher than 5, grows when we increase only the value of  $K_{min}$ . The networks with  $K_{min} = 5$  become more clustered than the GSFNs with  $K_{min} = 2$ , and at the same time, these networks diminish the length of the linear segments. On the other hand, by decreasing the value of  $K_{max}$  and keeping  $K_{min}$  constant, compare, for instance, the panels from the first row of Fig. 2.8, we increase the linear paths and the emergence of nodes with high degree is less probable. In the limiting case  $K_{min} = K_{max}$ , one obtains networks formed by nodes with the same degree, similar to the dendrimers, but they do not inherit their perfect symmetry.

In Fig.2.9, as another application of the network theory, we have a schematic representation of a scale-free network, where Eq.(2.32) is obeyed, with a focus on the spreading of a disease, let's say, COVID-19. In this work, Galiceanu *et al.* consider an epidemiological model

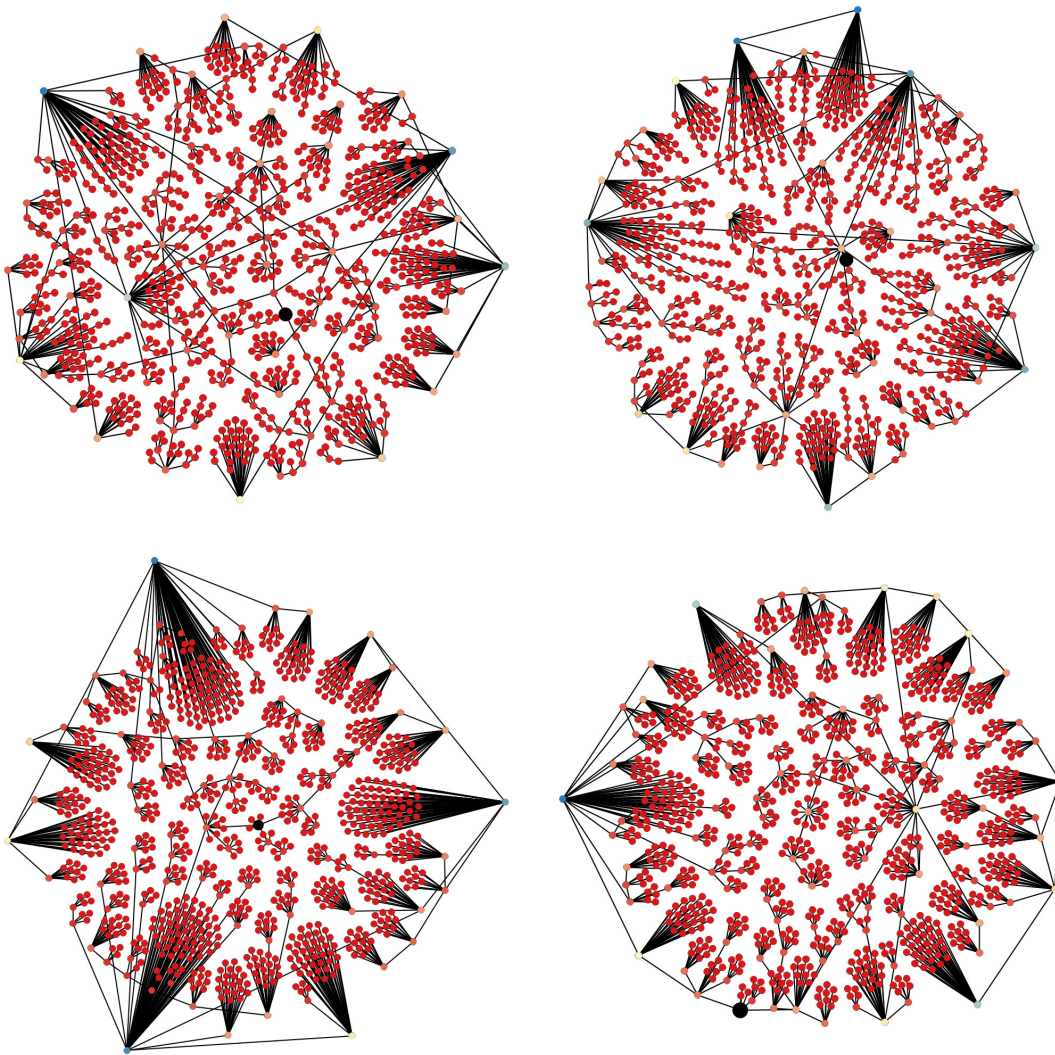


**Figure 2.8** - Realizations of GSFNs with  $N = 1000$ ,  $\gamma = 2.5$  and the parameters' set  $(K_{min}, K_{max})$ : (Top left) (2, 999), (Top right) (2, 50), (Down left) (5, 999), and (Down right) (5, 50). Source: [39]

based on a version of a  $A + B \rightarrow B$  chemical reaction model where the epidemiological model can be interpreted as a modified SIR model. The individuals can be Susceptible, Infected, or Removed and are acting on an irregular lattice, which in the case is of a scale-free network type.

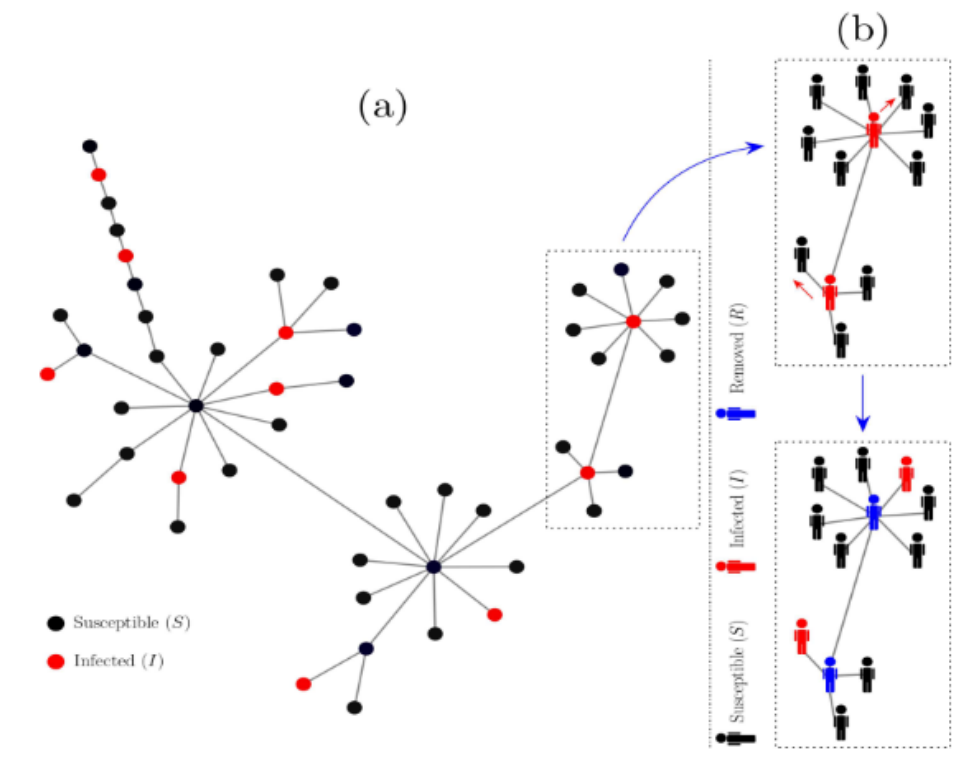


**Figure 2.9** - (a) Schematic representation of a scale-free network of size  $N = 50$ ,  $\gamma = 2.5$ ,  $K_{min} = 2$ , and  $K_{max} = 49$  and ten random walkers, shown by red color. (b) The visualization of the one step evolution of the infectious randomwalkers on the network. The black color represents susceptible individuals, red the infectious, and blue the individuals removed from the network. Source: [17]

---

# Theoretical Models

---

Rouse developed the first successful molecular model of polymer dynamics and is one of polymer physics's fundamental and classical paper. It has been the subject of intensive investigation, experimentally and theoretically, over many year [69–73]. The theoretical investigation of flexible polymers' conformational and dynamical properties often proceeds from a very simplified model, the Rouse model [31]. In this model the polymer is considered as being a sequence of beads connected via harmonic (entropic) springs (Gaussian chain); the chain incessantly changes its shape due to thermal agitation. Though this model disregards many features of a physical chain *e.g.*, the excluded volume effect, hydrodynamic interactions, and semiflexible effects it works in a series of cases *e.g.*, semidilute solution. It melts below the entanglement limit to a reasonable description of the physical situation [32,74]. The extension of Rouse's approach from linear chains to other polymer systems is relatively straightforward and eventually leads to the concept of generalized Gaussian structures (GGS). In the framework of the GGS approach, a polymer system is modeled as a collection of beads (subject to viscous friction) connected through elastic springs in a system-specific way [33]. On the other hand, the Rouse model describes very well polymer chain, where the excluded volume interaction and the hydrodynamic interaction are disregarded [74]. In this work, we consider the framework of GGS. Usually, in studies of polymer dynamics, semiflexibility is modeled by introducing angular constraints (of freely-rotating type) on the orientations of the bonds. The basic idea here is to take semiflexibility into account through restrictions on the orientations of neighboring bonds. Introducing semiflexibility into the GGS consists in the appearance of additional terms in the connectivity matrix Eq. (2.11) [75]. In this chapter, we will be to show the models in framework GGS but applied to a new type of hyperbranched polymers: the Generalized Scale-free Networks 2. I

## 3.1 Rouse Model

In the Rouse model, a polymer is represented through  $N$  connected beads with position vector  $(\mathbf{R}_1, \dots, \mathbf{R}_N)$ , where the distances between any two directly connected beads, say  $i$  and  $j$ , are assumed to obey Gaussian statistics, see Fig 3.1. In this way one is led for  $\mathbf{R}_i$  to the following probability distribution:

$$P(\mathbf{R}_i) = \left(\frac{3}{2\pi l^2}\right)^{3M/2} \exp\left(-\frac{3}{2l^2} \sum_{(i,j)} (\mathbf{R}_i - \mathbf{R}_j)^2\right). \quad (3.1)$$

Here the sum goes over all  $M$  directly connected  $(i, j)$  -pairs of beads and  $l^2$  is the mean-

square distance between them. Eq. (3.1) can be envisaged as being a Boltzmann distribution,  $\exp(U(R)/k_B T)$ , where  $k_B$  is the Boltzmann constant and  $U_{elastic}(R)$  is the potential energy.

The potential energy ( $U_{elastic}(R)$ ) contains only harmonics terms between monomers directly bound each other:

$$U_{elastic}(\mathbf{R}) = \frac{\kappa}{2} \sum_{bond} (\mathbf{R}_i - \mathbf{R}_j)^2 = \frac{\kappa}{2} \sum_{i=1}^N \sum_{j=1}^N A_{ij} \mathbf{R}_i \mathbf{R}_j, \quad (3.2)$$

where  $\mathbf{R}_i(t) = (X_i(t), Y_i(t), Z_i(t))$  and  $\mathbf{R}_j(t) = (X_j(t), Y_j(t), Z_j(t))$  are the position vectors of the  $i$ th and  $j$ th GGS beads, respectively. The summation in the first sum of Eq. (3.3) goes over all pairs of beads ( $i, j$ ) directly connected by elastic springs (bonds). The quantity  $K = 3k_B T/l^2$  is the elastic constant of a harmonic spring, where  $k_B$  is the Boltzmann constant,  $T$  is the temperature, and  $l^2$  is the mean square end-to-end distance for the unstretched spring. The symmetric  $N \times N$  matrix  $\mathbf{A} = (A_{ij})$ , which is the Connectivity Matrix Eq.(2.11), reflects the topology of the particular structure [33, 76]: the nondiagonal elements  $A_{ij}$  equal 1 if the  $i$ th and  $j$ th beads are directly connected and 0 otherwise and the diagonal elements  $A_{ii}$  equal the number of connections of the  $i$ th bead. By construction, the  $\det \mathbf{A} = 0$ ; therefore, at least one of its eigenvalues vanishes.

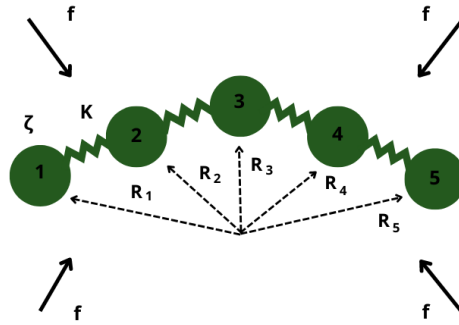


Figure 3.1 - Rouse Model.

The dynamics of the whole network is described by the set of  $N$  linearly independent Langevin equations [74], which have the forces determined from the potential  $U(R_i)$  through  $\frac{\partial U(\mathbf{R}_k)}{\partial \mathbf{R}_i}$ . Thus, for a bead  $i$  has the form [32–34, 68, 76, 77]:

$$\frac{\partial \mathbf{R}_i(t)}{\partial t} + \sigma \sum_{j=1}^N A_{ij} \mathbf{R}_j(t) = \mathbf{w}_i(t) + \frac{\mathbf{F}_i}{\zeta}, \quad (3.3)$$

where  $\zeta = 6\pi\rho a$  is the friction constant of the beads, usually formulated in terms of an effective radius  $a$  and viscosity of the solvent  $\rho$  and  $\sigma = K/\zeta$  is the bond rate constant. Furthermore,  $\mathbf{w}_i$  and  $\mathbf{F}_i$  are the external forces acting on the  $i$ th bead, which in our models we will consider to vanish.

However,  $\mathbf{w}_i$  represents the stochastic force that acts on the  $i$ th bead. Due to the fluctuation-dissipation theorem, this force is connected with the dissipative force (or friction) [33, 68] and is assumed to be Gaussian with zero mean value, so that one has

$$\langle w_i(t) \rangle = 0, \quad (3.4)$$

$$\langle w_{i\alpha}(t)w_{j\beta}(t') \rangle = 2\zeta\kappa_B T \delta_{ij}\delta_{\alpha\beta}\delta(t-t'), \quad (3.5)$$

where  $\alpha$  and  $\beta$  denote the directions  $(x, y, z)$ ,  $\delta_{ij}$  and  $\delta_{\alpha\beta}$  are the Kronecker delta.

The solution of Eq. (3.3) can be written as

$$\mathbf{R}(t) = \int_{-\infty}^t dt' \exp[-\sigma(t-t')\mathbf{A}][w(t') + \frac{\mathbf{F}(t')}{\zeta}]. \quad (3.6)$$

The connectivity matrix  $\mathbf{A}$  can be diagonalized, for determining  $\mathbf{R}(t)$  from Eq. (3.6). Given the eigenvectors  $\mathbf{Q}_i$  of  $\mathbf{A}$ , that  $\mathbf{A}\mathbf{Q}_i = \lambda_i\mathbf{Q}_i$ , so we define  $\mathbf{Q} \equiv (\mathbf{Q}_1, \mathbf{Q}_2, \dots, \mathbf{Q}_N)$ . We use the matrix  $\mathbf{Q}$  to diagonalize  $\mathbf{A}$ , since

$$\mathbf{A} = \mathbf{Q}\mathbf{\Lambda}\mathbf{Q}^{-1}, \quad (3.7)$$

where  $\mathbf{Q}^{-1}$  is the inverse of  $\mathbf{Q}$ . So, this relation follows from  $\mathbf{A}\mathbf{Q} = \mathbf{\Lambda}\mathbf{Q}$ , being  $\mathbf{\Lambda}$  the diagonal matrix whose elements are  $\lambda_i$  of  $\mathbf{A}$ .

Knowing that any function of  $\mathbf{A}$  can be written

$$f(\mathbf{A}) = \mathbf{Q}f(\mathbf{\Lambda})\mathbf{Q}^{-1}, \quad (3.8)$$

especially one has

$$\exp(\mathbf{A}t) = \mathbf{Q}\exp(\mathbf{\Lambda}t)\mathbf{Q}^{-1}. \quad (3.9)$$

Thus Eq. (3.6) can be written in terms of these eigenvalues and eigenvectors

$$\mathbf{R}(t) = \int_{-\infty}^t dt' \mathbf{Q} \exp[-\sigma(t-t')\mathbf{\Lambda}]\mathbf{Q}^{-1}[\mathbf{w}(t') + \frac{\mathbf{F}(t')}{\zeta}]. \quad (3.10)$$

The mean displacement  $\langle \mathbf{R}(t) \rangle$  can be obtained by averaging Eq. (3.10). For this, we use the relations (3.4) and (3.5). Thus, Eq. (3.10) simplifies to:

$$\langle \mathbf{R}(t) \rangle = \int_{-\infty}^t dt' \mathbf{Q} \exp[-\sigma(t-t')\mathbf{\Lambda}] \mathbf{Q}^{-1} \frac{\mathbf{F}(t')}{\zeta}. \quad (3.11)$$

The Eq. (3.11) represents the average displacement under the action of the external forces. Assume that the external force pulls the  $m$ th bead then stay constant. We also let the force be switched on at  $t = 0$  and then stay constant. Choosing the  $y$ -coordinate in the direction of the force we have

$$\mathbf{F}_m(t) \equiv F_0 \Gamma(t) \mathbf{e}_y. \quad (3.12)$$

and  $\mathbf{F}_j(t) = 0$  for  $j \neq m$ . In Eq. (3.12) is the Heaviside step function.

We now turn to the determination of the mean displacement of the  $m$ th bead under a constant step force acting on it. From Eq. (3.11) the motion of this bead in  $y$ -direction is:

$$\langle Y_m(t) \rangle = \frac{F_0}{\zeta} \sum_{m=1}^N \int_0^t dt' Q_{m,i} \exp[-\sigma(t-t')\lambda_i] Q_{i,m}^{-1} = \quad (3.13)$$

$$= \frac{F_0 t}{N\zeta} + \frac{F_0}{\sigma\zeta} \sum_{i=2}^N \int_0^t dt' Q_{m,i} \frac{1 - \exp(-\sigma\lambda_i t)}{\lambda_i} Q_{i,m}^{-1}, \quad (3.14)$$

where we set  $(\mathbf{Q}^{-1})_{i,m} \equiv Q_{i,m}^{-1}$ .

A particular situation arises when the external force acts on a charged monomer contained in a GGS. When the position of the charge inside the structure is random (quenched disorder), the ensemble-averaged monomer displacement can be calculated from Eq.(3.11), by averaging over all monomer positions, which is a double average, both over the fluctuations of the random forces and over the positions of the charges. Nonetheless, the ensuing expression turns out to be simpler than Eq.(3.11), since for its determination only the eigenvalues of  $\mathbf{A}$ , but not its eigenvectors are required [32, 68, 77, 78]. To show this, one remarks that when monitoring the bead on which the external force acts, one has from Eq.(3.11) and Eq.(3.13)

$$\langle \langle Y(t) \rangle \rangle = \frac{1}{N} \sum_{i=2}^N \langle \langle Y_m(t) \rangle \rangle = \quad (3.15)$$

$$= \frac{F_0}{N\zeta} \int_0^t dt' \mathbf{Tr}(\mathbf{Q} \exp[-\sigma(t-t')\mathbf{\Lambda}] \mathbf{Q}^{-1}) \quad (3.16)$$

$$= \frac{F_0}{N\zeta} \int_0^t dt' \mathbf{Tr}(\exp[-\sigma(t-t')\mathbf{\Lambda}]) \quad (3.17)$$

$$= \frac{F_0}{N\zeta} \int_0^t dt' \sum_{i=2}^N (\exp[-\sigma\lambda_i(t-t')]). \quad (3.18)$$

This equation can be readily integrated; noting that only  $\lambda_1$  vanishes,  $\lambda_1 = 0$ , one has:

$$\langle\langle Y(t) \rangle\rangle = \frac{F_0 t}{N\zeta} + \frac{F_0}{\sigma N\zeta} \sum_{i=2}^N \frac{1 - \exp(-\sigma\lambda_i t)}{\lambda_i}. \quad (3.19)$$

In this model, the average displacement depends only on the eigenvalues  $\lambda_n$  of the connectivity matrix  $\mathbf{A}$ , but not on its eigenvectors.

### 3.1.1 Viscoelastic Relaxation Moduli

The dynamics of polymers in solution can be studied by measuring their viscoelastic properties. In this work, we won't study the interaction with solution. Newton's law of viscosity defines viscosity  $\eta$  by stating that stress  $\sigma$  is proportional to the velocity gradient in the liquid [79]

$$\sigma = \eta \frac{\partial v}{\partial y}, \quad (3.20)$$

where  $v$  is the velocity and  $y$  is the direction of the velocity gradient. For a velocity gradient in the  $xy$  plane

$$\sigma_{xy} = \eta \left( \frac{\partial v_x}{\partial y} + \frac{\partial v_y}{\partial x} \right), \quad (3.21)$$

The terms  $\partial v_x/\partial y$  and  $\partial v_y/\partial x$  are the velocity gradients in the  $y$  and  $x$  directions.

Since  $v_x = \partial u/\partial t$  and  $v_y = \partial w/\partial t$ , where  $u$  and  $w$  are the displacements in the  $x$  and  $y$  directions, respectively, we have

$$\sigma_{xy} = \eta \left[ \frac{\partial}{\partial y} \left( \frac{\partial u}{\partial t} \right) + \frac{\partial}{\partial x} \left( \frac{\partial w}{\partial t} \right) \right] \quad (3.22)$$

$$= \eta \frac{\partial}{\partial t} \left( \frac{\partial u}{\partial y} + \frac{\partial w}{\partial x} \right) \quad (3.23)$$

$$= \eta \frac{\partial e_{xy}}{\partial t}. \quad (3.24)$$

It can be seen that the shear stress  $\sigma_{xy}$  is directly proportional to the rate of change of shear strain with time.

If the shear rate  $\kappa(t) = \partial e_{xy}/\partial t$  is small enough, the shear stress depends linearly on  $\kappa(t)$  and can be written as [74, 80]

$$\sigma_{xy}(t) = \int_{-\infty}^t dt' G(t-t') \kappa(t'), \quad (3.25)$$

where  $G(t)$  is called the shear relaxation modulus. For dilute solutions, in which the effect of the polymer is small, it is convenient to write Eq. (3.25) as

$$\sigma_{xy}(t) = \eta_s \kappa(t) + \int_{-\infty}^t dt' G^p(t-t') \kappa(t') \quad (3.26)$$

The first term represents the property of the pure solvent and the second term represents the effect of the polymers ( $G^p$ ).

We have one case very important case where there is an oscillatory flow:

$$\kappa(t) = \kappa_0 \cos(\omega t) = \kappa_0 \operatorname{Re}(\exp^{i\omega t}), \quad (3.27)$$

where  $\operatorname{Re}$  stands for the real part. The response for this flow defines the complex modulus  $G^*(\omega)$ :

$$\sigma_{xy}(t) = \kappa_0 \operatorname{Re}\left(\frac{G^*(\omega)}{i\omega} \exp^{i\omega t}\right). \quad (3.28)$$

Since Eq. (3.26) gives

$$\sigma_{xy}(t) = \kappa_0 \operatorname{Re}\left(\exp^{i\omega t} \eta_s + \int_{-\infty}^t dt' G^p(t-t') \exp^{i\omega t'}\right) \quad (3.29)$$

$$= \kappa_0 \operatorname{Re}\left[\exp^{i\omega t} \left(\eta_s + \int_{-\infty}^t dt' G^p(t') \exp^{-i\omega t'}\right)\right]. \quad (3.30)$$

$G^*(\omega)$  is written as [31, 33, 74, 79]

$$G^*(\omega) = i\omega \eta_s + i\omega \int_0^\infty dt \exp^{-i\omega t} G^p(t) \quad (3.31)$$

$$= G'(\omega) + iG''(\omega). \quad (3.32)$$

The real component of  $G^*(\omega)$ ,  $G'(\omega)$ , is called *the dynamic storage modulus* and the imaginary part,  $G''(\omega)$ , is called *the dynamic loss modulus*. For GGS according to [74] in Eqs. (4.159) and (4.160),

$$G'(\omega) = \int_0^\infty dt \omega \sin(\omega t) \sum_i \exp(-t/\tau_i) = \sum_{i=2}^\infty \frac{(\omega\tau_i)^2}{1 + (\omega\tau_i)^2} \quad (3.33)$$

and

$$G''(\omega) = \int_0^\infty dt \omega \cos(\omega t) \sum_i \exp(-t/\tau_i) = \sum_{i=2}^\infty \frac{\omega\tau_i}{1 + (\omega\tau_i)^2}, \quad (3.34)$$

the reduced storage  $G'(\omega)$  and loss  $G''(\omega)$ , moduli read [33]:

$$G'(\omega) = \nu k_B T \frac{1}{N} \sum_{n=2}^N \frac{\omega^2}{\omega^2 + (2\sigma\lambda_n)^2} \quad (3.35)$$

and

$$G''(\omega) = \nu k_B T \frac{1}{N} \sum_{n=2}^N \frac{2\sigma\omega\lambda_n}{\omega^2 + (2\sigma\lambda_n)^2}. \quad (3.36)$$

where  $\nu$  is the number of polymer segments (beads) per unit volume and  $\sigma = K/\zeta$ . We can see that the Eqs. (3.35) and (3.36) depend only on the eigenvalues ( $\lambda_i$ ) of the connectivity matrix  $\mathbf{A}$ . In these equations the  $\lambda_1 = 0$  mode corresponds to the translation of the whole structure and may influence  $G''(\omega)$  only in the very close vicinity of  $\omega = 0$ . Note that the factor 2 in the relaxation times  $\tau_i = \tau_0/2\lambda_i$  arises from the second moment of the displacement involved in computing the stress required in the evaluation of the  $G^*(\omega)$  [74, 95].

From Eqs. (3.35) and (3.36) the limiting connectivity-independent behaviors, very high  $\omega$  are clearly evident. For small frequencies, the reduced storage and loss moduli can be written as

$$\lim_{\omega \rightarrow 0} [G'(\omega)] = \nu k_B T \frac{1}{N} \lim_{\omega \rightarrow 0} \left( \sum_{n=2}^N \frac{\omega^2}{\omega^2 + (2\sigma\lambda_n)^2} \right) \simeq \sum_{i=2}^N \frac{\omega^2}{(2\lambda_n)^2} \sim (\omega)^2 \quad (3.37)$$

and

$$\lim_{\omega \rightarrow 0} [G''(\omega)] = \nu k_B T \frac{1}{N} \lim_{\omega \rightarrow 0} \left( \sum_{n=2}^N \frac{2\sigma\omega\lambda_n}{\omega^2 + (2\sigma\lambda_n)^2} \right) \simeq \sum_{n=2}^N \frac{\omega}{2\lambda_n} \sim \omega. \quad (3.38)$$

In the high frequency region, the storage and loss moduli depend on  $\omega$  as

$$\lim_{\omega \rightarrow \infty} [G'(\omega)] = \nu k_B T \frac{1}{N} \lim_{\omega \rightarrow \infty} \left( \sum_{n=2}^N \frac{\omega^2}{\omega^2 + (2\sigma\lambda_n)^2} \right) \simeq \sum_{i=2}^N \frac{\omega^2}{\omega^2} \sim \omega^0 \quad (3.39)$$

and

$$\lim_{\omega \rightarrow \infty} [G''(\omega)] = \nu k_B T \frac{1}{N} \lim_{\omega \rightarrow \infty} \left( \sum_{n=2}^N \frac{2\sigma\omega\lambda_n}{\omega^2 + (2\sigma\lambda_n)^2} \right) \simeq \sum_{n=2}^N \frac{2\lambda_n}{\omega} \sim \omega^{-1}. \quad (3.40)$$

## 3.2 Semiflexible Model

In this section, we summarize the concepts and the main equations of the Semiflexible Treelike Polymers (STPs) model, focusing on the relaxation dynamics of polymers. Here, semiflexibility is introduced by restricting the orientations of the bonds, and it is modeled through the interactions between the next-nearest neighboring beads. The polymer network comprises  $N$  beads, described by a set of position vectors  $\mathbf{R}_i$  ( $i = 1, 2, \dots, N$ ). The neighboring beads are connected by elastic springs,  $\mathbf{d}_a = \mathbf{R}_i - \mathbf{R}_j$ , and these springs possess the same elasticity constant  $K$  and obey Gaussian statistics. The dynamics of the polymer network are described by a set of linear Langevin equations, which for the  $Y$ -component of bead  $i$  can be written as [33, 34, 82, 83]:

$$\zeta \frac{\partial Y_i(t)}{\partial t} + \frac{\partial V_{STP}(\{\mathbf{R}_k\})}{\partial Y_i} = \tilde{f}_i(t), \quad (3.41)$$

where  $\tilde{f}_i$  corresponds to the  $Y$  component of the stochastic Gaussian force acting on the  $i$ th bead, with their moments given by  $\langle \tilde{f}(t) \rangle = 0$  and  $\langle \tilde{f}_i(t) \tilde{f}_j(t') \rangle = 2k_B T \zeta \delta_{ij} \delta(t-t')$  ( $k_B$  is the Boltzmann constant,  $T$  is the temperature and  $\zeta$  denotes the friction coefficient).

The potential  $V_{STP}(\{\mathbf{R}_k\})$  accounts for the connections between beads and in this model it includes also the semiflexibility effects. Considering that the bonds are Gaussian-distributed and correlated [86] and by making use of some traditional typical conditions, explained in details in Refs. [35, 36, 38, 84–86, 88–90] we express the potential as:

$$V_{STP}(\mathbf{d}_a) = \frac{K}{2} \sum_{a,b} \mathbf{W}_{ab}^{STP} \mathbf{d}_a \cdot \mathbf{d}_b. \quad (3.42)$$

The general form of the potential  $V_{STP}$  allows to impose restrictions on the angles between the bonds of the GGS through the matrix  $\mathbf{W} \equiv (W_{ab})$  [36]. The elements of the matrix  $\mathbf{W}$  are determined through the bond–bond correlations and having the  $\mathbf{d}_a$  Gaussian,

$$\langle \mathbf{d}_a \cdot \mathbf{d}_b \rangle = l^2 (\mathbf{W}^{-1})_{ab}. \quad (3.43)$$

Hence the knowledge of all  $\langle \mathbf{d}_a \cdot \mathbf{d}_b \rangle$  is sufficient in order to determine  $\mathbf{W}$  through a matrix inversion. Following the traditional choice [35, 36, 38, 84–86],

$$\langle \mathbf{d}_a \cdot \mathbf{d}_b \rangle = l^2, \quad (3.44)$$

and for adjacent bonds  $a$  and  $b$  (connected, say, by the  $i$ th bead),

$$\langle \mathbf{d}_a \cdot \mathbf{d}_b \rangle = \pm l^2 q_i, \quad (3.45)$$

where  $q_i$  reflects the stiffness of junction  $i$ .

We envisage the bonds to be directed, so that the plus sign holds for a head to tail arrangement and the minus sign in the other cases. For nonadjacent bonds  $a$  and  $c$  we consider, in the spirit of the freely rotating chain model [91],

$$\langle \mathbf{d}_a \cdot \mathbf{d}_c \rangle = \langle \mathbf{d}_a \cdot \mathbf{d}_{b_1} \rangle \langle \mathbf{d}_{b_1} \cdot \mathbf{d}_{b_2} \rangle \dots \langle \mathbf{d}_{b_k} \cdot \mathbf{d}_c \rangle l^{-2k}, \quad (3.46)$$

where  $(b_1, b_2, \dots, b_k)$  denotes the shortest path that connects  $a$  with  $c$ .

In Eq. (3.45), the stiffness parameter  $q_i$  is associated with the bead  $i$ ; by this, we assume equal average values for all bond pairs connected by this bead. In the limit  $q_i \rightarrow 0$  for all  $i$ , all averages involving different bonds vanish, and the potential Eq. (3.42) takes the simple diagonal form which corresponds to a flexible polymer Eq.(3.3). In the opposite limit, an upper bound for  $q_i$  follows from the fact that the sum of the cosines of the angles between all pairs of bonds adjacent to monomers of functionality  $f_i$  is bounded by  $\sum_{a<b} \cos \theta_{ab} \geq -f_i/2$ . Thus if all the averages of Eq. (3.46) are equal, one obtains  $q_i \leq 1/(f_i - 1)$ . For all  $\cos \theta_{ab} = \theta$  (without averaging), i.e.

$\cos \theta = 1/(f_i - 1)$ , is realizable in three dimensions only for functionalities  $f_i \leq 4$ . For higher functionalities, this limit is attainable only on average, i.e., for  $\langle \mathbf{d}_a \cdot \mathbf{d}_b \rangle$  [35, 36, 86, 91].

The matrix  $\mathbf{W}$  defines the potential energy in the bond representation. The set of Langevin equations, Eq.(3.41), requires that the potential  $V_{STP}$  be written in position variables. The transformation from bonds' to positions' variables,  $\mathbf{d}_a = \mathbf{R}_i - \mathbf{R}_j$ , can be written in terms of the incidence matrix  $\mathbf{G}$  [92] as

$$\mathbf{d}_a = \sum_k (\mathbf{G}^T)_{ak} \mathbf{R}_k. \quad (3.47)$$

In the last equation  $\mathbf{G}^T$  is the transpose of the incidence matrix  $G$ , whose elements are  $G_{ja} = 1$  and  $G_{ia} = 1$ , when the bond  $a$  connects the beads  $i$  and  $j$ , and zero otherwise. By replacing Eq. (3.47) into Eq. (3.42) we encounter the potential in position variables:

$$V_{STP}(\{\mathbf{R}_i\}) = \frac{K}{2} \sum_{m,n} A_{mn}^{STP} \mathbf{R}_m \cdot \mathbf{R}_n. \quad (3.48)$$

Here,  $\mathbf{A}^{STP}$  is the so-called dynamical matrix and it is given by  $\mathbf{A}^{STP} = \mathbf{G}\mathbf{W}\mathbf{G}^T$ , where the matrix  $\mathbf{G}$  is the incidence matrix [86]. The elements of the dynamical matrix  $\mathbf{A}^{STP} = (A_{ij}^{STP})$  are known in the closed form [35, 86] and depend on the functionalities and stiffness parameters, see Eqs. (3)-(5) from Ref. [86]. However, these equations are simplified by considering a homogeneous situation, for which an inner node  $i$  with functionality  $f_i$  ( $f_i > 1$ ) has the stiffness parameter  $q_i = \frac{q}{f_i - 1}$ . Thus, the parameter  $q$  will be the only parameter responsible for the stiffness. This real number allows us to monitor the transition between a pure flexible polymer ( $q = 0$ ) and a completely rigid polymer ( $q = 1$ ).

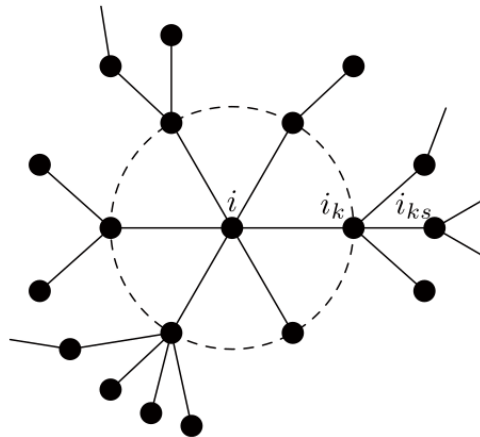


**Figure 3.2** - Schematic drawing of the nearest and next-nearest neighbors of a bead  $i$  in a treelike network. Source: [86]

The non-vanishing elements of matrix  $\mathbf{A}^{STP}$  can be written as a function of the stiffness parameter  $q$  and they can be classified into three distinct groups [86]. Here it is worthwhile to

introduce a notation to present the situation of the bead sites, see Fig. 3.2. The first group contains the diagonal elements and are equal to

$$A_{ii}^{STP} = 1 + \frac{q^2}{(f_{i_k} - 1 + q)(1 - q)} \quad (3.49)$$

if  $i$  is a peripheral node,  $f_i = 1$ , and

$$A_{ii}^{STP} = \frac{f_i}{1 - q} + \sum_{i_k \in \Delta_i} \frac{q^2}{(f_{i_k} - 1 + q)(1 - q)} \quad (3.50)$$

if the node  $i$  has functionality  $f_i > 1$ . In the last equation the set  $\Delta_i$  contains only the neighbors  $i_k$  of node  $i$ .

In the second group we have the non-diagonal nearest-neighboring elements of matrix  $\mathbf{A}^{STP}$ . These elements are given by

$$A_{ii_k}^{STP} = -\frac{1}{1 - q} \quad (3.51)$$

if either  $i$  or  $i_k$  is a peripheral bead and

$$A_{ii_k}^{STP} = -\frac{1 + q}{1 - q}. \quad (3.52)$$

if both  $i$  and  $i_k$  beads have functionalities larger than 1.

The last group is formed by the non-diagonal next nearest-neighboring elements. These elements depend only on the functionality of bead  $i_k$ , which is the nearest neighbor of both beads  $i$  and  $i_{ks}$  and are expressed as:

$$A_{ii_{ks}}^{STP} = \frac{q}{(f_{i_k} - 1 + q)(1 - q)}. \quad (3.53)$$

The solution of Eq. (3.41), which is found by deploying a normal mode analysis, can be averaged both over the fluctuating forces and over all the bead positions. Thus, the average monomer displacement along the  $Y$ -axis is an expression that depends only on the eigenvalues of  $\mathbf{A}^{STP}$  [38, 82, 93] and is calculated substituting in Eq. (3.19). Here, we are mainly interested in the slope of  $\langle\langle Y \rangle\rangle$  and we consider for simplicity that  $\frac{2l^2 K}{\zeta} = 1$  and  $2l^2 = 1$ . In same form, the storage  $G'(\omega)$ , Eq. (3.35), and loss  $G''(\omega)$ , Eq. (3.36), moduli in the Rouse-type formalism depend now only on the eigenvalues of  $\mathbf{A}^{STP}$ . In these equations the vanishing eigenvalue ( $\lambda_1 = 0$ ), which corresponds to the translation of the system as a whole, is not considered.

### 3.3 Copolymer Model

The polymers are subunits of two different ( $A$ - and  $B$ -) types, modeled as beads. The type of every bead is chosen randomly and will be kept unaltered during the calculations. All  $N$  beads of the polymer network are connected to their neighbors by Gaussian elastic springs (*i.e.* obeying Gaussian statistics) with the same elasticity constant  $K$ . The dynamical properties of the two kinds of monomers ( $A$ - and  $B$ -) differ; thus, we focus on the situation that the friction

constants  $\zeta_A$  and  $\zeta_B$  are different [44, 94].

Our growth procedure of the generalized scale-free copolymer network is given by the construction steps seen in chapter 2 with the additional step that every node of the network is randomly chosen to be of  $A$ - or  $B$ -type of monomer. The type is chosen by maintaining constant the ratio between the number of monomers of type  $A$  and  $B$ :  $\eta = \frac{N_A}{N_B}$ . In Fig. 3.3 we exemplify the above steps for small networks. The filled circles are the nodes that received the degree from the distribution (2.32), while the other nodes are shown by open circles. In panel (e) we depict the scale-free network of panel (c) as a copolymer network, in which the type of all monomers was chosen by maintaining constant the ratio between the number of monomers of type  $A$  and  $B$ . In this last panel we displayed a network with  $\eta = 0.5$  with the monomers' type being picked at random.

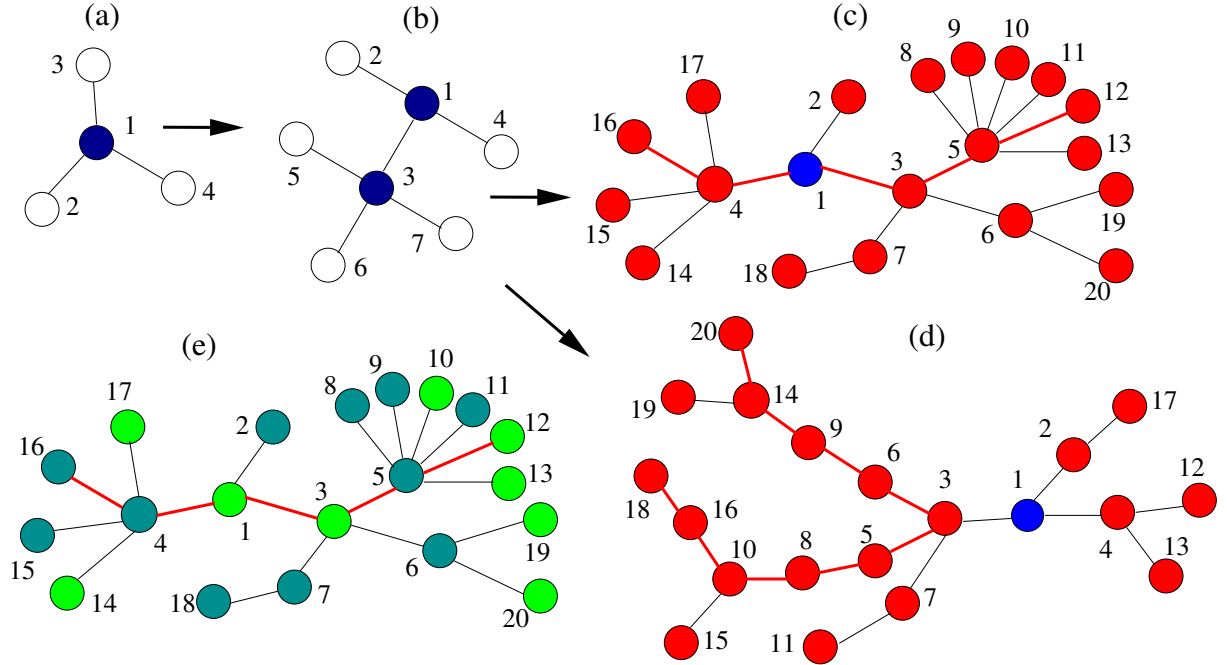


**Figure 3.3** - Construction procedure of a GSFN: (a) and (b) Construction procedure in detail for realization of the GSFN construction procedure with  $N = 20$  and the parameters' set  $(\gamma, K_{min}, K_{max})$  equal to: (c) (1.0, 2, 19) and (d) (4.0, 2, 19). (e) Copolymer GSFN obtained from network (c) by choosing at random the  $A$ -type (green) and  $B$ -type (gray) monomers.

The configuration of any GGS with  $N$  beads is given by a set of position vectors  $\mathbf{R}_i$  ( $i = 1, 2, \dots, N$ ), where  $\mathbf{R}_i(t) = (X_i(t), Y_i(t), Z_i(t))$  is the three-dimensional position vector of the  $i$ th bead at time  $t$ . The dynamics of the network are described by a set of  $N$  linearly independent Langevin equations, which for an arbitrary bead  $i$  can be written as [32, 68, 74, 82, 96]

$$\zeta_i \frac{d\mathbf{R}_i(t)}{dt} + K \sum_{j=1}^N A_{ij} \mathbf{R}_j(t) = \mathbf{f}_i(t), \quad (3.54)$$

where  $\zeta_i$  is the friction constant of bead  $i$ ,  $\mathbf{f}_i$  represents the stochastic force acting on  $i$ th bead, and  $\mathbf{A} = (A_{ij})$  is the connectivity matrix (or Laplace-matrix). This  $N \times N$  real symmetric matrix

has its non-diagonal elements  $A_{ij}$  equal to  $-1$  if the beads  $i$ th and  $j$ th are directly connected and  $0$  otherwise; while its diagonal elements  $A_{ii}$  equal the number of connections of bead  $i$ . It is important to mention that the sets  $\zeta_i$  and  $\mathbf{f}_i$  are correlated through the fluctuation-dissipation theorem [74]. However, we do not enter into details because we will be interested only in the eigenvalues of the system, which depends on  $\mathbf{A}$ . In the GGS framework the right-hand-side term vanishes after a thermally averaging  $\mathbf{R}_i$  [44, 45], thus we have to focus only on the homogeneous equation of the differential equation (3.54).

We consider beads of type  $A$  as the reference and we introduce the characteristic relaxation time of the network  $\tau_0 \equiv \zeta_A/K$ . Implementing these assumptions the homogeneous part of Eq. (3.54) reads as [44, 45, 94]

$$\frac{d\mathbf{R}_i(t)}{dt} + (1/\tau_0) \sum_{j=1}^N \tilde{A}_{ij} \mathbf{R}_j(t) = 0, \quad (3.55)$$

where the elements of the matrix  $\tilde{\mathbf{A}}$  are given by

$$\tilde{A}_{ij} = \sigma_i A_{ij} \quad (3.56)$$

with

$$\sigma_i = \frac{\zeta_A}{\zeta_i}. \quad (3.57)$$

The new matrix  $\tilde{\mathbf{A}}$  is obtained from the connectivity matrix  $\mathbf{A}$  by multiplying its rows with  $\sigma_i$ . In general, this matrix is not symmetric, but it was shown [44] that all its eigenvalues are real and nonnegative. Here, we consider two types of beads  $A-$  and  $B-$ , thus from Eq. (3.57) one can clearly see that  $\sigma_i$  takes two values:  $\zeta_A/\zeta_A = 1$  and  $\zeta_A/\zeta_B = \sigma$ .

From the wealth of physical quantities dependent on the relaxation times  $\tau_i$  of the networks, which are related to the eigenvalues  $\tilde{\lambda}_i = 1/\tau_i$  of Eq. (3.55), we choose the complex dynamic modulus  $G^*(\omega)$ . In typical mechanical experiments the real and the imaginary components of this modulus, namely the storage  $G'(\omega)$  and the loss  $G''(\omega)$  moduli, are determined by applying an external harmonic strain to the polymer network. The storage and loss moduli in the GGS framework depend only on the eigenvalues of the matrix  $\tilde{\mathbf{A}}$ . In Eqs. (3.58) and (3.59)  $\nu$  is the number of polymer segments (beads) per unit volume,  $K_B$  is the Boltzmann constant and  $T$  is the temperature. In these equations the vanishing eigenvalue  $\lambda_1 = 0$  is not considered, while the factor 2 in the relaxations times  $\tau_i = \tau_0/2\lambda_i$  arises from the second moment of the displacements involved in calculating the stress [74]. Our main interest are the slopes and not the prefactors, thus in Eqs. (3.58) and (3.59) we will consider only the reduced storage and loss moduli, obtained by setting  $\nu K_B T = 1$  and  $\tau_0 = 1$ .

$$G'(\omega) = \nu K_B T \frac{1}{N} \sum_{i=2}^N \frac{\omega^2}{\omega^2 + \left(\frac{2\tilde{\lambda}_i}{\tau_0}\right)^2}, \quad (3.58)$$

and

$$G''(\omega) = \nu K_B T \frac{1}{N} \sum_{i=2}^N \frac{\omega \left( \frac{2\tilde{\lambda}_i}{\tau_0} \right)}{\omega^2 + \left( \frac{2\tilde{\lambda}_i}{\tau_0} \right)^2}. \quad (3.59)$$

# Results

In this chapter, we focus on the relaxation dynamics of Generalized Scale-free Polymer Networks (GSFNs) applied to the Rouse, Semiflexible, and Copolymer Model using the algorithm described in chapter 2. In all models, we fix the number of the monomers  $N$  and the number of realizations of the construction algorithm  $S$ , and we change the parameters  $\gamma$ ,  $K_{min}$  and  $K_{max}$  of the Eq. (2.32). After this, we built the connectivity matrix for each model. In the Rouse Model, the dynamical matrix  $\mathbf{A}$  is its Laplacian matrix (connectivity matrix) seen Eq. (2.11). However, in the semiflexible model, we need to add the stiffness parameter  $q$  and, as a consequence, the dynamical matrix is  $\mathbf{A}^{STP}$  with the elements are seen in section 3.2. In the Copolymer model, we increase the parameters  $\sigma$  and  $\eta$ , and the dynamical matrix  $\tilde{A}$  is represented by Eq.(3.56).

## 4.1 Eigenvalue spectra

The eigenvalue spectrum  $\lambda$  of the Dynamical Matrix of the Models plays a fundamental role in the static and dynamic properties of polymers. In all the figures, the results are displays are in double logarithmic scale.

### 4.1.1 Rouse Model

In Fig. 4.1, we plot the eigenvalues in progressive order for networks of  $N = 1000$  nodes and averaged over  $S = 1000$  realizations. This eigenvalue with the highest degeneracy is situated in the intermediate part of the spectra. We fix  $K_{min}$  constant to 4, and we investigate the influence on the eigenvalue spectrum of the other parameter,  $K_{max}$ . In fig. 4.1 the parameter  $K_{max}$  is equal to  $N - 1$ , Fig. 4.1(a),  $0.02N = 20$ , Fig. 4.1 (b),  $0.05N = 50$ , Fig. 4.1(c),  $0.1N = 100$  and  $N = 1000$  Fig. 4.1(d).

For this value of  $K_{min}$ , a very high  $\gamma$  corresponds to a network with nodes connected in a "fish-bonelike" or "dendriticlike" fashion or a combination of both. We note that the effect of  $K_{max}$  is mainly related to the decrease of  $\gamma$  for GSFPNs. For large values of  $\gamma$ , the maximum allowed degree  $K_{max}$  does not play an important role because the networks are homologous; that is, they are structures built by nodes of the same degree  $K_{min}$ . Decreasing the value of  $K_{max}$ , the degeneracy of the eigenvalue  $\lambda = 1$  gets lower. For the same  $K_{max}$ , the degeneracy of the eigenvalue  $\lambda = 1$  decreases as  $\gamma$  increases. Another point, for a star with  $N - 1$  arms we get three eigenvalues:  $\lambda_1 = 0$ ,  $\lambda_N = N$ , and the  $(N - 2)$ -fold degenerated eigenvalue  $\lambda_2, \dots, \lambda_{N-1} = 1$ . The number of appearances of eigenvalue  $\lambda = 1$  diminishes by increasing the value of  $\gamma$ , which corresponds to dendritic-like ( $K_{min} \geq 3$ ) segments. The lowest nonzero eigenvalue is  $\lambda \approx 0.001$ , except for GSFPNs with  $K_{max} = 999$  and  $\gamma = 1.0$ , as shown in Fig. 4.1 (d), for which we have

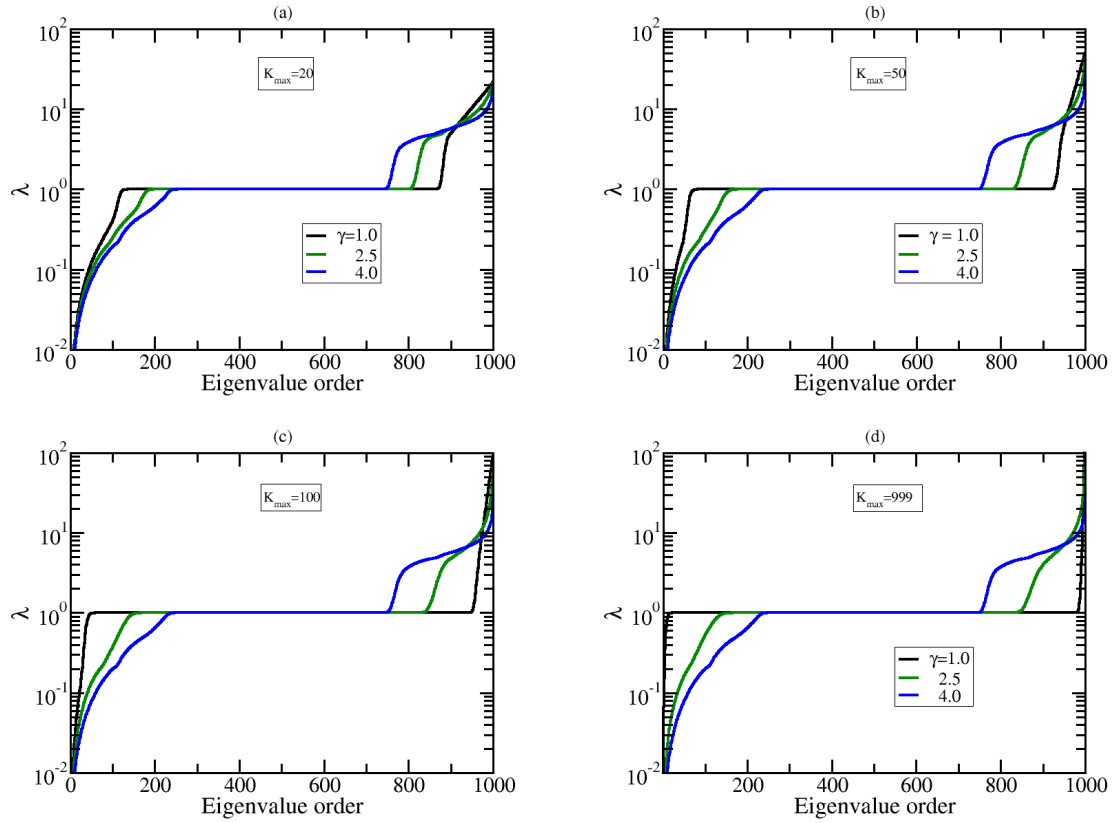


**Figure 4.1** - (a-d) Eigenvalues in progressive order for GSFPNs with  $N = 1000$  and  $K_{min} = 4$ .

0.039. The highest eigenvalue depends more on  $K_{max}$ , for example, in the case of  $\gamma = 1.0$ , we have  $\lambda_{max} \approx 584, 93$ , and  $21.54$  for  $K_{max} = N - 1, 100$  and  $20$ , respectively. The eigenvalue spectrum plays an important role in the Relaxation Patterns.

### 4.1.2 Semiflexible Model

In figures we display in ascending order the eigenvalues of  $\mathbf{A}^{STP}$  for  $S = 250$  Semiflexible Generalized Scale-Free polymer Networks (SGSFPNs) consisting of  $N = 4000$  nodes. In Fig. 4.2, we focus on the influence of  $q$ , on the eigenvalues spectrum, while we keep constant the parameters  $K_{min}$  and  $K_{max}$ . In Fig. 4.3 we fix  $\gamma$  to 2.5 and vary the parameter  $K_{min}$ , we monitor the influence of the minimum allowed degree  $K_{min}$  on the eigenvalue spectrum. In Fig. 4.4 we focus on the influence of  $\gamma$ , which controls the topology of the networks, while we keep constant the stiffness parameter  $q$  to 0.1. As shown in all figures, the degeneracy of eigenvalue  $\lambda^{STP} \approx 1$  is immediately visible, representing a fingerprint of the branching density we find in our networks. This eigenvalue corresponds to the case where the movement of the polymer is to the movement of two dangling neighbors.

In Fig. 4.2 (a) and (b), we monitor the influence of the stiffness parameter on the eigenvalue spectrum. We observe that with growing stiffness, the largest eigenvalues increase while the small eigenvalues decrease slightly. The degeneracy of the eigenvalues is comparable in both cases. The eigenvalue with the highest degeneracy is  $\lambda_d^{STP} = \frac{f}{(f+q)}$ , with  $f$  being the

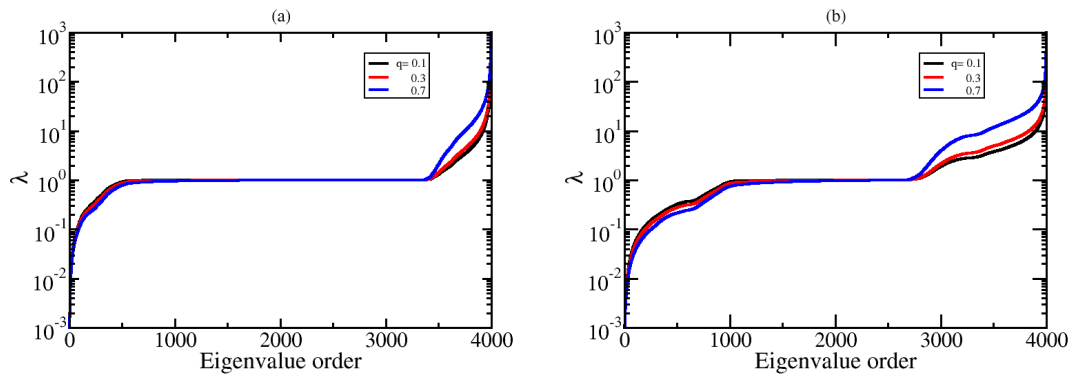


**Figure 4.2** - Eigenvalue spectra for SGSFNs with  $N = 4000$  nodes and  $S = 250$  realizations. Other parameters are:  $(\gamma, K_{min}, K_{max}, q)$ : (a)  $(2, 2, 3999, \text{variable})$ , (b)  $(2.5, 2, 3999, \text{variable})$ .

degree of the node. The degeneracy of  $\lambda_d^{STP}$  is closely related to the topology of the networks, i.e.  $\gamma$ . With low  $\gamma$ , the polymer network is composed predominantly of dendritic-like or star-like structures, while high  $\gamma$  contains mostly long linear segments. The pseudogap between  $\lambda_d$  and the largest eigenvalue increases slightly as  $q$  increases, in contrast to symmetric networks, such as dendrimers or recursive small-world networks [24, 75, 86].

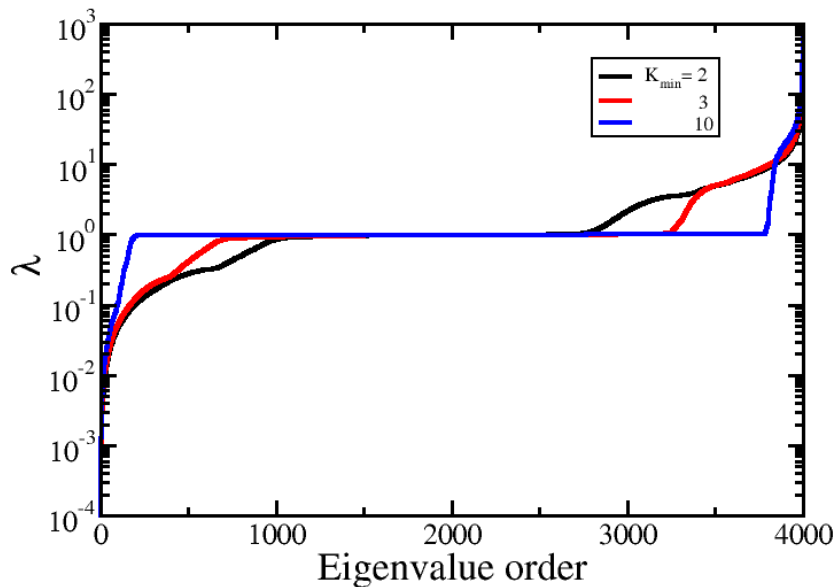


**Figure 4.3** - Eigenvalue spectra for SGSFNs with  $N = 4000$  nodes and  $S = 250$  realizations for the parameters  $(\gamma, K_{min}, K_{max}, q)$  being  $(2.5, \text{variable}, 3999, 0.3)$ .

In Fig. 4.3, we monitor the influence of the minimum allowed degree  $K_{min}$  on the eigenvalue spectrum, while the stiffness parameter is kept constant to  $q = 0.3$  and  $K_{max} = 3999$

for  $\gamma = 2.5$ . By increasing  $K_{min}$ , our networks are composed of nodes with higher degrees, i.e., stars with more branches, and their longest linear path diminishes. This aspect is easily observed by focusing on the highest degenerated eigenvalue. Its degeneracy is strongly influenced by the minimum allowed degree, which directly influences the size of the stars and the number of dangling beads. For instance, a slight increase of  $K_{min}$ , such as the change from 2 to 3, will alter the degeneracy of  $\lambda_d$  by almost 1000. This corresponds to a topological transition between networks with and without linear segments, which, in terms of the eigenvalue spectrum, corresponds to a more discretized spectrum.

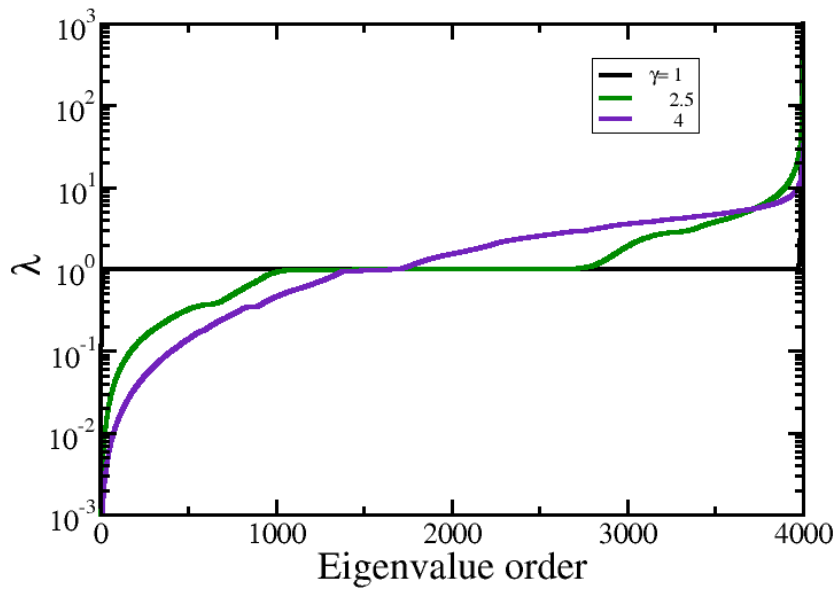


**Figure 4.4** - Eigenvalue spectra for SGSFNs with  $N = 4000$  nodes and  $S = 250$  realizations for the parameters  $(\gamma, K_{min}, K_{max}, q)$  are *variable, 2, 3999, 0.1*.

In Fig. 4.4, we display the spectra for different  $\gamma$ -values and a fixed stiffness parameter  $q = 0.1$ . For very high  $\gamma$  the probability of having a node with high functionality is low [38]; see Eq. (2.32). In this case, the structure will have more chainlike segments than nodes with high functionality (Hubs). In this situation, the structures obtained from the degree distribution are more similar to a linear chain topology. This behavior can be seen through the degeneracy of the eigenvalues, with growing  $\gamma$  the largest eigenvalues increase. For very small  $\gamma$  the probability of getting vertices with high functionalities increases [38]; thus, we can get structures with a starlike topology or an ensemble of starlike segments.

### 4.1.3 Copolymers Model

Our Generalized Scale-Free Copolymer Networks (GSFCNs) involve randomness in the network construction and also in the choice of monomer' type. Thus, for every choice of the parameters' set  $(N, \gamma, K_{min}, K_{max}, \sigma, \eta)$  we consider averages over  $S$  distinct realizations of the

steps growth algorithm of Chapter 2. In our model, these irregular hyperbranched trees can be described by two parameters: the network-related and the polymer-based quantities. In the first class, we have the number of nodes  $N$ , the connectivity parameter  $\gamma$ , the minimum and the maximum allowed degrees,  $K_{min}$  and  $K_{max}$ , respectively. The second class is composed of the ratio between the frictions,  $\sigma$ , and the ratio between the numbers of monomers of the two types,  $\eta$ . In this section, we consider  $S = 100$  GSFCNs with  $N = 4000$  nodes. We monitor how the eigenvalue spectrum of the dynamical matrix  $\tilde{\mathbf{A}}$  and the complex dynamic modulus are influenced by the network topology, which is controlled through changes of  $\gamma$ ,  $K_{min}$  and  $K_{max}$ , or by the copolymer parameters:  $\sigma$  or  $\eta$ .

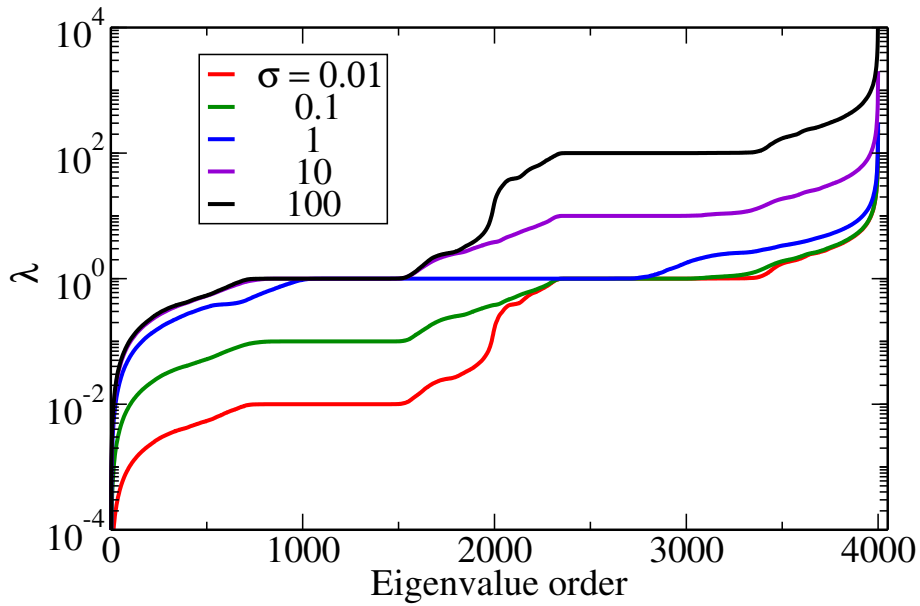


**Figure 4.5** - Eigenvalue spectra for GSFCNs with  $N = 4000$ . The parameters  $(\gamma, K_{min}, K_{max}, \sigma, \eta)$  are:  $(2.5, 2, 3999, \text{variable}, 1.0)$ .

In Fig. 4.5 we let  $\sigma$  to vary between 0.01 and 100, keeping constant the topological parameters:  $\gamma = 2.5$ ,  $K_{min} = 2$ , and  $K_{max} = N - 1$ . Here, we consider that the number of monomers of type  $B$  and  $A$  is the same:  $N_B = N_A$ , *i.e.*  $\eta = 1$ . The value  $\sigma = \zeta_A/\zeta_B = 1$  corresponds to the homopolymer situation, and we encounter the results for Generalized Scale-Free Polymer Networks [68]. For the networks considered in this panel,  $\gamma = 2.5$ , we have a good mixture between stars and linear segments. For our GSFNs the eigenvalue with the highest degeneracy,  $\tilde{\lambda} = 1$ , has a degeneracy of 1486 for the homopolymer case. By considering copolymers, this eigenvalue splits into two subgroups: one is composed of the eigenvalue  $\tilde{\lambda} = 1$ , and the other corresponds to eigenvalue  $\tilde{\lambda} = \sigma$ . Both eigenvalues correspond to the *nonsymmetric* case, for which only two dangling monomers of the same type are moving against each other. The degeneracy of each eigenvalue depends on the number of such independent pairs that one can form and can be understood by considering a star with  $N$  monomers. The eigenvalues  $\tilde{\lambda} = \sigma$  and  $\lambda = 1$  are surrounded by regions of continuous spectrum, which is typical for linear segments.

The highest and the lowest eigenvalues,  $\tilde{\lambda}_{max}$  and  $\tilde{\lambda}_{min}$ , are increasing when  $\sigma$  increases. For our GSFCNs considered in Fig. 4.5 we encounter that the average  $\tilde{\lambda}_{max}$  over  $S$  networks varies between 236.4 ( $\sigma = 0.01$ ) and 18259.9 ( $\sigma = 100$ ), while for the average of  $\tilde{\lambda}_{min}$  we have  $4.7 \cdot 10^{-6}$  ( $\sigma = 0.01$ ) and  $4.68 \cdot 10^{-4}$  ( $\sigma = 100$ ). For homopolymers ( $\sigma = 1$ ) we found  $\tilde{\lambda}_{max} = 309.7$  and  $\tilde{\lambda}_{min} = 2.3 \cdot 10^{-4}$ .

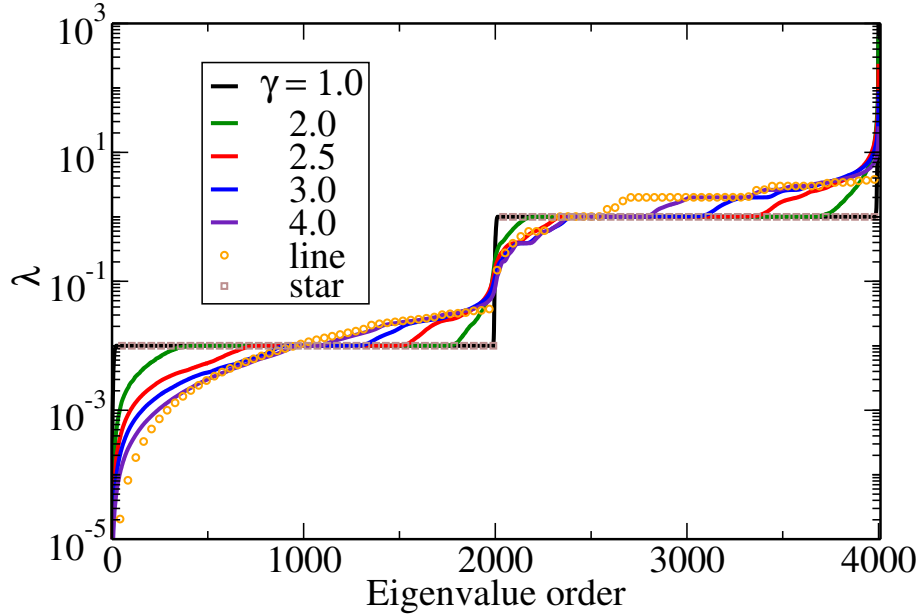


**Figure 4.6** - Eigenvalue spectra for GSFCNs with  $N = 4000$ . The parameters  $(\gamma, K_{min}, K_{max}, \sigma, \eta)$  are:  $(variable, 2, 3999, 0.01, 1.0)$ .

In Fig. 4.6 we monitor the influence of  $\gamma$  on the eigenvalue spectrum. We display the results for GSFCNs with  $\sigma = 0.01$  and  $\eta = 1$ , stressing that similar findings were encountered for other  $\sigma$ -values. The eigenvalue spectrum of our GSFCNs is bounded by two limiting topological cases: random stars with  $N - 1$  arms and random linear copolymers. For these kind of random stars we have only two distinct situations: an  $A$ -core star and a  $B$ -core star, both having a very discrete spectrum composed of only five eigenvalues. The most degenerated eigenvalues are equal to  $\sigma$  and 1.0. Random linear copolymers display a more continuous spectrum, having only some degenerate eigenvalues. These eigenvalues are bounded by two limiting situations: an alternating sequence of  $A$ - and  $B$ -type monomers and a two block sequence of the same monomers' type. Our GSFCNs have star-like segments, thus their eigenvalue spectrum is degenerated, having the eigenvalues  $\sigma$  and 1 as the most degenerated. GSFCNs with low  $\gamma$ -values are mostly formed by star-like segments, while GSFCNs with high  $\gamma$  contain predominantly linear segments. Thus, as seen also in Fig. 4.6, by increasing the value of  $\gamma$  the spectrum becomes less discrete. The lowest nonvanishing and the highest eigenvalues are decreasing when  $\gamma$  increases. The ratio between dendritic and linear segments of a network can be also monitor through the degree of branching, which for homopolymer GSFNs was determined in Ref. [39].

In Fig. 4.7, we check the influence of the minimum and the maximum allowed degree

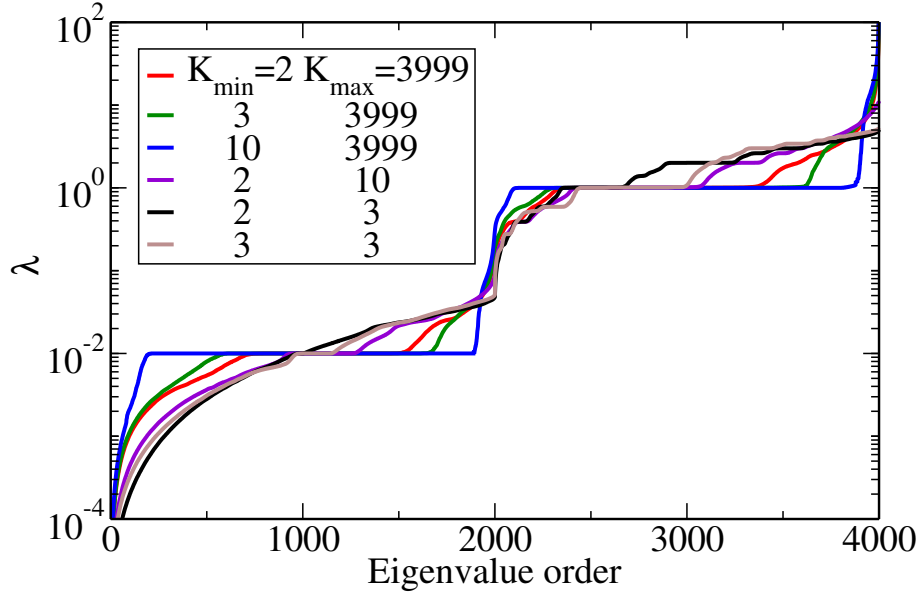


**Figure 4.7** - Eigenvalue spectra for GSFCNs with  $N = 4000$ . The parameters  $(\gamma, K_{min}, K_{max}, \sigma, \eta)$  are:  $(2.5, \text{variable}, \text{variable}, 0.01, 1.0)$ .

$K_{min}$  and  $K_{max}$  on the eigenvalue spectrum. Here, we plot the results for GSFCNs with  $\gamma = 2.5$ ,  $\sigma = 0.01$  and  $\eta = 1$ . Topologically, by fixing  $K_{max}$  and increasing  $K_{min}$ , our networks will be composed of nodes with higher degrees, *i.e.* larger size of the stars. Due to this aspect, we notice an increase in the degeneracy of eigenvalues  $\sigma$  and 1.0, which are the most degenerated eigenvalues of a copolymer star. Their degeneracy is strongly influenced by the minimum allowed degree; even a small change of  $K_{min}$  is very impactful. For example, the eigenvalue 1 is 578-fold degenerated for networks with  $(K_{min}, K_{max}) = (2, N - 1)$  and appears 1666 times for  $(10, N - 1)$ . Between the two most degenerated eigenvalues is created a pseudogap, which becomes thinner when  $K_{min}$  increases. Its limiting size is about two eigenvalues, encountered when  $K_{min} = K_{max} = N - 1$ , *i.e.* a copolymer star with  $N - 1$  arms. In this panel, we also investigate the influence of  $K_{max}$  and display the results for GSFCNs with  $K_{min} = 2$ . Overall, we observe a not too strong influence on  $K_{max}$  than on  $K_{min}$ , although we diminished  $K_{max}$  from  $N - 1$  to 10 or 3. The degeneracy of the eigenvalues  $\sigma$  and 1 decreases while the size of the pseudogap between them increase. The average of the highest eigenvalue is the only quantity suffering big changes when  $K_{max}$  equals 3: it decreases from 236.4 (for  $K_{max} = N - 1$ ) to 5.03. All the features mentioned above can also be explained by the topological changes of our networks, namely, more linear segments and smaller stars are found when  $K_{max}$  is diminished. For comparison reasons, we also plot the results for networks resembling dendrimers because they have the same degree for all nodes ( $K_{min} = K_{max} = 3$ ). However, our copolymers do not inherit the perfect symmetry of dendrimers or the ratio  $\eta$  between  $A$ - and  $B$ -type monomers. For copolymeric dendrimers with alternating monomers having an  $A$ -core  $\eta$  is equal to  $\frac{2^{G+1}-1}{2^{G-1}}$  (if  $G$  is even) and  $\frac{2^G-1}{2^{G+1}-1}$  (if  $G$  is odd), where  $G$  is the dendrimer generation. In the limit of very large copolymers, the ratio equals 2 (even  $G$ ) or 0.5 (odd  $G$ ). For this particular kind of copolymers, it is possible to determine the eigenvalues in a semi-analytical fashion [45].

In Fig. 4.7, the big difference between the last two curves is in the degeneracy of eigenvalue 1, which is higher for networks with  $K_{min} = K_{max} = 3$ , and a higher number of eigenvalues around 2, which is higher for  $(K_{min}, K_{max}) = (2, 3)$ . This feature is a consequence of the linear segments for linear copolymers.

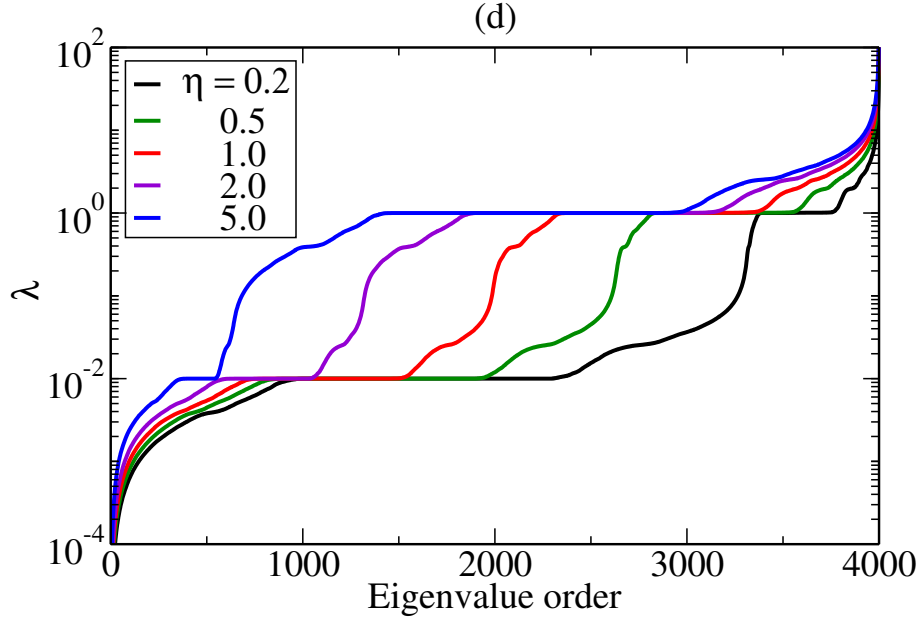


**Figure 4.8** - Eigenvalue spectra for GSFCNs with  $N = 4000$ . The parameters  $(\gamma, K_{min}, K_{max}, \sigma, \eta)$  are:  $(2.5, 2, 3999, 0.01, variable)$ .

In Fig. 4.8 we vary only the ratio  $\eta = N_A/N_B$  between the  $A$ - and  $B$ -type monomers, keeping fixed the parameters  $\gamma = 2.5$ ,  $\sigma = 0.01$ ,  $K_{min} = 2$  and  $K_{max} = N - 1 = 3999$ . The value  $\eta = 1$  corresponds to an equal number of  $A$  and  $B$  monomers, while for  $\eta > 1$  the GSFCNs have more  $A$  monomers and for  $\eta < 1$  we have more  $B$  monomers. Immediately apparent is the degeneracy of eigenvalues  $\sigma$  and 1. GSFCNs with more  $A$  type monomers have higher degeneracy of 1, while copolymers with more  $B$  monomers have more eigenvalues equal to  $\sigma$ . The responsible for this behavior are the star-like segments. For small star copolymers with predominant  $A$  monomers have the eigenvalue 1, while for predominant  $B$  monomers we get the eigenvalue  $\sigma$  as the most degenerated. The networks considered in Fig. 4.8 have a good number of star-like segments, thus the ratio  $\eta$  will control which of the two eigenvalues is the most degenerated. The lowest nonvanishing and the highest eigenvalues get higher when  $\eta$  increases, *i.e.* when the number of  $A$  monomers increases. In Fig. 4.8 the average of  $\tilde{\lambda}_{min}$  is between  $2.5 \cdot 10^{-6}$  ( $\eta = 0.2$ ) and  $1.3 \cdot 10^{-5}$  ( $\eta = 5$ ), while for  $\tilde{\lambda}_{max}$  we have the interval 106.6 ( $\eta = 0.2$ ) to 288.3 ( $\eta = 5$ ).

## 4.2 Mechanical Relaxation

We are now in the position to compute the mechanical moduli  $G'(\omega)$ , Eq. (3.35) and  $G''(\omega)$ , Eq. (3.36), and their derivatives,  $\alpha' = \frac{d(\log_{10} G')}{d(\log_{10} \omega)}$  and  $\alpha'' = \frac{d(\log_{10} G'')}{d(\log_{10} \omega)}$ , respectively, of GSFCNs built from the algorithm described in chapter 2 and with their eigenvalue spectrum dis-

cussed in section 4.1. Most polymer measurements are monitored in the frequency domain; moreover, they are accompanied by macroscopic changes. The moduli are given by Eqs (3.35) and (3.36), where we set  $\frac{\nu K_B T}{N} = 1$  and  $\sigma = 1$ . Clearly evident in all figures are the limiting, connectivity-independent behaviors at very small and very large  $\omega$ ; for very small  $\omega$  one has  $G'(\omega) \sim \omega^2$  and  $G''(\omega) \sim \omega^1$ , which represents the mechanical response of the entire polymer network and very large  $\omega$  has  $G'(\omega) \sim \omega^0$  and  $G''(\omega) \sim \omega^{-1}$  which signifies single-bead mechanical response. These scaling behaviors are universal, being independent of network topology or the model implemented and they are not associated with the microscopic structure.

The average monomer displacement  $\langle\langle Y(t) \rangle\rangle$  Eq.(3.27) we show in double logarithmic scale with  $\frac{F}{\zeta} = 1$  and  $\sigma = 1$ . In the limit of very short times and sufficiently large  $N$  one has  $\langle\langle Y(t) \rangle\rangle = Ft/\zeta$ , and for very long times, we have  $\langle\langle Y(t) \rangle\rangle = Ft/N\zeta$ . The physical interpretation is as follows: For very short times, only one bead is moving, whereas for very long times, the whole GGS diffuses, which increases the friction from  $\zeta$  to  $N\zeta$ . In the intermediate time region the particular topology of the GGS under investigation will come into play; the behavior of the averaged displacement indeed depends on the eigenvalues of the connectivity matrixes  $\mathbf{A}$  and  $\mathbf{A}^{STP}$  for Rouse and Semiflexible Models, respectively [34, 38, 39].

### 4.2.1 Rouse Model

Fig. 4.9 shows the behavior of the storage modulus,  $G'(\omega)$  and Figure 4.10 of the loss modulus,  $G''(\omega)$ , calculated for GSFPNs of size  $N = 4000$  and averaged over ensembles consisting of  $S = 250$  realizations. The minimum allowed degree,  $K_{min}$ , was kept constant to 3 for  $G'(\omega)$  and to 5 for  $G''(\omega)$  and  $\gamma$  was varied: 1.0, 2.5 and 4.0. The scales on all panels of the figure are double logarithmic to basis 10. We restricted the maximum allowed degree to  $K_{max} = N/200 = 20$  and in  $K_{max} = N/400 = 100$ .

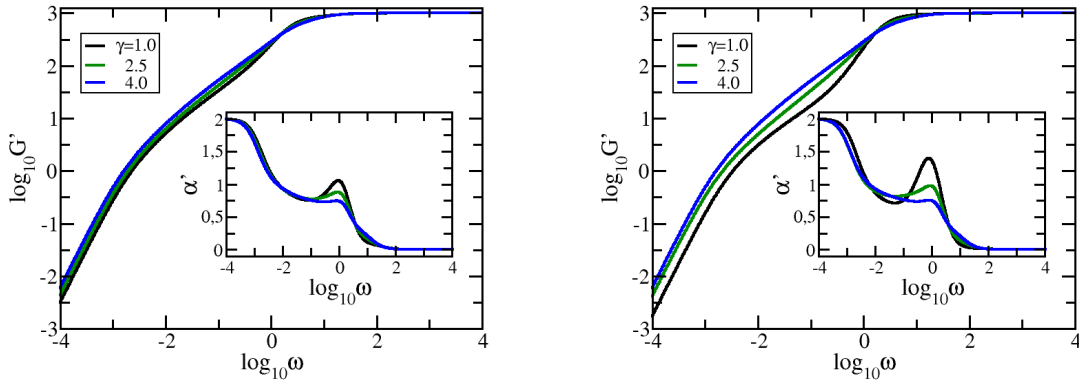


**Figure 4.9** - The storage modulus  $G'(\omega)$  for GSFPNs with  $N = 1000$  and  $\gamma = \text{variable}$ . The parameters' set  $(K_{min}, K_{max})$  is equal to: (Left) (3, 20) and (Right) (3, 100).

The intermediate frequency range is typical of the topological details of the structure being examined. The shape of the curves in the intermediate frequency range suggests that different

types of networks were formed as a function of the parameter  $\gamma$ . In both panels, for  $\gamma = 1$  and 2.5 the intermediate frequency domain splits into two regions which suggests that the achieved networks consists of two major components. The splits increased when  $K_{max}$  change the value to 100. The splitting of the intermediate region indicates the existence of two relaxation processes, with each component of the network relaxing independently of the other components within its frequency range. When the value of  $\gamma$  is greater than 1, the intermediate domain is not split, suggesting that the resulting network is a single component. For a better visualization of the intermediate frequency domain, we plot the derivative  $\alpha' = \frac{d(\log_{10}G')}{d(\log_{10}\omega)}$  as an inset for the same curves of Fig. 4.9. As expected, the very low and very high frequency limiting behavior applies to slope 2 and slope 0. However, in the intermediate frequency range, all four curves become wavy. In Fig. 4.9 left-hand side panel, we notice a peak at  $\log_{10}\omega \approx -0.21$ , which starts to fade away when  $\gamma$  increases and Fig. 4.9 right-hand side panel happen when the peak is  $\log_{10}\omega \approx -0.11$  when  $\gamma$  increases. We observe that only by reducing the maximum allowed degree,  $K_{max}$ , the curves corresponding to different values of  $\gamma$  tend to stick together and the overall  $\gamma$  dependent behavior is preserved.

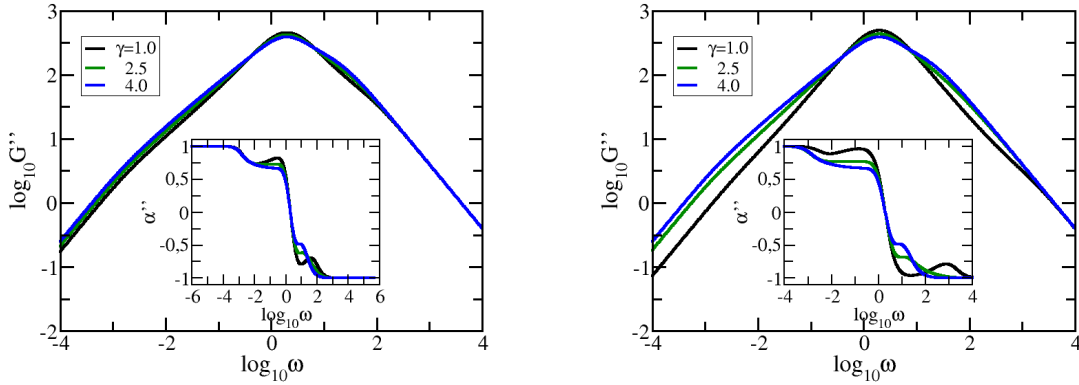


**Figure 4.10** - The loss modulus  $G''(\omega)$  for GSFPNs with  $N = 1000$  and  $\gamma = \text{variable}$ . The parameters' set  $(K_{min}, K_{max})$  is equal to: (Right) (5, 50), and (Left) (5, 1000).

Now, we turn our attention to the loss modulus,  $G''(\omega)$ . In Fig. 4.10 left-hand side panel, we fixed the maximum allowed degree  $K_{max} = N/80$  and in right-hand panel  $K_{max} = N/4$ . In both panels, the restrictive and connection-independent behavior at very small  $\omega$  and very large  $\omega$  is clearly visible; for very small  $\omega$  has  $G''(\omega) \approx \omega$ , and for very large  $G''(\omega) \approx \omega^{-1}$ . What we are interested in is the intermediate frequency range where we can determine the topology of the structure [34, 68]. We find that for  $\gamma = 1$  and 4, the intermediate frequency region of the loss modulus is decomposed into two regions, indicating the existence of a two-component network and two independent relaxation processes. In Fig. 4.10 right-hand side panel,  $K_{max} = 50$ , for values of  $\gamma = 2.5$  and 4 the in-between frequency domain does not decompose and one obtains single-component networks. To have a better insight in the intermediate domain, we plot as inset graph the derivative  $\alpha'' = \frac{d(\log_{10}G'')}{d(\log_{10}\omega)}$ . When  $K_{max}$  is decreased, the curves corresponding to different

values of  $\gamma$  form a kind of similar main curve and tend to maintain the same pattern. This constant slope is similar in both panels and spans nearly two orders of magnitude,  $\alpha'' \approx 0.77$ . For  $\gamma = 4.0$ , this region with constant slope disappears. In the frequencies' interval  $\log_{10}\omega \approx (-1, 1)$  a very pronounced peak at  $\gamma = 1.0$  is observed and transformed into a small plateau when  $\gamma$  increases. This situation is reminiscent of a star-shape geometry: a polymer with a core and  $N - 1$  arms [34, 68].

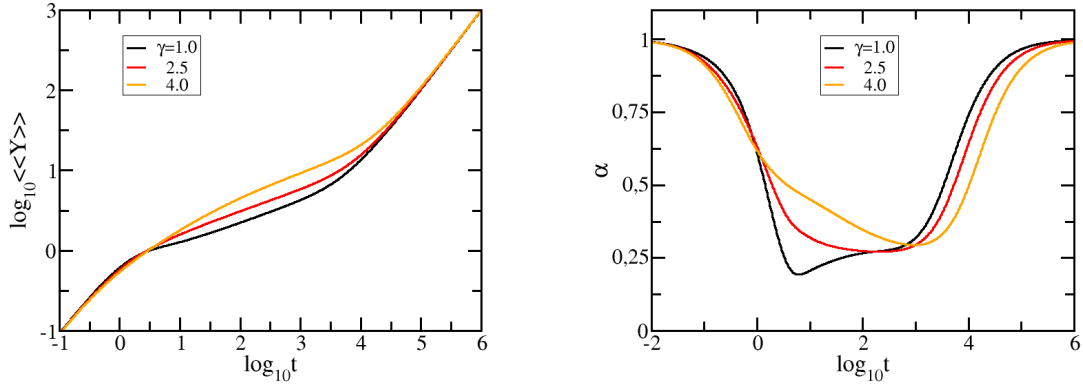


**Figure 4.11** - The average monomer displacement for GSFPNs with  $N = 1000$  its derivative for GSFPNs corresponds to  $K_{min} = 2$ ,  $K_{max} = 50$ ,  $\gamma = variable$ .

In the Figures 4.11 and 4.12, we plot in double logarithmical scale the average monomer displacement for GSFPNs with  $N = 4000$ . In Fig. 4.11 left-hand side panel, we focus on the role of  $\gamma$ , keeping unchanged the other two parameters:  $K_{min} = 2$  and  $K_{max} = N/20 = 50$  and right-hand panel, we show their derivatives,  $\alpha' = \frac{d\log_{10}\langle\langle Y(t) \rangle\rangle}{d\log_{10}t}$ . In Fig. 4.12 left-hand side panel, we focus on the role of  $K_{min}$ , keeping unchanged the other two parameters:  $K_{max} = N$  and  $\gamma = 2.5$  and right-hand panel, we show their derivatives,  $\alpha'$ . In Fig. 4.11 here we took all the values  $\gamma$  from 1 to 4. We observe the limiting cases are clearly observed: linear  $t$  dependence for short and long times. We notice that all the curves reach faster long-time linear behavior than a pure linear chain ( $\gamma = 4$ ), but slower than a  $N - 1$  arms star polymer ( $\gamma = 1$ ). One can easily spot the slope equal to 1 for short and long times and its inverted shape for all the curves. Between  $\alpha \approx 0.2$  and  $0.45$ , the slope decreases when the value  $\gamma$  increases. In Fig. 4.12, we observe that if the value of  $K_{min}$  increases the intermediate time region with this slope gets larger.

### 4.2.2 Semiflexible Model

In Figs. 4.13 and Fig. 4.14 we display in double logarithmic scale the storage modulus, Eq. (3.35), for SGSFNs with  $N = 4000$  and  $S = 100$ . In the inset panels we show the derivatives of the curves from the main panel  $\alpha' = \frac{d(\log_{10}G'(\omega))}{d(\log_{10}\omega)}$  in semi-logarithmic scale. From all panels of Figs. 4.13 and 4.14 immediately apparent are the two limiting behaviors, namely for very low frequencies one encounters an  $\omega^2$ -behavior and for very high frequencies one obtains a plateau. These scaling behaviors are universal, *i.e.* independent of topology or the model implemented, valid

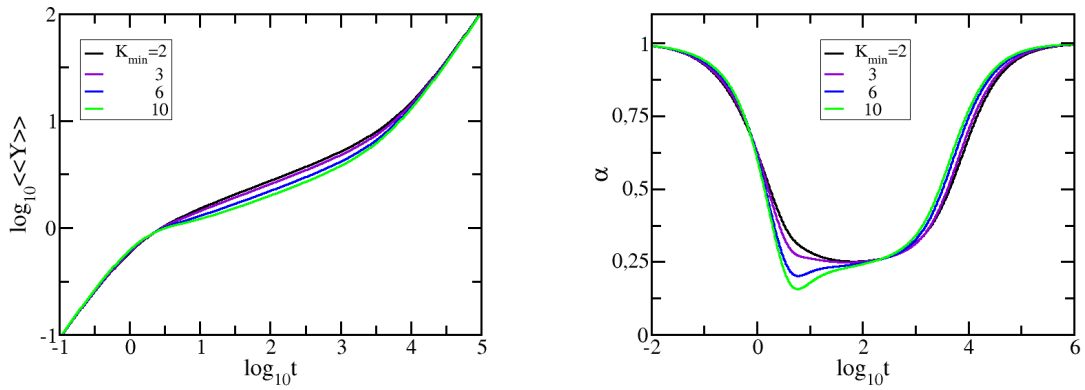


**Figure 4.12** - The average monomer displacement and its derivative for GSFPNs with  $N = 1000$ . Left-hand side panel corresponds to  $K_{min} = \text{variable}$ ,  $K_{max} = 1000$ ,  $\gamma = 25$ .

for all polymer networks [33], and they are not associated with the microscopic structure. The microscopic properties of the polymers are exposed only in the region of intermediate frequency.

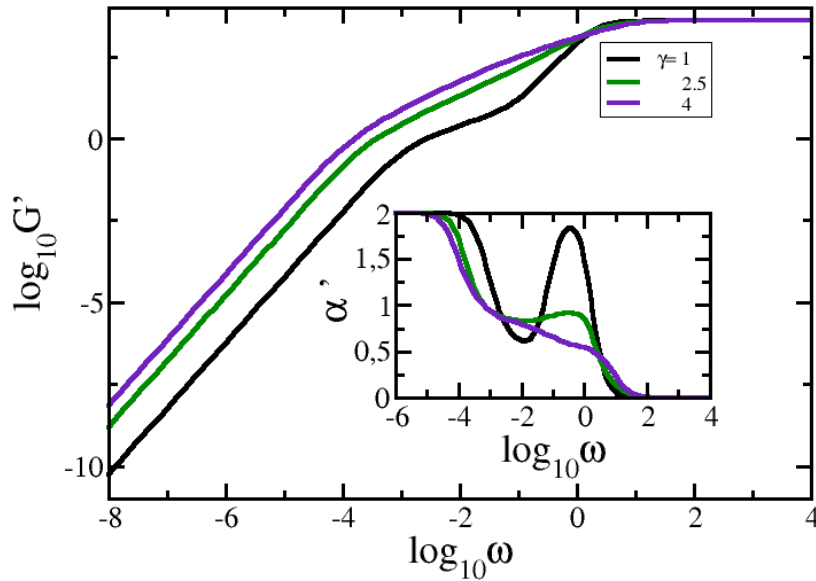


**Figure 4.13** - Storage modulus and its derivative for SGSFNs with  $N = 4000$  and  $S = 100$  realizations for the parameters  $(\gamma, K_{min}, K_{max}, q)$  are  $(\text{variable}, 2, 3999, 0.1)$ .

In Fig. 4.13 we monitor the influence of the parameter  $\gamma$ , for SGSFNs with fixed values of  $K_{min} = 2$ ,  $K_{max} = 3999$ , and low stiffness:  $q = 0.1$ . Here, we vary  $\gamma = 1.0, 2.5$  and  $4.0$  and one can easily notice a transition from SGSFNs with predominant star-like segments (low  $\gamma$ s) to SGSFNs with long linear segments (high  $\gamma$ s). The differences between distinct curves are better visualized in the derivative,  $\alpha'$ . For  $\gamma = 1$  we encounter a high peak at  $\log_{10} \omega \approx -0.5$ , which is a

consequence of having an eigenvalue with a very high degeneracy,  $\lambda^* = f/(f + q)$ . This peak will be drastically diminished by a small increase of  $\gamma$ , such as 2.5. In the same time a small region of almost constant slope appears between  $\log_{10}\omega = -2$  and  $-1$ , which becomes broader for SGSFNs with  $\gamma = 4$ . However, due to a significant number of nodes with higher functionalities, SGSFNs with  $\gamma = 2.5$  has  $\alpha' \approx 0.83$  and only for about two orders of magnitude. The overall behavior of the curves keeps the same, namely networks with  $\gamma = 1$  show a high peak due to the starlike topology, while SGSFNs with  $\gamma = 2.5$  show a mixture of linear-like chain with some dendrimer-like segments. For these networks we notice a split for intermediate frequencies: a concave downward behavior, which is typical for dendrimers [33], and a short plateau, which is a trademark of linear chains.

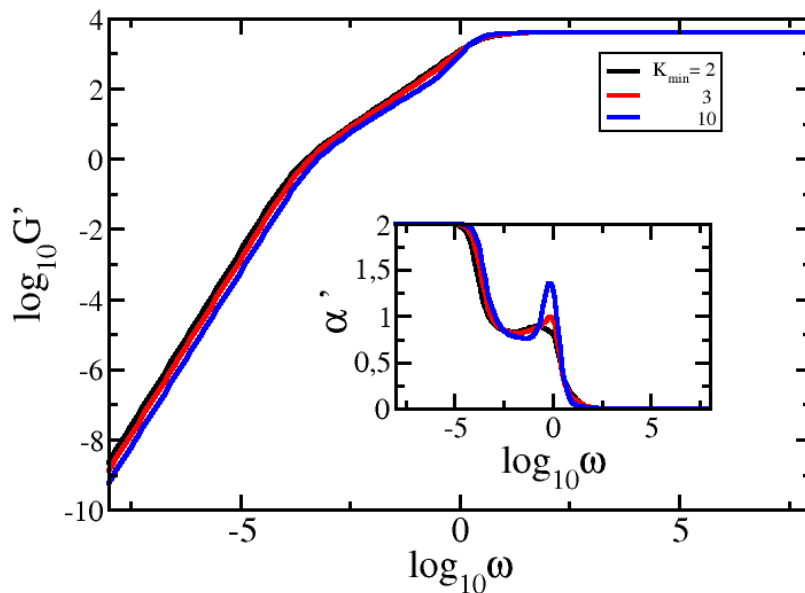


**Figure 4.14** - Storage modulus and its derivative for SGSFNs with  $N = 4000$  and  $S = 100$  realizations for the parameters  $(\gamma, K_{min}, K_{max}, q)$  are  $(2.5, \text{variable}, 3999, 0.3)$ .

In Fig. 4.14 we increase the stiffness parameter to  $q = 0.3$  and we focus on the influence of  $K_{min}$  on  $G$ . Networks with  $K_{min} = 2$  are allowed to have nodes with degree 2, thus the linear segments between branching nodes increase. However, starting from  $K_{min} = 3$  the topology changes drastically to networks formed by stars of different sizes. This change in topology is seen also in the panel: a peak around  $\omega \approx 1.0$  becomes visible and a complete destruction of any constant slope plateau. These drastic changes could be understood also in terms of the eigenvalue spectrum. SGSFNs with higher  $K_{min}$  have a more discrete spectrum, *i.e.* less distinct eigenvalues, but higher degeneracies.

In Fig. 4.15 we monitor how the stiffness parameter  $q$  affects the storage modulus. We consider the same SGSFNs, which have  $\gamma = 2.5$ ,  $K_{min} = 2$  and  $K_{max} = 3999$ . By switching

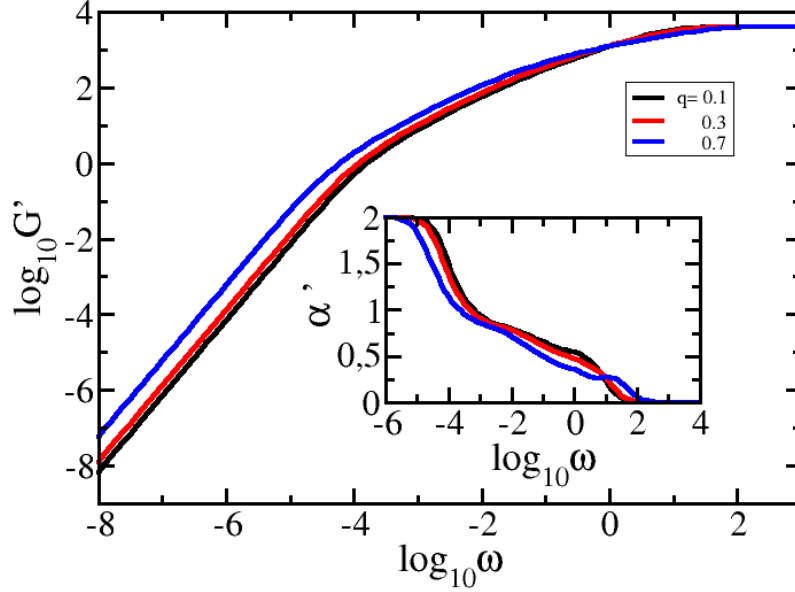


**Figure 4.15** - Storage modulus and its derivative for SGSFNs with  $N = 4000$  and  $S = 100$  realizations. The parameters  $(\gamma, K_{min}, K_{max}, q)$  are  $(2, 2, 3999, \text{variable})$ .

on the stiffness we manage to smoothen this peak and for  $q = 0.3$  we encounter the broadest constant slope,  $\alpha' \approx 0.83$ , in the region of intermediate frequencies. However, this behavior is destroyed gradually by further increasing the  $q$ -value. We also notice that the elevation around  $\omega \approx 10$  becomes more visible and with higher values of the derivative when the stiffness parameter increases. This elevation is encountered for medium and high values of  $q$ ; for  $q = 0.5$  the derivative ranges between  $\alpha' \approx 0.3$  and  $0.1$ . Similar values were also found for linear chains and large values of stiffness parameter [36]. In the region between  $\omega \approx 0.1$  and  $1.0$  we have noticed a decrease in the net values of  $G'$  for all the curves.

In Fig. 4.16 we plot in double logarithmical scale the reduced loss modulus, Eq. (3.36), where we consider  $\nu k_B T/N = 1$  and  $\sigma = 1$ . We display the results for  $S = 100$  networks with  $N = 4000$  monomers. In all panels we show as inset the derivative  $\alpha'' = \frac{d(\log_{10} G'')}{d(\log_{10} \omega)}$  of all the curves from the main subfigure. First, we focus on the influence of the networks's topology, which is controlled by the parameter  $\gamma$ , on the relaxation dynamics. In Fig. 4.16 (right) we set the stiffness parameter to  $q = 0.3$ , while in Fig. 4.16 (down) we have  $q = 0.7$ . In both panels, the connectivity parameter takes  $\gamma$ -values between 1 and 4. Immediately apparent are the limiting behaviors for all the curves, namely an  $\omega^1$ -law for very low frequencies and an  $\omega^{-1}$ -law for very high frequencies. For  $\gamma = 1$  we encounter a high peak at  $\log_{10} \omega \approx -1$ , which is a consequence of having an eigenvalue with a very high degeneracy,  $\lambda^* = f/(f + q)$ . Due to big changes of networks's topology, the peak is not so evident anymore even for increase of  $\gamma$  and it disappears completely for networks with  $\gamma = 4$ . For SGSFNs with  $\gamma = 2.5$  we encounter a small region of almost constant slope ( $\alpha'' \approx 0.76$ ),

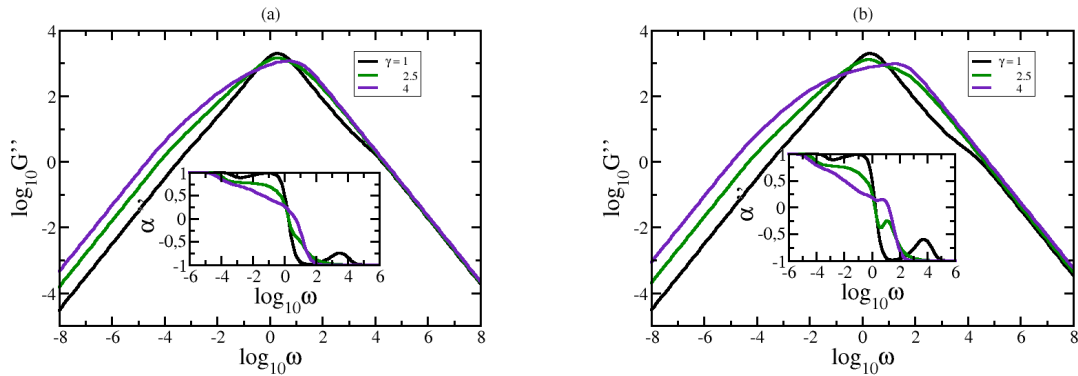


**Figure 4.16** - Loss modulus and its derivative for SGSFNs with  $N = 4000$  and  $S = 100$  realizations. Other parameters are:  $(\gamma, K_{min}, K_{max}, q)$ : (Left) (variable, 2, 3999, 0.3) and (Right) (variable, 2, 3999, 0.7).

which is broader when  $q$  is smaller. For example, it extends for more than one order of magnitude when  $q = 0.3$  and only to one order when  $q = 0.7$  is considered, by comparing Figs. 4.16 (right) and (left). Similar values of the slope were encountered experimentally for cross-linked polymer gel based on reversible covalent acylhydrazone bond [97] and Poly(vinyl chloride) plastisol gels [98]. In Ref. [99], the authors encountered slopes between 0.5 and 0.7 in the intermediate frequency region when studying dendronized polymers with generations 1 – 3 and backbone nominal degrees of polymerization in the range of 50 – 3000. For frequencies between  $10^{-3}$  and  $10^{-4}$  we notice another very prominent peak for networks with  $\gamma = 1$ , which is shifted in the direction of lower frequencies when  $\gamma$  increases. The existence of this peak is due to the presence of larger stars; the same behavior being encountered also for flexible scale-free networks [34,68]. For small to medium values of the stiffness parameter, like in panel 4.16 (a), the peak slowly disappears, but for high values of  $q$  it moves towards lower frequencies when  $\gamma$  is increased.

In Fig. 4.17 we investigate the influence of  $K_{max}$  on the loss modulus for SGSFNs with  $\gamma = 2.5$ ,  $K_{min} = 2$ , and the stiffness parameter  $q = 0.1$ . In this case the usual slope for a linear chain, namely 0.5, is perfectly recovered; a higher stiffness value diminishes the length of the constant slope. Even by a small increase of  $K_{max}$  we notice a clear transformation of the curves in the intermediate frequency region. The constant slope of 0.5 vanishes and we notice a monotonous decay of the derivative, due to the presence of many nodes with degree higher than two. Networks with very high  $\gamma$  show a constant slope of  $\alpha'' \approx 0.76$ , extended for almost two orders of magnitude. By comparing these results with Fig. 4.14 we can conclude that a change of  $K_{max}$  is not that striking as a change of  $K_{min}$ .

In Fig. 4.18 we focus on the influence of the stiffness parameter  $q$  on the loss modulus, choosing to display the results for SGSFNs with  $\gamma = 2.5$ ,  $K_{min} = 3$  and  $K_{max} = 3999$ . In the region of lower intermediate frequencies we observe a constant slope with  $\alpha'' \approx 0.76$ . For all the other  $q$ -values the slope continues to be the same, but its width gets narrower. For higher intermediate

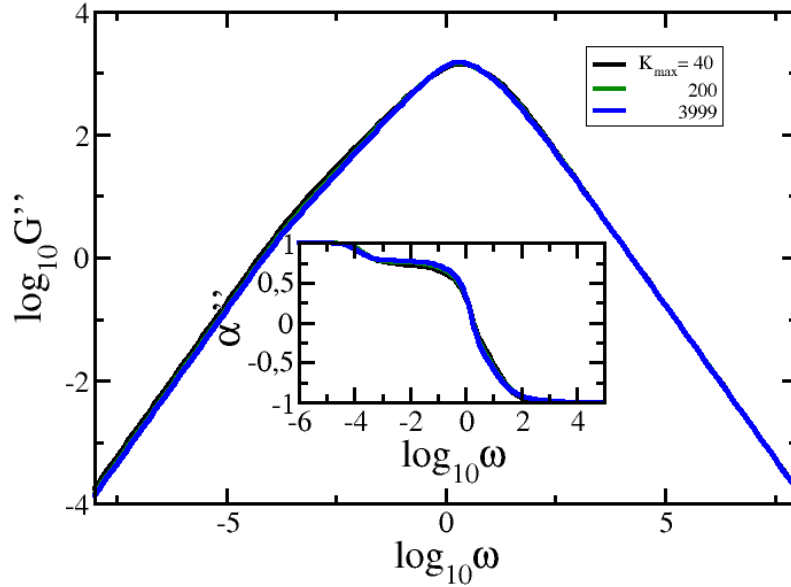


**Figure 4.17** - Loss modulus and its derivative for SGSFNs with  $N = 4000$  and  $S = 100$  realizations for the parameters  $(\gamma, K_{min}, K_{max}, q)$  are  $(2.5, 2, \text{variable}, 0.1)$ .

region we observe a monotonous decay of the derivative for lower values of  $q$ , followed by a local minimum and a peak for medium to high values of  $q$ . However, this minimum is not as sharp as in the case of dendritic semiflexible polymers [84] or dendrimers [36, 89] because the pseudogap in the region of high eigenvalues is smoothened by the scale-free topology. Similar findings were encountered for some particular semiflexible scale-free networks ( $K_{min} = 2$  and  $K_{max} = N - 1$ ) [38] or small-world networks [93]. In the region of high frequencies the loss modulus gets wider if the stiffness parameter  $q$  is increased. This aspect is related to an increase in the value of the highest eigenvalues, as noticed also in other semiflexible hyperbranched polymer networks [38, 84–86].

In figures 4.19 and 4.20 we display in double logarithmical scale the average monomer displacement,  $\langle\langle Y \rangle\rangle$ , calculated based on Eq.(3.19), for  $S = 100$  SGSFNs with  $N = 4000$  monomers. In Fig. 4.19 we monitor how the stiffness parameter  $q$  influences the average monomer displacement, choosing to display the results for SGSFNs with  $\gamma = 2.5$ ,  $K_{min} = 2$ , and  $K_{max} = 3999$ . For these networks we have noticed a constant slope in the region of intermediate times when  $q = 0.3$ , see Fig. 4.19. Now, by varying  $q$  we observe almost the same behavior for all the  $q$ -values. The most significant difference is given by the width of the constant slope region. When  $q$  increases the length of the constant slope diminishes and a region of monotonous decay appears for lower intermediate times. It is worth reminding that we observe scaling only for SGSFNs with  $\gamma = 2.5$ , but this small increase of the slope for lower intermediate times is valid for other values of  $\gamma$ . This is a direct consequence of the increase of the highest eigenvalues, as can be seen in Fig. 4.2 (c).

In Fig. 4.20 (a) we focus on the influence of the networks' topology, by varying only  $\gamma$ .

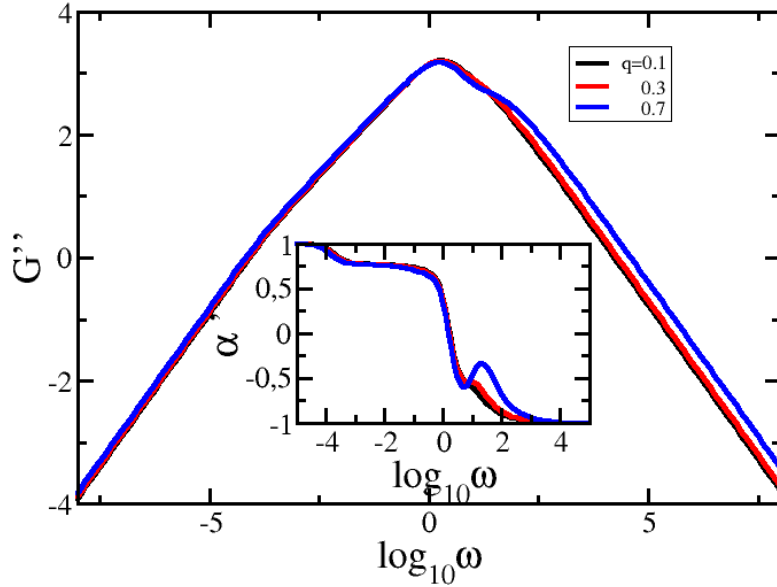


**Figure 4.18** - Loss modulus and its derivative for SGSFNs with  $N = 4000$  and  $S = 100$  realizations for the parameters  $(\gamma, K_{min}, K_{max}, q)$  are  $(2.5, 2, 3999, \text{variable})$ .

Here, we display the results for SGSFNs with  $(K_{min}, K_{max}) = (2, 3999)$  and the stiffness parameter  $q = 0.3$ . All the curves lay between the curves for a linear chain and a star with  $N - 1$  arms; features from both these limiting topologies being observed. In the intermediate time domain we notice an almost constant slope of  $\alpha \approx 0.53$  for a linear chain, which is slightly different than 0.5 obtained for the Rouse flexible linear chain ( $q = 0$ ). For the single star we notice a complete lack of scaling, having only a steep decay until a minimum followed by a fast increase of the derivative. Networks with low values of  $\gamma$  maintain the behavior of a star, while SGSFNs with high  $\gamma$ s are approaching the linearlike behavior, but it will not be reached due to the presence of nodes with higher degree. The most interesting situation is encountered for SGSFNs with  $\gamma = 2.5$ . For these networks we found a constant slope of 0.23 for more than two orders of magnitude. This low value of the slope is characteristic for some semiflexible topologies, like linear chains [100], stars [36] or other hyperbranched polymers [93]. In Fig. 4.20 (b) we focus on the influence of  $K_{min}$ , keeping constant all the other parameters. For having a constant slope in the intermediate time region we choose again the SGSFNs with  $\gamma = 2.5$  and  $K_{max} = 3999$  with the stiffness parameter being equal to  $q = 0.3$ . When  $K_{min}$  is increased, we obtain hyperbranched polymers with a nontrivial mixture of linear segments and stars of various sizes for  $K_{min} = 2$  and formed only by stars for  $K_{min} > 2$ . This topological transition can be observe also in the figure, especially in the region of lower intermediate times. SGSFNs with  $K_{min} > 2$  show a local minimum, which gets lower by increasing  $K_{min}$ . Remarkably, this local minimum extends by one order of magnitude the region of constant slope for networks with  $K_{min} = 2$  and 3. The effect of diminishing the width of the

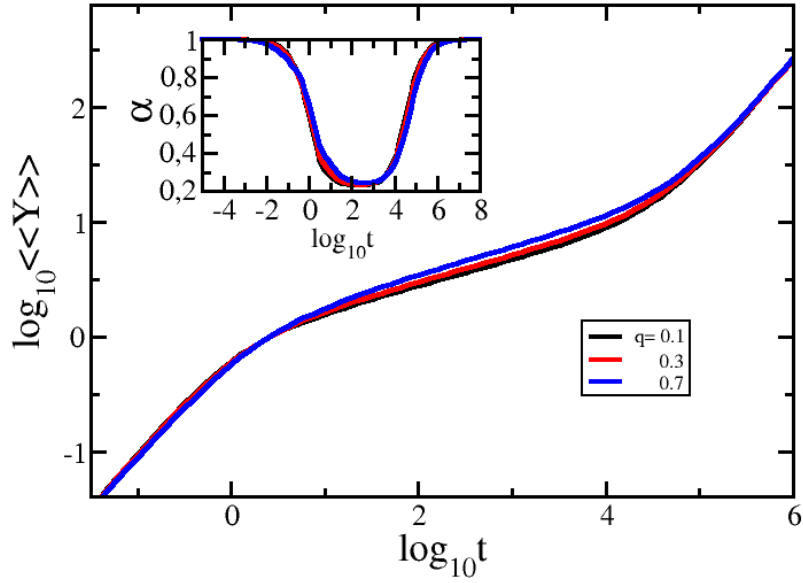


**Figure 4.19** - Average monomer displacement and its derivative for SGSFNs. The parameters' set is:  $(N, \gamma, K_{min}, K_{max}, q)$ : (Left) (4000, 2, 2,  $N1$ , variable), (Right) (4000, 2.5, 2, 3999, variable)

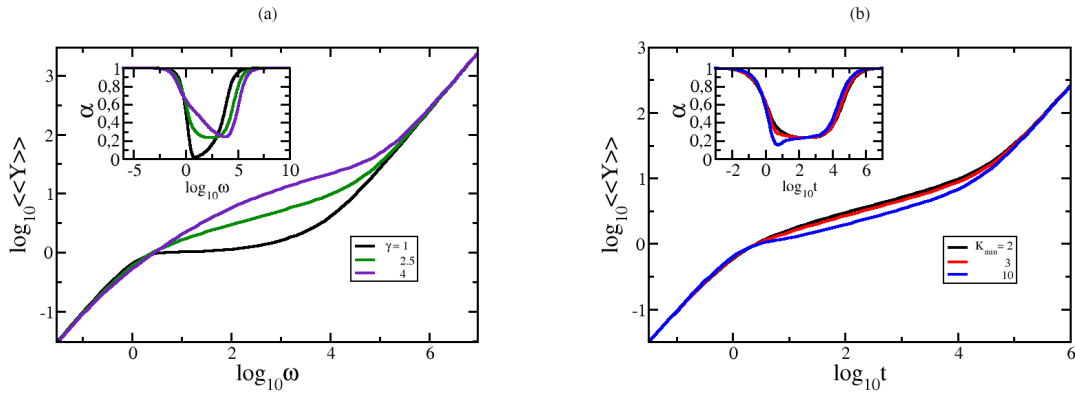


**Figure 4.20** - Average monomer displacement and its derivative for SGSFNs. The parameters' set is:  $(N, \gamma, K_{min}, K_{max}, q)$ : (a) (4000, variable, 2, 3999, 0.3), (b) (4000, 2.5, variable, 3999, 0.3).

constant slope when  $q$  is increased, observed in 4.19, is canceled by a slight increase of  $K_{min}$ . Thus, a similar behavior can be obtained when both  $\gamma$  and  $K_{min}$  are varied in a proper manner.

### 4.2.3 Copolymers Model

Here we study systematically the influence of the parameters, namely  $\gamma$ ,  $K_{min}$ ,  $K_{max}$ ,  $\sigma$  and  $\eta$ , on both mechanical moduli. For each parameter we display in the same figure the results for the storage and loss moduli  $G'(\omega)$  and  $G''(\omega)$ , given by Eqs. (3.35) and (3.36) and their derivatives. As in the model had seen, we can see in all figures, at very small and very large frequencies  $G' \sim \omega^2$

and  $G'' \sim \omega^1$  for  $\omega \leq 1$  and  $G' \sim \omega^0$  and  $G'' \sim \omega^{-1}$  for  $\omega \geq 1$ . These scaling behaviors are universal, independent of network topology or the model implemented, and they are not associated with the microscopic structure.

In Figs. 4.21 and 4.22 we study the influence of changes in  $\sigma$ , which is varied between 0.01 and 100. The particular case  $\sigma = \zeta_A/\zeta_B = 1$  corresponds to homopolymers (blue color in the panels) and reproduces the results of homopolymer GSFNs [68]. Even a small deviation from 1 leads to significant differences in the behavior of both moduli. For relatively small differences from 1, such as  $\sigma = 0.1$  or 10, we encounter a new feature: a short quasi-plateau ( $\alpha' \approx 0.3$  and  $\alpha'' \approx 0.05$ ) localized to the left (to the right) from the curve with  $\sigma = 1$ , when  $\sigma$  is smaller (larger) than 1. By further increasing the distance from 1, for example  $\sigma = 0.01$  or 100, the quasi-plateau disappears and a pronounced peak appears to the left (to the right) from the curve with  $\sigma = 1$ . For  $\sigma \gg 1$  the  $B$ -type monomers are more mobile than the  $A$  monomers, thus the relaxation dynamics starts earlier than in the case of homopolymers,  $\sigma = 1$ . In the region of high frequencies only the  $B$  monomers move, while the  $A$  monomers are practically immobile. These monomers start to move only if one goes towards much lower frequencies. This clear scale separation between monomers is responsible for the quasi-plateaus and the peaks already mentioned. The scaling behavior encountered for homopolymer GSFNs in the low frequency domain (frequencies between  $10^{-3}$  and  $10^0$ ) remains practically unaltered when  $\sigma$  is switched on. The broadening of this constant slope is almost the same and is noticed only a shift towards low (high) frequencies when  $\sigma$  is smaller (larger) than 1. This shift exits due to the difference between the mobility of the two monomer types:  $\zeta_A$  and  $\zeta_B$ . The value of the slope keeps the same, namely  $\alpha' \approx 0.3$  and  $\alpha'' \approx 0.05$ , because it is mainly dependent of the topology of the network. In this figure the construction parameters which control the topology  $\gamma$ ,  $K_{min}$ , and  $K_{max}$ , are kept constant, thus for all the curves the topological changes are minimal. The high symmetry between  $\sigma$  and  $1/\sigma$  curves is due to the fact that all the networks have the same number of  $A$  and  $B$  type monomers, as it was observed for linear alternating copolymer chains [44]. Different values of  $\eta$  infer some discrepancies between  $\sigma$  and  $1/\sigma$  curves, *i.e.* interchange the monomers type. This aspect creates an asymmetric behavior, which was also observed for copolymeric dendrimers built from alternating monomers [45].

In Figs. 4.23 and 4.24 we study the influence of the network topology on the moduli by changing only the parameter  $\gamma$ . GSFNs with low  $\gamma$  (1 in our figure) have predominantly star-like segments, while for high  $\gamma$  (4 in the figure) we obtain networks with more linear-like segments [68]. For comparison we display the results of the limiting cases: the random linear copolymers, depicted by circle symbols in the figure, and random stars with  $N - 1$  arms, shown through square symbols in the figure. For linear copolymers is clearly noticed a plateau with  $\alpha' = \alpha'' = 0.5$ , which is typical for a linear homopolymer. This happens because at low frequencies only half of the beads, *i.e.* the higher mobility monomers, start to move. It is important to remark that a similar behavior is encountered for alternating copolymer chains [44]. The big difference between them occurs in the intermediate frequency region, more precisely in the intensity of the peaks. The symmetric arrangement of the alternating copolymer gives the highest difference between peaks, while for the

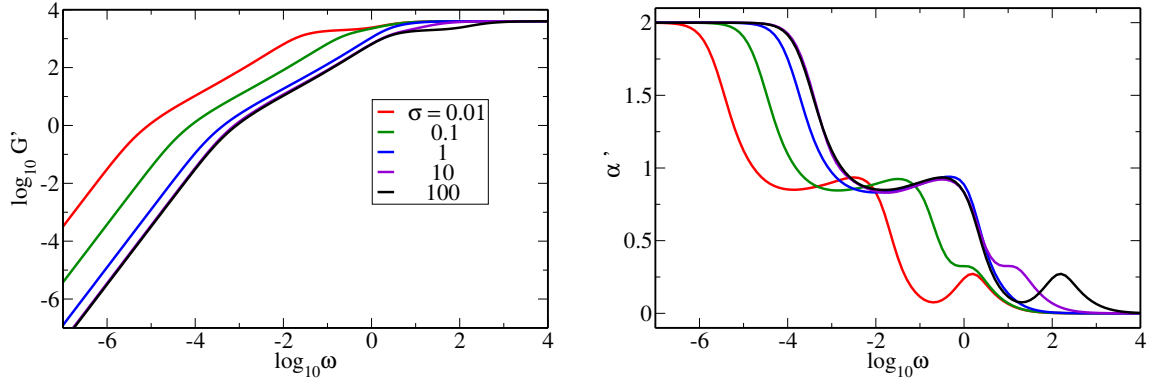


**Figure 4.21** - Storage modulus  $G'(\omega)$  and your derivative for GSFCNs with  $N = 4000$  with the parameters  $(\gamma, K_{min}, K_{max}, \sigma, \eta) = (2.5, 2, 3999, \text{variable}, 1.0)$ .

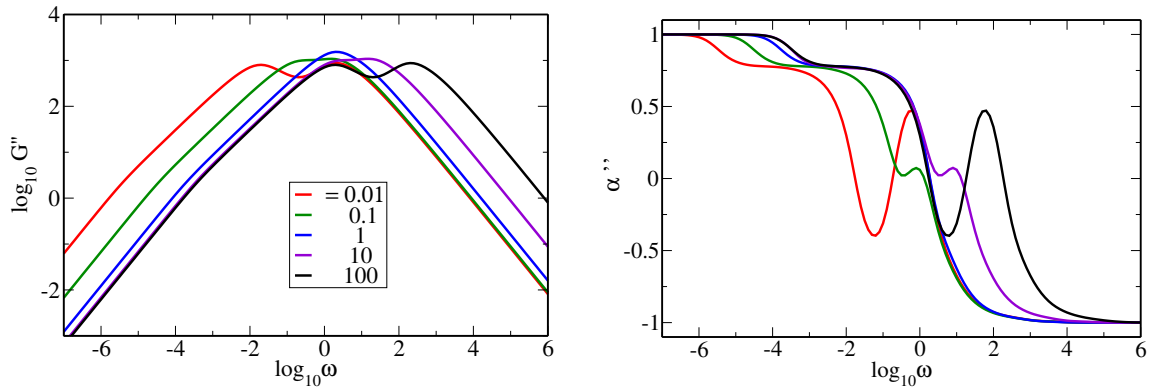


**Figure 4.22** - Loss modulus  $G''(\omega)$  and your derivative  $\alpha''$  for GSFCNs with  $N = 4000$  with the parameters  $(\gamma, K_{min}, K_{max}, \sigma, \eta) = (2.5, 2, 3999, \text{variable}, 1.0)$ .

block copolymer the variation in the slope is the lowest. The slope of the peaks for any random linear copolymers is situated between the above-mentioned limiting situations. The results of  $G'$  and  $G''$  for random copolymer linear chains are similar to our GSFCNs of  $\gamma = 4.0$ , but only in the region of intermediate to high frequencies ( $\omega \geq 10^{-2}$ ). In the region of small frequencies the difference between these two topologies are still significant: the GSFCNs contain a good number of hyperbranched segments. The same behavior is encountered when one compares both  $G'$  and  $G''$  of random stars with  $N - 1$  arms to the GSFCNs with  $\gamma = 1$ . Differently than a star with  $N - 1$  arms our GSFCNs possess a significant number of linear segments. In the low intermediate domain we observed constant slopes for almost two orders of magnitude, namely  $\alpha' \approx 0.77$  for GSFCNs with  $\gamma = 3.0$  and  $\alpha'' \approx 0.85$  for GSFCNs with  $\gamma \leq 2.5$ . This distinct behavior between the slopes of the moduli was encountered also for the scale-free homopolymer networks, but for slightly different  $\gamma$ -values, namely 2.75 (for storage modulus) and 2.25 (for loss modulus) [34]. This fact also confirms our findings from Fig. 4.21 that changes in  $\sigma$  appear more clearly in the region of higher frequencies if  $\sigma < 1$ . For high frequencies ( $\omega \geq 10^3$ ) the random stars with  $N - 1$  arms display an increase in the slope of the  $G''$ , which is due to the presence of the core, *i.e.* a

monomer with very high degree. This behavior is encountered also for our random GSFCNs of  $\gamma = 1.0$  because they also contain monomers with high degree. Remarkably, GSFCNs with  $\gamma = 2.0$  transform this peak in the slope into a small region of constant slope  $\alpha'' \approx -0.9$ .

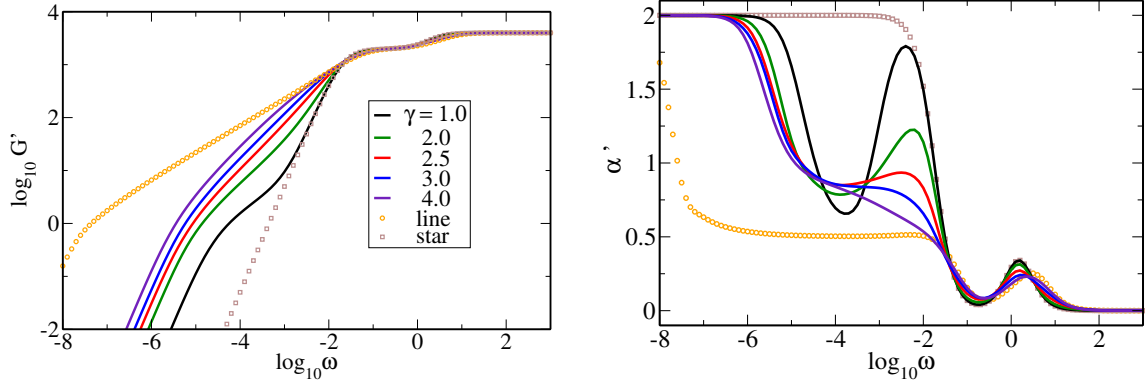


**Figure 4.23** - Storage modulus  $G'(\omega)$  and your derivative for GSFCNs with  $N = 4000$  with the parameters  $(\gamma, K_{min}, K_{max}, \sigma, \eta) = (\text{variable}, 2, 3999, 0.01, 1.0)$

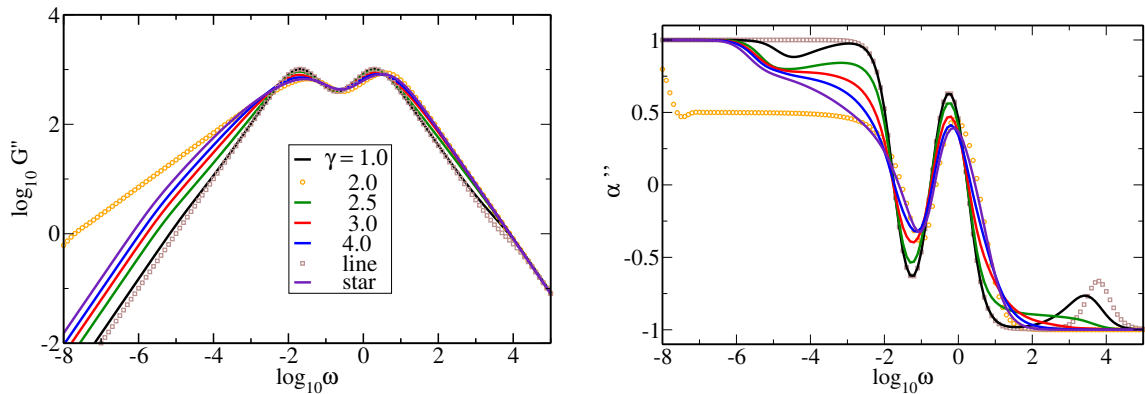


**Figure 4.24** - Loss modulus  $G''(\omega)$  and your derivative  $\alpha''$  for GSFCNs with  $N = 4000$  with the parameters  $(\gamma, K_{min}, K_{max}, \sigma, \eta) = (\text{variable}, 2, 3999, 0.01, 1.0)$

In Figs. 4.25 and 4.26 we monitor how the modularity parameters  $K_{min}$  and  $K_{max}$  influence the storage and loss moduli. For the first three curves we gradually increase the value of  $K_{min}$ , keeping constant  $K_{max}$ . There is a topological transition between networks with  $K_{min} = 2$  and  $K_{min} = 3$ , more precise a transition from networks with linear segments to networks composed of stars of different sizes. This transition provides very little changes for GSFCNs, which are better seen in the slopes  $\alpha'$  and  $\alpha''$ . In the intermediate frequency domain, around  $\omega \approx 10^{-2}$ , we notice only a slight increase of the slopes. This situation is different than semiflexible GSFNs with  $K_{min} = 3$  [39], for which a peak becomes more prominent and destroys the constant slope. Copolymer and semiflexible GSFNs with  $K_{min} = 10$  show a very similar behavior in the intermediate frequency domain, see Fig. 4 (d) of [39] for more details. These two polymer types become distinct in the region of higher intermediate frequencies, when a new peak appears for copolymers. Remarkably, the loss modulus keeps almost unaltered when the transition  $K_{min} = 2 \rightarrow 3$  occurs, but copolymers

with  $K_{min} = 10$  increases by almost two order of magnitude the constant slope  $\alpha'' \approx 0.77$ . In Fig. 4.25 becomes more evident the presence of a new peak around  $\omega \approx 10^{1.5}$ , for having to deal with stars of higher sizes. These results can be understood also in terms of the eigenvalue spectrum, see Fig. 4.7. GSFCNs with  $K_{min} = 10$  increase the degeneracy of the most degenerated eigenvalues:  $\tilde{\lambda} \approx \sigma$  and  $\tilde{\lambda} \approx 1$ , *i.e.* gaining a more discrete spectrum. In Fig. 4.25 we keep constant  $K_{min}$  to 2 and vary the  $K_{max}$  from 3999 (first curve) to 10 (fourth curve) and 3 (fifth curve). By doing this, from the topological point of view we are decreasing the size of the stars in our networks. For the limiting value,  $K_{max} = 3$ , we get a combination of linear and dendritic segments. The slopes  $\alpha'$  and  $\alpha''$  show more clearly that the constant slope is completely destroyed in the intermediate frequency domain by decreasing  $K_{min}$ . However, for the curve with  $K_{max} = 3$  the constant slope around 0.5 starts to appear (more clearly for  $G'$ ), which is a feature typical to single linear chains. Another impactful change occurs for  $G''$  in the region of  $\omega \approx 10^{1.5}$ : the peak observed for  $(K_{min}, K_{max}) = (10, 3999)$  vanishes. Thus, the appearance of this peak is strictly related to stars of high sizes. In the last curve of Fig. 4.25 we display the results of nonsymmetric modified dendrimers, *i.e.* networks composed of monomers with functionality 3 without preserving the high symmetry of dendrimers. Also for these nonsymmetric dendrimers the lack of scaling in the intermediate frequency domain is evident, which was observed also for alternating copolymeric dendrimers as shown in Ref. [45]. By having the same number of  $A$ - and  $B$ - type of monomers the two peaks of  $\alpha''$  show the same height for all curves. However, the behavior of the derivatives of the last three curves are similar: a complete loss of scaling for low intermediate  $\omega$ -values followed by a maximum around  $\omega = 1$ .

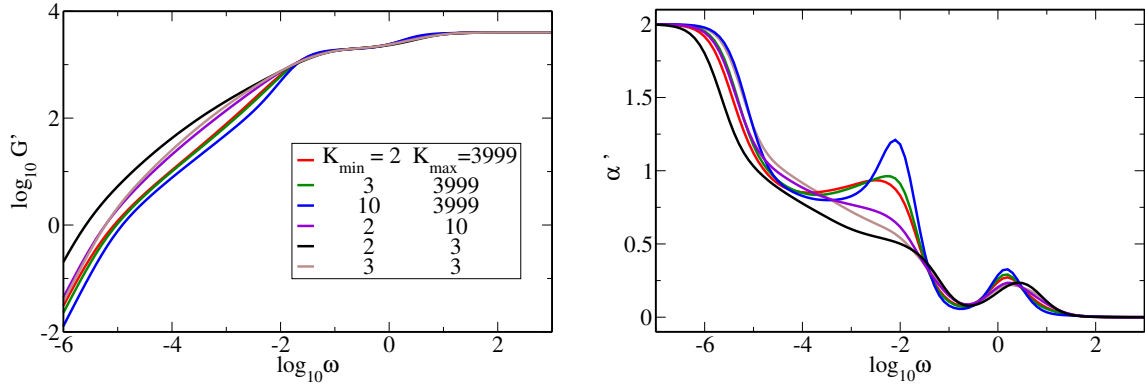


**Figure 4.25** - Storage modulus  $G'(\omega)$  and your derivative for GSFCNs with  $N = 4000$  with the parameters  $(\gamma, K_{min}, K_{max}, \sigma, \eta) = (2.5, \text{variable}, \text{variable}, 0.01, 1.0)$

In Figs. 4.27 and 4.28 we study the influence of the ratio between the numbers of monomers of the two types,  $\eta = \frac{N_A}{N_B}$ , on the moduli. The construction of our networks allows us to choose any value between  $\eta = 0$  (all monomers are of type  $B$ ) and  $\infty$  (all monomers are of type  $A$ ). For an equal number of  $A$  and  $B$  monomers one has to choose  $\eta = 1$ . In Fig. 4.27 we choose symmetric values for this parameter, such that one value is obtained by inversion of another  $\eta$ -value. For instance,  $\eta = 0.2$  corresponds to copolymer networks containing on average

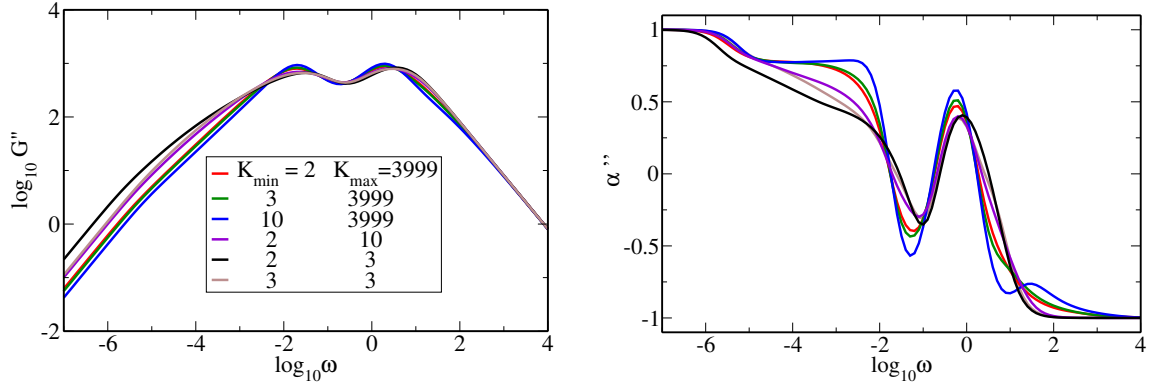


**Figure 4.26** - Loss modulus  $G''(\omega)$  and your derivative  $\alpha''$  for GSFCNs with  $N = 4000$  with the parameters  $(\gamma, K_{\min}, K_{\max}, \sigma, \eta) = (2.5, \text{variable}, \text{variable}, 0.01, 1.0)$

$N_A = 667$  monomers of type  $A$  from a total of  $N = 4000$  monomers, while its inverse  $\eta = 5.0$  provides networks with roughly  $N_B = 667$   $B$ -type monomers. The distribution of the  $A$  or  $B$ -type monomers on the network is chosen at random, as described in chapter 3. In Fig. 4.27 we display the results for  $\sigma = 0.01$ , *i.e.* monomers of type  $B$  are 100 times heavier. By decreasing the number of  $B$  monomers, *i.e.* increasing  $\eta$ , the width of the constant slope in the region of low intermediate frequency gets shorter. In the region of  $\omega \approx 1$  a new peak appears when  $\eta$  is switched on, its height being proportional to the value of  $\eta$ . For comparison we depict by circles the results for alternating copolymer dendrimers of generation  $G = 10$ , which have  $N = 3070$  monomers. For this class of copolymer dendrimers [45] one monomer type dominates, depending on the dendrimer generation number  $G$ . If one considers that the central monomer ( $G = 0$ ) is of  $A$ -type, for  $G$  *even* the  $A$  monomers predominates, while for  $G$  *odd* the majority of the monomers are  $B$ -type. More precise, the ratio between the  $A$  and  $B$  monomers  $\eta = \frac{N_A}{N_B}$  is equal to  $\frac{2^{G+1}-1}{2^G-1}$  or  $\frac{2^G-1}{2^{G+1}-1}$  if  $G$  is *even* or *odd*, respectively. In Fig. 4.27 our dendrimers have  $\eta = \frac{2^{11}-1}{2^{10}-1} \approx 2.0009$ . The hierarchical organization of the dendrimers provides a complete lost of scaling in the low intermediate frequency domain. The second peak of the derivatives, encountered for  $\omega \approx 1$ , shows a similar behavior as our GSFCNs with  $\eta = 2.0$ , especially for the  $G'$  modulus. Thus, we conclude that the size of the peak in the region of  $\omega \approx 1$  is related to the value of  $\eta$ . The two peaks observed for  $G''$  have almost the same height, *i.e.* the curve is more symmetric, when the network has the same number of  $A$  and  $B$  monomers ( $\eta = 1$ ). However, it is possible to fine tune this symmetry by choosing an appropriate distribution of the monomers' type

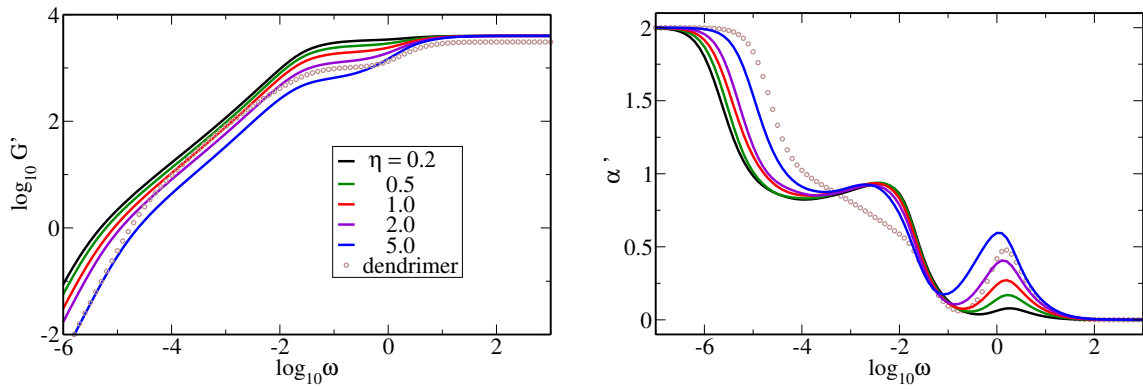


**Figure 4.27** - Storage modulus  $G'(\omega)$  and your derivative for GSFCNs with  $N = 4000$  with the parameters  $(\gamma, K_{min}, K_{max}, \sigma, \eta) = (2.5, 2, 3999, 0.01, \text{variable})$

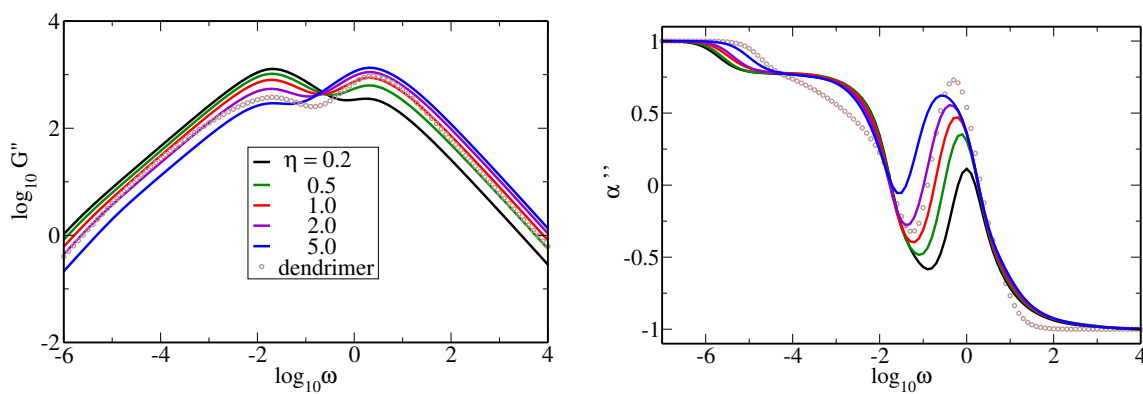


**Figure 4.28** - Loss modulus  $G''(\omega)$  and your derivative  $\alpha''$  for GSFCNs with  $N = 4000$  with the parameters  $(\gamma, K_{min}, K_{max}, \sigma, \eta) = (2.5, 2, 3999, 0.01, \text{variable})$

---

# Conclusion

---

We presented a systematic theoretical investigation of the dynamic properties of polymer networks in the framework of the generalized Gaussian structures. The main goal of this work is to explore the impact of various Theoretical Models such as Rouse, Semiflexible, and Copolymer models, applied to the same networks type: scale-free networks. In the models the dynamics is fully determined by knowing the complete eigenvalues' spectrum of the dynamical matrix. Firstly, we have introduced a new type of scale-free network by considering two new modularity parameters for the usual power-law degree distribution of these hyperbranched trees. They were built by using the degree distribution given by Eq. (2.32) where  $K_{min}$  parameter restricts the minimum allowed degree,  $K_{max}$ , controls the maximum allowed degree, and  $\gamma$  controls the topology from linear to hyperbranched networks. Secondly, based on the eigenvalue spectra, we have investigated the mechanical relaxation  $G'(\omega), G''(\omega)$  and the average displacement  $\langle\langle Y(t) \rangle\rangle$ .

We have analyzed the structural properties of networks for the Rouse Model. Of help here is that in the Rouse-regime, the main relaxation patterns depend only on the eigenvalues, but not on the eigenvectors of the connectivity matrix [33,34,37,38,82]. The eigenvalue spectrum strongly depends on  $K_{min}$  for GSFNs of any  $\gamma$ -value. Increasing the value of  $K_{min}$  we have observed a gap in the spectrum, located between  $\lambda = 1$  and the next higher eigenvalue. This gap was encountered for all  $\gamma$ s, and it gets broader as long as  $K_{min}$  increases. The influence of  $K_{max}$  on the eigenvalue spectrum is less pronounced. The most important feature, which is more evident for lower  $\gamma$ s, is a decrease in the degeneracy of the eigenvalue  $\gamma = 1$  when  $K_{max}$  gets lower. The dynamics of the networks have been analyzed through the average monomer displacement and the mechanical moduli. As observed for the static properties, the parameter  $K_{min}$  has also a stronger influence on the dynamical properties of the networks than the parameter  $K_{max}$ . We have shown that if only the parameter  $K_{max}$  is decreased, the moduli for all  $\gamma$ -values tend to the same curve, and usually the value of the slope is maintained. When we varied the parameter  $K_{min}$ , we have observed for intermediate frequencies various regions of constant slopes for different values of the parameters set  $(\gamma, K_{min})$ . We have highlighted the scaling behavior in the intermediate frequency region for  $(K_{min}, \gamma) = (3, 2.5)$ . In analyzing the dynamical behavior of the average monomer displacement, we have mainly concentrated on the influence of  $K_{min}$  for a particular choice of  $\gamma$ , specifically  $\gamma = 2.5$ . Varying the parameter  $K_{min}$ , while  $K_{max}$  is fixed, we have been able to increase the width of the scaling region by one order of magnitude, obtaining a larger power-law behavior for  $K_{min} > 2$ . This remarkable finding was extended to GSFPNs with higher  $\gamma$ s that don't show scaling for  $K_{min} = 2$ , but will scale when  $K_{min}$  is increased to a certain value.

We have considered the Semiflexible model on generalized scale-free polymer networks. The stiffness effects were considered by assuming correlations between bonds of a freely rotating chain. Thus, we have investigated the influence of the stiffness strength  $q$  and of the networks' topology, controlled by  $\gamma$ ,  $K_{min}$ , and  $K_{max}$  on the eigenvalue spectrum. The impact of the stiffness parameter can be reduced to two main aspects: the highest eigenvalues increase and the lowest eigenvalues decrease if  $q$  gets higher, while the most degenerated eigenvalue depends on the  $q$ -value, for not dealing with highly symmetric networks. The influence of other parameters is richer because by changing at least one of these parameters, we switch to a distinct topology. In the intermediate frequency domain of the mechanical moduli, we encounter networks with  $\gamma = 2.5$ , for which we found a constant slope of 0.83 for about two orders of magnitude. By increasing the stiffness parameter, we increase the width of this constant slope region for another order of magnitude (for networks with  $q = 0.3$ ). Networks with no scaling in the intermediate frequency domain show scaling by carefully choosing all our parameters:  $\gamma$ ,  $q$ ,  $K_{min}$ , and  $K_{max}$ . The behavior of the mechanical moduli show a stronger dependence on  $K_{min}$  than on  $K_{max}$ , since the change in the topology is more efficient. In the intermediate time region of the averaged monomer displacement, we have observed scaling for networks with  $\gamma = 2.5$ . For these networks, the width of the scaling region is diminished by increasing the stiffness parameter, but it is increased by more than one order of magnitude if  $3 \leq K_{min} \leq 5$ . Thus, by an interplay between  $q$  and  $K_{min}$ , we obtain networks with different topologies but similar behavior.

In the theoretical model of copolymers, the two monomer types, namely  $A$  and  $B$ , are also assumed to have different friction constants, with  $\sigma$  being the ratio between them. In the limiting case of equal friction constant or single monomer type, the results of scale-free homopolymer networks [38, 68] were well recovered. By varying the minimum and the maximum allowed degree,  $K_{min}$  and  $K_{max}$ , and the exponent  $\gamma$  of the power-law degree distribution, we obtained irregular hyperbranched networks within two limiting topologies: linear and star polymer. The type of each monomer was chosen at random, and the ratio  $\eta$  between the number of  $A$ - and  $B$ -beads was established at the beginning of the construction. Thus, we have built *random* copolymers from a scale-free network, but the special cases of *block* copolymers or copolymers with *alternating* monomers were possible. In our theoretical model, by knowing the whole eigenvalue spectrum of a new dynamical matrix, we were able to compute the storage and the loss moduli, which can be measured in rheological experiments. For star copolymers, no scaling behavior is observed in the intermediate frequency region, while for random linear copolymers, a scaling with slope 0.5 is seen. For GSFCNs we encountered an additional constant slope for low intermediate frequencies, namely 0.77 for  $G'$  ( $\gamma = 3.0$ ) and 0.85 for  $G''$  ( $\gamma = 2.5$ ). For relatively high frequencies, the random star copolymers and GSFCNs with  $\gamma = 1.0$  have shown a peak for the derivative of  $G''$  because the networks contain monomers with very high degree. This peak was transformed into a new region of constant slope for GSFCNs with  $\gamma = 2.0$  and was completely lost when  $\gamma$  was higher. The topological transition between GSFCNs with ( $K_{min} = 2$ ) and without ( $K_{min} = 3$ ) linear segments have shown very little changes for  $G'$ . The situation is drastically different when

$K_{min}$  gets higher: the constant slope observed for GSFCNs with  $\gamma = 2.5$  was almost destroyed for  $G'$ , but was increased by almost two orders of magnitude for  $G''$ . The parameter  $K_{max}$  was decreased while  $K_{min}$  was kept unaltered; thus, the size of the stars in our networks got higher. For both moduli, the scaling behavior was completely destroyed and for  $K_{max} = 3$  the constant slope around 0.5 started to appear, reminding single linear chains.

The influence of the ratio  $\eta$  for GSFCNs with more  $A$  type monomers have higher degeneracy of 1, while copolymers with more  $B$  monomers have more eigenvalues equal to  $\sigma$ . The ones responsible for this behavior are the star-like segments. For small star copolymers with predominant  $A$  monomers, they have the eigenvalue 1, while for predominant  $B$  monomers, we get the eigenvalue  $\sigma$  as the most degenerated. For  $G'$ , when decreasing the number of  $B$  monomers, *i.e.* increase  $\eta$ , the width of the constant slope in the region of low intermediate frequency gets shorter. In the region of  $\omega \approx 1$  a new peak appears when  $\eta$  is switched on, its height being proportional to the value of  $\eta$ . The second peak of the derivatives, encountered for  $\omega \approx 1$ , shows a similar behavior as our GSFCNs with  $\eta = 2.0$ , especially for the  $G'$  modulus, which influence in the size of the peak in the region of  $\omega \approx 1$  is related to the value of  $\eta$ .

In these three models, the dynamics are fully determined by knowing the complete eigenvalues' spectrum of a dynamical matrix. However, unlike what one finds for flexible (Rouse) GGS, the mechanic relaxation forms for SGSFNs and GSFCNs are not similar. In all models, we have displayed the mechanical storage and loss moduli and average displacement. In the limit of very small and very large frequencies we obtained the well-known behaviors: for the storage modulus  $G'$  a  $\omega^2$  dependence and a plateau, respectively, while for the loss modulus  $G''$  a  $\omega^1$  and a  $\omega^{-1}$  dependence, respectively. For Semiflexible model, with the increasing stiffness parameter  $q$ , the  $G''$  curves get broader especially in the high frequency domain (showing that the stiffness is very important at the local scales) and they start to show a local minimum and another minor peak in the in-between region. Already for the copolymers,  $G'$  and  $G''$ , we can observe two peaks with the size of the peak in the region of  $\omega \approx 1$  being related to the values of  $\sigma$  and  $\eta$ , and for  $G''$  have almost the same height, *i.e.* the curve is more symmetric, when the network has the same number of  $A$  and  $B$  monomers ( $\eta = 1$ ).

Further perspectives of this thesis include studying two situations: the application of the semiflexible to copolymers and to work with three type monomers, both for Generalized Scale-Free Copolymer Network. In both situations, we study the behavior of the mechanical relaxation moduli through the eigenvalues of the new dynamical matrix.

---

# BIBLIOGRAPHY

---

- [1] SHIELDS, Rob. Cultural topology: The seven bridges of Königsburg, 1736. **Theory, Culture Society**, v. 29, n. 4-5, p. 43-57, 2012.
- [2] GOH, K.-I. et al. The human disease network. **Proceedings of the National Academy of Sciences of the United States of America**, v. 104, n. 21, p. 8685–8690, 2007.
- [3] ERDŐS, Paul et al. On the evolution of random graphs. **Publ. Math. Inst. Hung. Acad. Sci.**, v. 5, n. 1, p. 17-60, 1960.
- [4] BARABASI, A.-L. **Network Science**. Cambridge, England: Cambridge University Press, 2016.
- [5] WATTS, Duncan J.; STROGATZ, Steven H. Collective dynamics of ‘small-world’ networks. **Nature**, v. 393, n. 6684, p. 440-442, 1998.
- [6] **Opte**. Disponível em: <<https://www.opte.org/>>. Acesso em: 19 oct. 2023.
- [7] BARABÁSI, Albert-László; ALBERT, Réka. Emergence of scaling in random networks. **Science**, v. 286, n. 5439, p. 509-512, 1999.
- [8] ZHANG, Yan-Chao et al. **The research of information dissemination model on online social network**. 2011.
- [9] JEONG, Hawoong et al. The large-scale organization of metabolic networks. **Nature**, v. 407, n. 6804, p. 651-654, 2000.
- [10] BUCHHOLZ, P. C. F.; ZEIL, C.; PLEISS, J. The scale-free nature of protein sequence space. **PloS one**, v. 13, n. 8, p. e0200815, 2018.
- [11] RAVASZ, Erzsébet et al. Hierarchical organization of modularity in metabolic networks. **Science**, v. 297, n. 5586, p. 1551-1555, 2002.
- [12] LACROIX, Vincent et al. An introduction to metabolic networks and their structural analysis. **IEEE/ACM transactions on computational biology and bioinformatics**, v. 5, n. 4, p. 594-617, 2008.
- [13] CALDARELLI, Guido. Cellular models for river networks. **Physical Review E**, v. 63, n. 2, p. 021118, 2001.
- [14] GARLASCHELLI, Diego; CALDARELLI, Guido; PIETRONERO, Luciano. Universal scaling relations in food webs. **Nature**, v. 423, n. 6936, p. 165-168, 2003.

- [15] VÁZQUEZ, Alexei; PASTOR-SATORRAS, Romualdo; VESPIGNANI, Alessandro. Large-scale topological and dynamical properties of the Internet. **Physical Review E**, v. 65, n. 6, p. 066130, 2002.
- [16] PASTOR-SATORRAS, Romualdo et al. Epidemic processes in complex networks. **Reviews of modern physics**, v. 87, n. 3, p. 925, 2015.
- [17] GALICEANU, M. et al. Mechanisms to decrease the diseases spreading on generalized scale-free networks. **Chaos (Woodbury, N.Y.)**, v. 31, n. 3, p. 033131, 2021.
- [18] NEWMAN, Mark EJ. The structure of scientific collaboration networks. **Proceedings of the national academy of sciences**, v. 98, n. 2, p. 404-409, 2001.
- [19] NEWMAN, Mark EJ. Who is the best connected scientist? A study of scientific coauthorship networks. **Physical Review E**, v. 64, n. 016131, 2001.
- [20] KIM, Hyun-Joo et al. Weighted scale-free network in financial correlations. **Journal of the Physical Society of Japan**, v. 71, n. 9, p. 2133-2136, 2002.
- [21] ONNELA, J.-P.; KASKI, Kimmo; KERTÉSZ, Janos. Clustering and information in correlation based financial networks. **The European Physical Journal B**, v. 38, p. 353-362, 2004.
- [22] BERCHE, Bertrand et al. Resilience of public transport networks against attacks. **The European Physical Journal B**, v. 71, p. 125-137, 2009.
- [23] ZHANG, Peng et al. The robustness of interdependent transportation networks under targeted attack. **Europhysics Letters**, v. 103, n. 6, p. 68005, 2013.
- [24] MACIEL, Cássio Macêdo et al. Quantum transport on generalized scale-free networks. **Physical Review A**, v. 102, n. 3, p. 032219, 2020.
- [25] SCHNEIDERMAN, Deborah K.; HILLMYER, Marc A. 50th anniversary perspective: There is a great future in sustainable polymers. **Macromolecules**, v. 50, n. 10, p. 3733-3749, 2017.
- [26] BOWER, D. I. **An introduction to polymer physics**. Cambridge, England: Cambridge University Press, 2012.
- [27] CEDERHOLM, Linnea et al. Design for Recycling: Polyester-and Polycarbonate-Based A-B-A Block Copolymers and Their Recyclability Back to Monomers. **Macromolecules**, 2023.
- [28] GUSEV, Andrei A.; SCHWARZ, Fabian. Molecular dynamics validation and applications of the maximum entropy homogenization procedure for predicting the elastic properties of Gaussian polymer networks. **Macromolecules**, v. 52, n. 24, p. 9445-9455, 2019.
- [29] RAO, Ameya; RAMÍREZ, Jorge; OLSEN, Bradley D. Mechanisms of Self-Diffusion of Linear Associative Polymers Studied by Brownian Dynamics Simulation. **Macromolecules**, v. 54, n. 24, p. 11212-11227, 2021.

- [30] TRUONG, Hoang P. et al. Single-Molecule Polypeptoid Stretching Reveals the Effects of Charge Sequence on Chain Conformation. **Macromolecules**, 2023.
- [31] ROUSE JR, Prince E. A theory of the linear viscoelastic properties of dilute solutions of coiling polymers. **The Journal of Chemical Physics**, v. 21, n. 7, p. 1272-1280, 1953.
- [32] SCHIESSEL, H. Unfold dynamics of generalized Gaussian structures. **Physical Review E**, v. 57, n. 5, p. 5775, 1998.
- [33] GURTOVENKO, Andrey A.; BLUMEN, Alexander. **Generalized gaussian structures: Models for polymer systems with complex topologies**. Springer Berlin Heidelberg, 2005.
- [34] GALICEANU, M. Relaxation dynamics of scale-free polymer networks. **Physical Review E - Statistical, Nonlinear, and Soft Matter Physics**, v. 86, n. 4, p. 1–11, 2012.
- [35] DOLGUSHEV, M.; BLUMEN, A. Dynamics of semiflexible treelike polymeric networks. **Journal of Chemical Physics**, v. 131, n. 4, 2009.
- [36] DOLGUSHEV, M.; BLUMEN, A. Dynamics of semiflexible chains, stars, and dendrimers. **Macromolecules**, v. 42, n. 14, p. 5378–5387, 2009.
- [37] DOLGUSHEV, M.; BEREZOVSKA, G.; BLUMEN, A. Cospectral polymers: Differentiation via semiflexibility. **Journal of Chemical Physics**, v. 133, n. 15, 2010.
- [38] GALICEANU, M.; REIS, A. S.; DOLGUSHEV, M. Dynamics of semiflexible scale-free polymer networks. **Journal of Chemical Physics**, v. 141, n. 14, p. 1–13, 2014.
- [39] ALVES RIBEIRO, M. V.; JURJIU, A.; GALICEANU, M. Dynamics of semiflexible generalized scale-free polymer networks. **Physica A: Statistical Mechanics and its Applications**, v. 606, p. 128136, 2022.
- [40] BUSTAMANTE, Carlos et al. Entropic elasticity of  $\lambda$ -phage DNA. **Science**, v. 265, n. 5178, p. 1599-1600, 1994.
- [41] KÄS, J. et al. F-actin, a model polymer for semiflexible chains in dilute, semidilute, and liquid crystalline solutions. **Biophysical journal**, v. 70, n. 2, p. 609-625, 1996.
- [42] GÖTTER, R. et al. Dynamic light scattering from semidilute actin solutions: a study of hydrodynamic screening, filament bending stiffness, and the effect of tropomyosin/troponin-binding. **Macromolecules**, v. 29, n. 1, p. 30-36, 1996.
- [43] LIN, Yi-Chia et al. Origins of elasticity in intermediate filament networks. **Physical Review Letters**, v. 104, n. 5, p. 058101, 2010.
- [44] SATMAREL, C.; GURTOVENKO, A. A.; BLUMEN, A. Viscoelastic Relaxation of Cross-Linked, Alternating Copolymers in the Free-Draining Limit. **Macromolecules**, v. 36, n. 2, p. 486–494, 1 jan. 2003.
- [45] SATMAREL, C.; VON FERBER, C.; BLUMEN, A. Dynamics of end-linked star-polymer structures. **Journal of Chemical Physics**, v. 123, n. 3, 2005.

- [46] WIKIPEDIA CONTRIBUTORS. **Seven Bridges of Königsberg**. Disponível em: <<https://en.wikipedia.org>>.
- [47] HAVLIN, Shlomo et al. Challenges in network science: Applications to infrastructures, climate, social systems and economics. **The European Physical Journal Special Topics**, v. 214, p. 273-293, 2012.
- [48] LILJEROS, Fredrik et al. The web of human sexual contacts. **Nature**, v. 411, n. 6840, p. 907-908, 2001.
- [49] HUBERMANN, B. A.; ADAMIC, L. A. Internet: Growth dynamics of the World-Wide Web. **Nature**, v. 401, 2000.
- [50] COHEN, Reuven; HAVLIN, Shlomo; BEN-AVRAHAM, Daniel. Efficient immunization strategies for computer networks and populations. **Physical review letters**, v. 91, n. 24, p. 247901, 2003.
- [51] RADICCHI, Filippo; FORTUNATO, Santo; VESPIGNANI, Alessandro. Citation networks. Models of science dynamics: Encounters between complexity theory and information sciences, p. 233-257, 2011.
- [52] NEWMAN, M. E. J. The structure and function of complex networks. **SIAM review. Society for Industrial and Applied Mathematics**, v. 45, n. 2, p. 167-256, 2003.
- [53] ZEYNEP; ALEXANDER; BUTENKO, S. Detecting large cohesive subgroups with high clustering coefficients in social networks. **Social Networks**, v. 46, p. 1-10, 2016.
- [54] WASSERMAN, M. L. E. Public expenditure and economic activity in Latin America from Old Regime: Buenos Aires in the 17th century. An Approach from Social Network Analysis. **Redes Revista hispana para el análisis de redes sociales**, v. 29, n. 1, p. 139, 2018.
- [55] ONNELA, J.-P. et al. Structure and tie strengths in mobile communication networks. **Proceedings of the national academy of sciences**, v. 104, n. 18, p. 7332-7336, 2007.
- [56] BELLINGERI, M. et al. Modeling the consequences of social distancing over epidemics spreading in complex social networks: From link removal analysis to SARS-CoV-2 prevention. **Frontiers in physics**, v. 9, 2021.
- [57] NEWMAN, M. **Networks: An Introduction**. Cary, NC, USA: Oxford University Press, 2010.
- [58] **Diffusion coefficient**. Disponível em: <<https://www.kruss-scientific.com/en/know-how/glossary/diffusion-coefficient>>. Acesso em: 28 nov. 2023.
- [59] DOROGOVTSSEV, S. N.; MENDES, J. F. F. Evolution of networks: From biological nets to the internet and WWW. **London, England: Oxford University Press**, 2003.
- [60] VOITALOV, I. et al. Scale-free networks well done. **Physical Review Research**, v. 1, n. 3, p. 33034, 2019.

- [61] BARABÁSI, Albert-László; ALBERT, Réka; JEONG, Hawoong. Mean-field theory for scale-free random networks. **Physica A: Statistical Mechanics and its Applications**, v. 272, n. 1-2, p. 173-187, 1999.
- [62] GALLOS, Lazaros K.; ARGYRAKIS, Panos. Absence of kinetic effects in reaction-diffusion processes in scale-free networks. **Physical Review Letters**, v. 92, n. 13, p. 138301, 2004.
- [63] IANG, J. et al. The Structure of Communities in Scale-free Networks. **Concurrency and Computation**, v. 29, 2017.
- [64] BIANCONI, Ginestra; BARABÁSI, A.-L. Competition and multiscaling in evolving networks. **Europhysics Letters**, v. 54, n. 4, p. 436, 2001.
- [65] GALICEANU, M. Relaxation of polymers modeled by generalized Husimi cacti. **Journal of Physics A: Mathematical and Theoretical**, v. 43, n. 30, p. 305002, 2010.
- [66] Gephi software's hyperlink: <https://gephi.org/>
- [67] GALICEANU, M.; BLUMEN, A. Target decay on irregular networks. **Journal of Physics: Condensed Matter**, v. 19, n. 6, p. 065122, 2007.
- [68] JURJIU, Aurel; GOMES MAIA JÚNIOR, Deuticilam; GALICEANU, Mircea. Relaxation dynamics of generalized scale-free polymer networks. **Scientific Reports**, v. 8, n. 1, p. 3731, 2018.
- [69] RAO, Ameya; RAMÍREZ, Jorge; OLSEN, Bradley D. Mechanisms of Self-Diffusion of Linear Associative Polymers Studied by Brownian Dynamics Simulation. **Macromolecules**, v. 54, n. 24, p. 11212-11227, 2021.
- [70] JIANG, Nuofei et al. Linear viscoelasticity of associative polymers: Sticky Rouse model and the role of bridges. **Macromolecules**, v. 53, n. 9, p. 3438-3451, 2020.
- [71] HUNG, Jui-Hsiang; MANGALARA, Jayachandra Hari; SIMMONS, David S. Heterogeneous rouse model predicts polymer chain translational normal mode decoupling. **Macromolecules**, v. 51, n. 8, p. 2887-2898, 2018.
- [72] RIEDEL, Clement et al. Rouse-model-based description of the dielectric relaxation of nontangled linear 1, 4-cis-polyisoprene. **Macromolecules**, v. 42, n. 21, p. 8492-8499, 2009.
- [73] TOSHCHEVIKOV, Vladimir P.; GOTLIB, Yuli Ya. Shear dynamic modulus of nematic elastomers: modified Rouse model. **Macromolecules**, v. 42, n. 9, p. 3417-3429, 2009.
- [74] DOI, M. M. and SF Edwards, Theory of Polymer Dynamics Clarendon Press. **Oxford**1988, 1986.
- [75] FÜRSTENBERG, F.; DOLGUSHEV, M.; BLUMEN, A. Analytical model for the dynamics of semiflexible dendritic polymers. **Journal of Chemical Physics**, v. 136, n. 15, 2012.
- [76] KLOCZKOWSKI, A.; MARK, J. E.; FRISCH, H. L. The relaxation spectrum for Gaussian networks. **Macromolecules**, v. 23, n. 14, p. 3481-3490, 1990.

- [77] BISWAS, Parbati; KANT, Rama; BLUMEN, Alexander. Polymer dynamics and topology: Extension of stars and dendrimers in external fields. **Macromolecular Theory and Simulations**, v. 9, n. 1, p. 56-67, 2000.
- [78] BISWAS, Parbati; KANT, Rama; BLUMEN, Alexander. Stretch dynamics of flexible dendritic polymers in solution. **The Journal of Chemical Physics**, v. 114, n. 5, p. 2430-2441, 2001.
- [79] WARD, Ian M.; SWEENEY, John. **Mechanical properties of solid polymers**. John Wiley Sons, 2012.
- [80] FERRY, John D. **Viscoelastic properties of polymers**. John Wiley Sons, 1980.
- [81] BLUMEN, A.; JURJIU, A. Multifractal spectra and the relaxation of model polymer networks. **The Journal of Chemical Physics**, v. 116, n. 6, p. 2636-2641, 2002.
- [82] BISWAS, Parbati; KANT, Rama; BLUMEN, Alexander. Polymer dynamics and topology: Extension of stars and dendrimers in external fields. **Macromolecular Theory and Simulations**, v. 9, n. 1, p. 56-67, 2000.
- [83] BLUMEN, A. Ch. von Ferber, A. Jurjiu, and Th. Koslowski. **Macromolecules**, v. 37, p. 638, 2004.
- [84] FÜRSTENBERG, Florian; DOLGUSHEV, Maxim; BLUMEN, Alexander. Analytical model for the dynamics of semiflexible dendritic polymers. **The Journal of Chemical Physics**, v. 136, n. 15, 2012.
- [85] FÜRSTENBERG, Florian; DOLGUSHEV, Maxim; BLUMEN, Alexander. Dynamics of semiflexible regular hyperbranched polymers. **The Journal of Chemical Physics**, v. 138, n. 3, 2013.
- [86] QI, Yi; DOLGUSHEV, Maxim; ZHANG, Zhongzhi. Dynamics of semiflexible recursive small-world polymer networks. **Scientific Reports**, v. 4, n. 1, p. 7576, 2014.
- [87] MIELKE, Jonas; DOLGUSHEV, Maxim. Relaxation dynamics of semiflexible fractal macromolecules. **Polymers**, v. 8, n. 7, p. 263, 2016.
- [88] KUMAR, Amit; BISWAS, Parbati. Conformational transitions in semiflexible dendrimers induced by bond orientations. **The Journal of Chemical Physics**, v. 137, n. 12, 2012.
- [89] VON FERBER, Ch; BLUMEN, A. Dynamics of dendrimers and of randomly built branched polymers. **The Journal of Chemical Physics**, v. 116, n. 19, p. 8616-8624, 2002.
- [90] KUMAR, Amit; BISWAS, Parbati. Intramolecular relaxation dynamics in semiflexible dendrimers. **The Journal of Chemical Physics**, v. 134, n. 21, 2011.
- [91] BIXON, Mordechai; ZWANZIG, Robert. Optimized Rouse-Zimm theory for stiff polymers. **The Journal of Chemical Physics**, v. 68, n. 4, p. 1896-1902, 1978.
- [92] BIGGS, Norman. **Algebraic graph theory**. Cambridge university press, 1993.

- 
- [93] OLIVEIRA, Edieliton S. et al. Relaxation dynamics of semiflexible treelike small-world polymer networks. **Physical Review E**, v. 100, n. 2, p. 022501, 2019.
- [94] HANSEN, D. R.; SHEN, M. Viscoelastic retardation time computations for homogeneous block copolymers. **Macromolecules**, v. 8, p. 343–348, 1975.
- [95] SOMMER, J. U.; BLUMEN, A. On the statistics of generalized Gaussian structures: Collapse and random external fields. **J. Phys. A**, v. 28, p. 6669–6674, 1995.
- [96] GALICEANU, Mircea; JURJIU, Aurel. Relaxation dynamics of multilayer triangular Husimi cacti. **The Journal of Chemical Physics**, v. 145, n. 10, 2016.
- [97] LIU, Fuyong et al. Rheological images of dynamic covalent polymer networks and mechanisms behind mechanical and self-healing properties. **Macromolecules**, v. 45, n. 3, p. 1636–1645, 2012.
- [98] TE NIJENHUIS, Klaas; WINTER, H. Henning. Mechanical properties at the gel point of a crystallizing poly (vinyl chloride) solution. **Macromolecules**, v. 22, n. 1, p. 411–414, 1989.
- [99] COSTANZO, Salvatore et al. Rheology and packing of Dendronized polymers. **Macromolecules**, v. 49, n. 18, p. 7054–7068, 2016.
- [100] BULACU, Monica; VAN DER GIESSEN, Erik. Effect of bending and torsion rigidity on self-diffusion in polymer melts: A molecular-dynamics study. **The Journal of Chemical Physics**, v. 123, n. 11, 2005.